Aus der Klinik für Neurologie

(Prof. Dr. med. M. Bähr)

der Medizinischen Fakultät der Universität Göttingen

Neural progenitor cell-derived extracellular vesicles enhance blood-brain barrier integrity in stroke mice

INAUGURAL-DISSERTATION

zur Erlangung des Doktorgrades

der Medizinischen Fakultät der

Georg-August-Universität zu Göttingen

vorgelegt von

Lin Zhang

aus

Anhui, China

Göttingen 2021

Dekan:	Prof. Dr. med. W. Brück

Betreuungsausschuss

Betreuer/in:	Prof. Dr. med. T. R. Döppner
Ko-Betreuer/in:	Prof. Dr. med. C. Binder

Prüfungskommission

Referent/in:	Prof. Dr. med. T. R. Döppner
Ko-Referent/in:	Prof. Dr. C. Binder
Drittreferent/in:	Prof. Dr. C. Kramm

Datum der mündlichen Prüfung: 08. 06. 2022

Hiermit erkläre ich, die Dissertation mit dem Titel „Neural progenitor cell-derived extracellular vesicles enhance blood-brain barrier integrity in stroke mice“ eigenständig angefertigt und keine anderen als die von mir angegebenen Quellen und Hilfsmittel verwendet zu haben.

Göttingen, den …… ……

(Unterschrift)

List of publications obtained during the doctoral thesis period

Publication as first author

Publication 1: Zhang L, Graf I, Kuang Y, Zheng X, Haupt M, Majid A, Kilic E, Hermann DM, Psychogios MN, Weber MS, et al. (2021): Neural Progenitor Cell-Derived Extracellular Vesicles Enhance Blood-Brain Barrier Integrity by NF-κB (Nuclear Factor-κB)-Dependent Regulation of ABCB1 (ATP-Binding Cassette Transporter B1) in Stroke Mice. Arterioscler Thromb Vasc Biol 41, 1127-1145

Other publications

Publication 2: Zheng X, **Zhang L**, Kuang Y, Venkataramani V, Jin F, Hein K, Zafeiriou MP, Lenz C, Moebius W, Kilic E, et al. (2021): Extracellular Vesicles Derived from Neural Progenitor Cells--a Preclinical Evaluation for Stroke Treatment in Mice. Transl Stroke Res 12, 185-203

Publication 3: Kuang Y, Zheng X, **Zhang L**, Ai X, Venkataramani V, Kilic E, Hermann DM, Majid A, Bähr M, Doeppner TR (2020): Adipose-derived mesenchymal stem cells reduce autophagy in stroke mice by extracellular vesicle transfer of miR-25. J Extracell Vesicles 10, e12024

Publication 4: Haupt M, Zechmeister B, Bosche B, Lieschke S, Zheng X, **Zhang L**, Venkataramani V, Jin F, Hein K, Weber MS, et al. (2020): Lithium enhances post-stroke blood-brain barrier integrity, activates the MAPK/ERK1/2 pathway and alters immune cell migration in mice. Neuropharmacology 181, 108357

The following thesis comprises methods and results published in the original paper Zhang et al. "Neural Progenitor Cell-Derived Extracellular Vesicles Enhance Blood-Brain Barrier Integrity by NF-κB (Nuclear Factor-κB)-Dependent Regulation of ABCB1 (ATP-Binding Cassette Transporter B1) in Stroke Mice".

Contents

Figures

Abbreviations

ABCB1	atp-binding cassette subfamily b member 1 transporter
ARRIVE	animal research reporting of *in vivo* experiments
BBB	blood-brain barrier
BSA	bovine serum albumin
BSS0	glucose-free balanced salt solution
CM	conditioned medium
ddH_2O	double distilled water
DMEM	dulbecco's modified eagle's medium
DS	donkey serum
EBA	evans blue-albumin
ECL	enhanced chemoluminescence
ECs	endothelial cells
EGF	epidermal growth factor
EVs	extracellular vesicles
FACS	fluorescence-activated cell sorting
FCS	fetal calf serum
FGF	fibroblast growth factor
IL-10	interleukin-10
ISEV	International Society for Extracellular Vesicles
LY	lucifer yellow
MCAO	middle cerebral artery occlusion
MMP-2	matrix metalloproteinase-2
MMP-9	matrix metalloproteinase-9
MSC	mesenchymal stem cell
NF-$\varkappa$B	nuclear factor-kappa B
NIH	National Institutes of Health
NPC	neural progenitor cell
NSC	neural stem cell
NTA	nanoparticle tracking analysis
OGD	oxygen-glucose deprivation
OGD/RO	oxygen-glucose deprivation/reoxygenation
PBS	phosphate-buffered saline
PEG	polyethylene glycol
R123	rhodamine 123
RO	reoxygenation

RT	room temperature
STAIR	Stroke Therapy Academic Industry Roundtable
SVZ	subventricular zone
TEM	transmission electron microscopy
TER	transcellular electrical resistance
TGF-β	transforming growth factor-β
UC	ultracentrifugation
VEGF	vascular endothelial growth factor
WHO	World Health Organization
ZO-1	zonula occludens-1

1 Introduction

1.1 Epidemiological and clinical aspects of ischemic stroke

Stroke is a major concern in terms of increasing morbidity and mortality worldwide and is categorized into two forms, i.e. ischemic and hemorrhagic stroke (WHO 2020). The majority of stroke cases are ischemic, while intracerebral hemorrhage accounts for less than 20 % of all stroke cases (Musuka et al. 2015). Of note, the present thesis focuses on ischemic strokes, also known as cerebral ischemia, and uses the term „stroke“ in this context only. Although systemic thrombolysis has been established for more than twenty years in modern stroke therapy, only a minority of patients (3.4 % to 5.2 %) are eligible for thrombolytic treatment due to a narrow therapeutic time window or side effects (Seitz 2016). The recent introduction of endovascular thrombectomy has revolutionized modern stroke therapy (Goyal et al. 2016). However, this treatment paradigm is reserved to a fraction of patients only. Hence, a great number of patients suffer from low life quality because of permanent brain injury after stroke. New treatment paradigms are therefore urgently needed. Although extensive neuroprotective approaches have been successfully employed in preclinical stroke models, their translation into the clinic has failed until recently (Gladstone et al. 2002; Green and Shuaib 2006; O'Collins et al. 2006; Schmidt-Pogoda et al. 2020; Venkat et al. 2018). Establishing novel therapeutic strategies to enhance the neurovascular protection for stroke patients during the acute course of stroke is therefore in order.

1.2 Neural progenitor cell (NPC) transplantation and NPC-derived extracellular vesicle (EV) delivery

Novel therapeutic strategies against ischemic stroke include cell-based therapies and neurotrophic drug-based therapies. However, the neurotrophic drug-based therapies entirely failed in clinical trials (O'Collins et al. 2006; Schmidt-Pogoda et al. 2020; Venkat et al. 2018; Xu and Pan 2013). Cell-based therapies using neural progenitor cells (NPCs) or bone marrow mesenchymal stem cells (MSCs) were shown to be a markedly valid therapy to facilitate neurological recovery and cerebral remodeling in preclinical stroke studies (Liu et al. 2014; Moskowitz et al. 2010). The effects induced by stem cells or progenitor cells are limited to neuroprotective mechanisms but imply neuroregenerative mechanisms as well. Hence, NPC transplantation induces both neurogenesis and angiogenesis via the regulation of vascular endothelial growth factor (VEGF) (Andres et al. 2011; Moriyama et al. 2013). These NPCs are usually derived from either the subgranular zone of the dentate gyrus or the subventricular zone (SVZ) of the lateral ventricles (Kaneko et al. 2011). In accordance with our previous studies, it was reported that NPC transplantation improves neurological recovery via pleiotropic mechanisms, including the stabilization of the blood-brain barrier (BBB), the reduction of microglial activation and the modulation of both peripheral and central immune responses that culminate in enhanced angioneurogenesis and axonal plasticity (Doeppner et al. 2014).

Increased poststroke functional recovery due to cell-based therapies is likely a consequence of paracrine mechanisms, among which are the transfer of cytokines, growth factors, and RNAs released from grafted stem cells into the brain parenchyma. Although cell-based therapies against stroke appear attractive, clinical concerns still remain, such as the efficiency of evading immune surveillance and crossing natural barriers including the BBB. Therefore, additional strategies are needed to further enhance neurovascular protection after stroke avoiding the aforementioned concerns.

As a matter of fact, the majority of biological alterations observed after stem cell transplantation appear to be the result of factors mediated by extracellular vesicles (EVs). The latter are secreted from virtually all eukaryotic cells including stem cells, thus providing a potential tool to avoid cell grafting itself. Previously, a great number of preclinical studies have reported that EVs derived from stem cells, both MSCs and NPCs, have beneficial effects on angiogenesis, neurogenesis, and immunomodulation against cerebral ischemia (Anderson et al. 2016; Bang and Kim 2019; Dabrowska et al. 2019; Webb et al. 2018). EVs comprise a heterogeneous group of vesicles ranging in size from 30-1000 nm that contain various non-coding RNAs, DNAs, and proteins (Kim et al. 2013; Mathivanan et al. 2012; Thery et al. 2018). EVs including exosomes and microvesicles are a consequence of direct outward budding or pinching of the plasma membrane, and microvesicles are the derivatives of multivesicular bodies (Doyle and Wang 2019). Previous results from our group suggest that NPC-derived EVs induce neurological recovery, neuroregeneration, and modulation of poststroke immune responses in a murine stroke model. Interestingly, NPC-EVs are not inferior to NPC transplantation in this respect (Zheng X et al. 2020). Consequently, NPC-EVs seem to be a mediator of cytokine or RNA transfer into the ischemic brain, which helps support both neuroprotection and cerebral remodeling. Given NPC transplantation stabilizing the BBB integrity (Doeppner et al. 2014; Doeppner et al. 2015), I proposed that NPC-EVs might enhance the preservation of the BBB integrity in acute ischemic stroke. However, the precise mechanisms of this key mechanism during stroke development are not fully understood and therefore deserve further scientific investigation.

1.3 Blood-Brain Barrier (BBB) and ABCB1 transporter in stroke

As a matter of fact, stroke induces BBB disruption, which allows intravascular molecules and immune cells to penetrate into the cerebral parenchymal extracellular space, in turn incurring subsequent inflammatory responses and further neurological impairment (Dirnagl et al. 1999). Previously, accumulating evidence suggests that early BBB protection promotes neurological recovery in stroke models involving various mechanisms such as immunomodulation. Ischemic stroke changes the microenvironment, including oxidative stress, chemokines, and modulation of endothelial cells (ECs) and astrocytes. This subsequently exacerbates BBB breakdown and initiates the recruitment of more immune cells into the brain, propagating tissue injury (Chamorro et al. 2012; Iadecola and Anrather 2011; Kamel and Iadecola 2012; Santos Samary

et al. 2016). Since NPC transplantation can stabilize the BBB as shown in our previous studies, I propose that the delivery of NPC-EVs also play a role in BBB protection.

The BBB is comprised of ECs lining cerebral microvessels, surrounded by a basal membrane. Various cell types including astrocytes, pericytes, neurons, and microglia form the neurovascular unit (Abbott et al. 2006; Abbott et al. 2010; Sa-Pereira et al. 2012). ECs constitute membrane domains between luminal (blood) and abluminal (brain) sides, and are interconnected by tight junctions which limit both paracellular and transcellular transport of molecules through the EC layer (Luissint et al. 2012; Sandoval and Witt 2008). This means that the exchange of substances through the BBB is modulated by specialized transporters, which involve the conveyance of nutrients to the brain side and potential toxins or other detrimental compounds to the blood side. Among the known BBB transporters, the ATP-binding cassette subfamily B member 1 transporter (ABCB1, also named P-gp or Mdr-1) is by far the most prominent one that has been studied in various disease models including stroke (Cen et al. 2013; ElAli and Hermann 2012; Ji et al. 2013; Qosa et al. 2015; Spudich et al. 2006).

ABCB1 binds to numerous structurally diverse molecules and is mostly located on the luminal sides of ECs in cerebral capillaries, transporting substances from the brain parenchyma to the blood side (Miller 2015). ABCB1 is upregulated as a consequence of inflammation, oxidative stress, radiation, and heat shock (Felix and Barrand 2002; Sanchez-Covarrubias et al. 2014; Zhou 2008). Recently, Spudich and colleagues showed that ABCB1 increased within three hours following transient middle cerebral artery occlusion (MCAO) in brain capillary ECs of ischemic areas and remained elevated up to twenty-four hours after reperfusion (Spudich et al. 2006). Although upregulation of ABCB1 in the ischemic brain is likely a physiological response to export toxic substances, it also excessively transports neuroprotective molecules and inflammatory chemokines to the luminal side (DeMars et al. 2017; ElAli and Hermann 2012; Hermann 2008; Patak and Hermann 2011). Importantly, the latter facilitates the recruitment of a great number of immune cells to the brain side and triggers a plethora of subsequent inflammatory responses. However, ABCB1 contributes to ischemic brain injury, since infarct sizes are significantly reduced in mdr1a (gene homolog of ABCB1 in rodents) knockout mice (Murozono et al. 2009). Although the underlying mechanisms of ABCB1 modulation after stroke are obscure, upregulation of ABCB1 is known to contribute to increased transport of chemokines that yield increased injury in models of neuroinflammation (Kooij et al. 2009; Kooij et al. 2011). As a matter of fact, up to 50 % of pharmaceutical compounds currently tested are related to ABCB1 substrates based on recent estimations (Abbott et al. 2002), as ABCB1 has been repeatedly reported to be upregulated under stroke conditions (Ji et al. 2013; Qosa et al. 2015). Thus, blocking of ABCB1 enhanced the efficacy of neuroprotective drug therapy in a mouse stroke model that was subjected to thirty and ninety minutes of MCAO (Spudich et al. 2006). In this context, ABCB1 is likely to be one key mediator in ischemic stroke.

1.4 Matrix metalloproteinases (MMPs) and NF-ϰB pathway in stroke

On the abluminal side of the BBB, end-feet of astrocytes encircle cerebral microvessels to closely support the integrity of the endothelial barrier (Abbott et al. 2010; Ronaldson and Davis 2012). However, when stimulated after ischemic stroke, activated astrocytes are an important source of MMPs, which contribute to degrading the extracellular matrix and facilitate BBB breakdown (Lakhan et al. 2013; Rempe et al. 2016; Yang Changjun and Candelario-Jalil 2017). Among the MMPs, accumulating evidence confirms that both MMP-2 and MMP-9 are involved in the poststroke BBB disruption. In the acute course, these two MMPs contribute to BBB opening, whereas severe and progressive BBB disruption is ascribed to the marked elevation of MMP-9 within the first forty-eight hours only. Several studies reported an extensive upregulation of MMP-9 in the ischemic hemisphere within twenty-four hours after reperfusion, while MMP-2 remained at its basal level (Fujimura et al. 1999; Park et al. 2009; Suofu et al. 2012).

Accumulating evidence indicates that both ABCB1 and MMP-9 are critically involved in the nuclear factor-kappa B (NF-ϰB) signaling pathway under conditions of cancer (Chiu et al. 2015; Katayama et al. 2014). Interestingly, MMP-9 is claimed to be modulated by the NF-ϰB pathway in stroke models as well (Lv et al. 2019; Wang Z et al. 2011). Several studies found ABCB1 regulation to be associated with the NF-ϰB pathway in various neurological diseases but not with stroke (Bauer et al. 2007; Zhang J et al. 2014). As a matter of fact, there are no studies analyzing the mutual interactions between ABCB1, MMP-9 and NF-ϰB pathway and the therapeutic impact of NPC-EVs on the aforementioned targets under preclinical conditions of ischemic stroke. The present thesis therefore strives to analyze whether or not NPC-EV application may modulate ABCB1 and MMP-9 levels by inhibiting the NF-ϰB pathway in order to stabilize the BBB in a murine stroke model.

1.5 Aim of the study

NPC transplantation has recently been described to generate neuroprotection, immunomodulation, and stabilization of the BBB under ischemic conditions. NPC-EVs are not inferior to NPC transplantation and may also contribute to enhancing the BBB integrity, albeit the underlying mechanisms of such an approach remain elusive. The aim of the present thesis was therefore to perform a proof-of-concept study using an *in vitro* BBB co-culture model of ECs and astrocytes as well as an *in vivo* murine stroke model. In detail, the impact of NPC-EVs on the integrity of the hypoxic/ischemic BBB, which involves the regulation of MMP-9 secretion by astrocytes and ABCB1 expression in ECs, and the regulation of the NF-ϰB signaling pathway are thoroughly studied.

2 Materials and Methods

2.1 Legal issues and ethical approval

In compliance with EU rules, animal experiments were developed following governmental approval according to the NIH guidelines for the care and housing of laboratory animals. Both the STAIR criteria and the ARRIVE guidelines have been followed. The mice were kept under a circadian rhythm in groups of five each and had free access to food and water. All animals were randomly assigned to the various experimental groups. For all phases of the study, the experimenter was blinded to the treatment protocols. This thesis does not contain any studies with human participants performed by the experimenter.

2.2 Primary culture of NPCs and EV isolation

The NPC preparation and EV enrichment were based on the method of Zheng et al (Zheng X et al. 2020). Briefly, C57BL/6J mouse pups at postnatal day 0-2 were decapitated, whole brains removed, and placed in cold HBSS. Thereafter, the cerebral SVZ was isolated under microscopic control, followed by digestion with 0.05 % trypsin for 15 min and centrifugation at 400 g for 15 min. The resulting pellet was resuspended with NPC medium, and the cells were plated in a cell culture dish. The neurospheres were observed within 72 h, and the cells were passaged every five days. After passage three, NPCs were transferred to T75 flasks with 30 mL NPC culture medium without growth factors. After 24 h of incubation under standard cell culture conditions, the conditioned medium (CM) of NPCs was collected. Large vesicles and debris were removed through 220 nm pore filters. EVs were enriched from the CM using either the polyethylene glycol (PEG) precipitation method or the ultracentrifugation only (UC) method as described before (Ludwig et al. 2018; Thery et al. 2018). Details of the procedures for these two methods can be found in Figure 1.

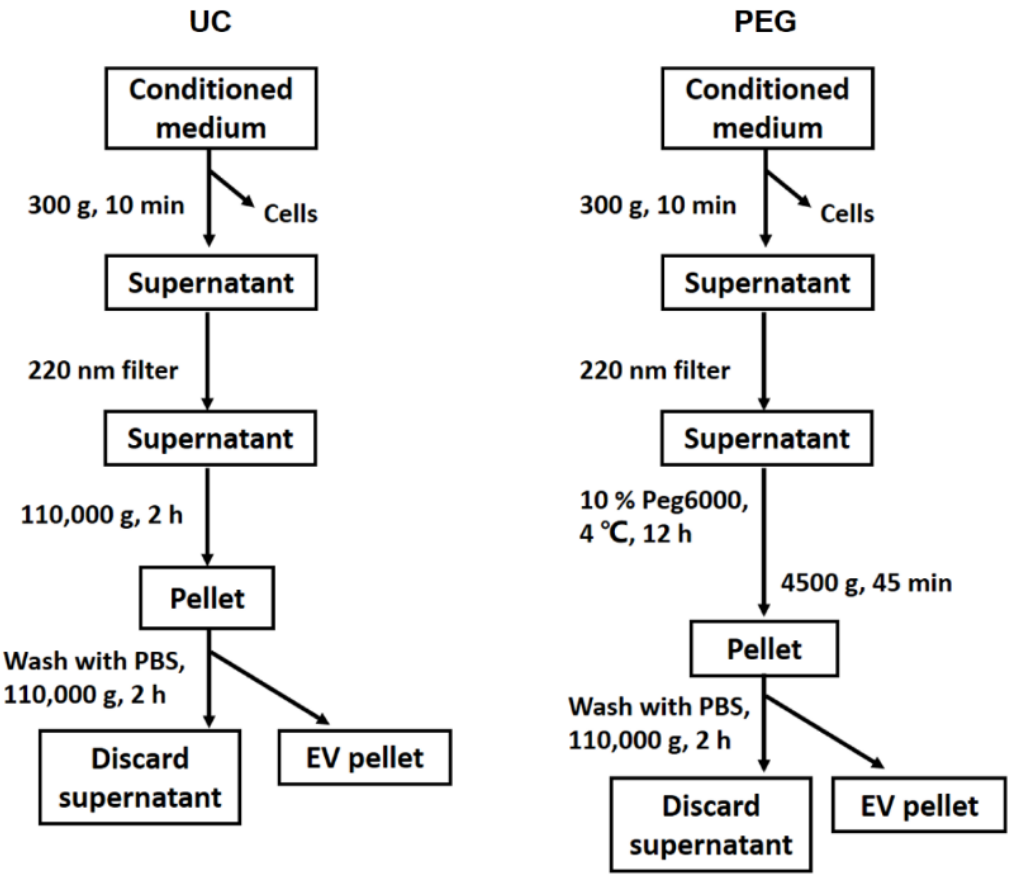

Figure 1: Schematic diagrams of the UC and PEG methods. In the schematic diagram, extracellular vesicles (EVs) were enriched from the conditioned medium of neural progenitor cells (NPCs) by UC and PEG methods. Abbreviations: UC, ultracentrifugation; PEG, polyethylene glycol (Zhang et al. 2021).

2.3 Characterization of NPC-EVs

There are many EV isolation methods. However, the optimal isolation method for EVs is still under debate (Buschmann et al. 2018). In the present thesis, I compared two different enrichment methods including the aforementioned UC only and the PEG approach. EVs were characterized with transmission electron microscopy (TEM), nanoparticle tracking analysis (NTA), Western blotting of EV specific markers, proteomic analysis, and iodixanol gradient centrifugation according to the ISEV guidelines (Thery et al. 2018). Details about the above mentioned procedures can be found in Supplement Materials and Methods (Zhang et al. 2021). Briefly, the characterization of EVs was confirmed by measuring the expression of specific markers Alix and Tsg101 and EV-associated protein markers such as CD63, CD81, and CD9. As EVs are on the nanoscale, ordinary fluorescence microscopy cannot confirm their microscopic structure. As such, TEM was performed by Dr. Möbius and colleagues from the Max Planck Institute of Experimental Medicine, Göttingen, to investigate the structure of NPC-EVs. In terms of both size and quantification analysis, NTA was employed by using a Nanosight platform. As previously reported (Sokolova et al. 2011), 1:1,000 PBS-diluted samples were

measured in duplicate with a video recording of each measurement. As described before, EVs achieve their biological functions by transferring their contents, such as proteins, towards the extracellular environment or directly to neighboring cells. Hence, the protein contents including cellular compartment markers of NPC-EVs were analyzed using mass spectrometric analyses, which was performed by Dr. Lenz and colleagues from the Core Facility Proteomics of the University Medical Center Göttingen. The details and the results of mass spectrometry analysis can be found in Supplement Data I (Zhang et al. 2021).

In addition, I further investigated the characteristics of EVs using iodixanol gradient centrifugation as reported by Kowal et al. (2016). The discontinuous iodixanol gradients (30 %, 20 % and 10 % iodixanol solutions) were prepared by diluting the OptiPrep™ solution (60 % w/v; STEMCELL Technologies, Vancouver, Canada) with 0.25 M sucrose/10 mM Tris buffer (pH 7.5). The EV pellets were resuspended in the 30 % iodixanol solution, and the overlaid gradient solutions (20 % and 10 % iodixanol solutions) were loaded on top, subsequently. After ultracentrifugation with 110,000 g for 2 h, ten fractions (F1-F10) were collected, washed with PBS, and recentrifuged at 110,000 g for 2 h. The resulting pellets were resuspended with PBS and analyzed for protein concentration and the presence of EV markers (Supplement Publication 1 Figure 2.D-E.).

When fluorescent EVs were needed for EV tracking, the supernatant was incubated with 10 μM DiI, a lipophilic membrane dye, for 1 h at 37 °C in the dark. DiI-labeled EVs were separated from extra DiI dye in the light fraction and protein aggregates in the dense fractions by the aforementioned iodixanol gradient centrifugation. Different fractions were washed with PBS and recentrifuged. Pellets with DiI-labeled EVs were applied for EV tracking, and the pellets from F9-10 fractions lacking EVs were used as negative controls for the following *in vitro* and *in vivo* experiments. As Figure 2. shows, DiI-labeled EVs (red signal) were incorporated by bEnd.3 and astrocytes (*in vitro*), and red spots depicting EVs were also shown to reach ECs and astrocytes of the mouse cerebral parenchyma (*in vivo*) when compared to the negative control groups.

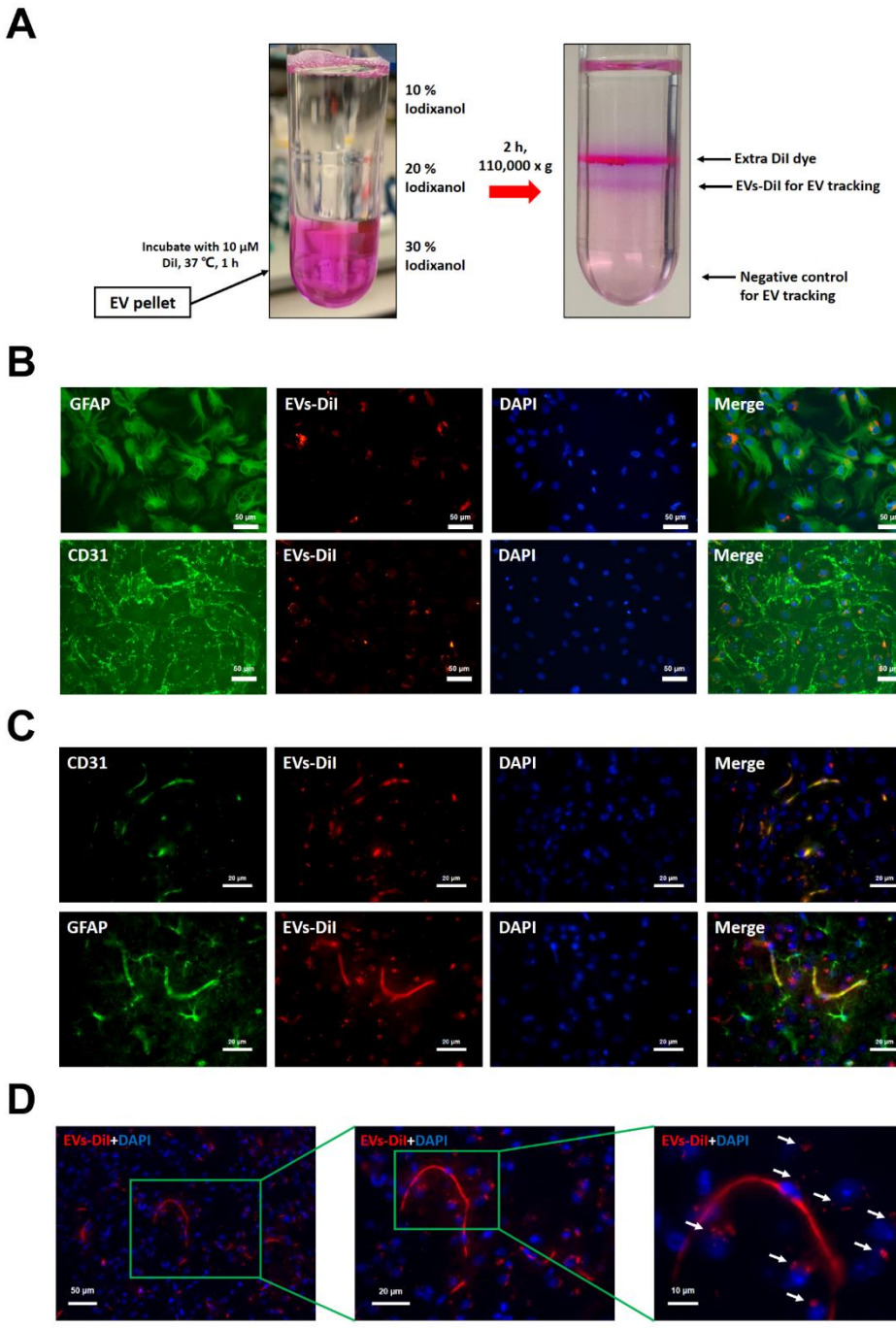

Figure 2: EV tracking with DiI dye. (A) DiI-labeled EVs were separated from excess DiI dye in the light fraction and protein aggregates lacking EVs in the dense fractions by iodixanol gradient centrifugation. After centrifugation, pellets with DiI-labeled EVs were applied for EV tracking, and the pellets from F9-10 fractions lacking EVs were used as negative controls for *in vitro* and *in vivo* experiments. (B) Representative immunofluorescence staining of EVs-DiI (red) taken up by bEnd.3 (CD31, green) and astrocytes (GFAP, green). (C) Representative immunofluorescence staining of EV tracking *in vivo* experiments. EVs labeled with DiI (red) reached ECs of the brain tissue as shown by immunofluorescence staining against CD31 (green). Furthermore, EVs-DiI (red spots) were also detected in the brain parenchyma outside of the microvessels with some positive signaling in astrocytes (GFAP, green). (D) High magnification photographs of representative immunofluorescence stain *in vivo* show that EVs-DiI cross the blood-brain barrier and reach the cerebral parenchyma (red spots represent EVs-DiI as indicated

by white arrows). Abbreviations: CD31, cluster of differentiation 31; EVs, extracellular vesicles; ECs, endothelial cells; GFAP, glial fibrillary acidic protein.

2.4 Oxygen-glucose deprivation (OGD) model and the *in vitro* experimental paradigm

ECs were exposed to OGD when they reached 90 % confluency. For OGD treatment, the cells were incubated in a glucose-free balanced salt solution (BSS0) and transferred to a hypoxic chamber containing 0.2 % O_2, 5 % CO_2, and 70 % humidity. As for the reoxygenation (RO) phase after OGD treatment, the cells were incubated in cell culture medium for 24 h under standard cell culture conditions. Thereafter, the cells were used for further analyses.

First, I employed the endothelial cell line bEnd.3 in the OGD/RO hypoxia model. In order to investigate the optimal hypoxic injury, I exposed bEnd.3 cells for different OGD time periods (8, 12, and 16 h) and the same RO time (24 h). By using Western blot analysis, BBB-related proteins (ABCB1 and ZO-1) were analyzed with a normoxia group as control (Figure 3.A-B.). Thereafter, I focused on an OGD time to reach an appropriate hypoxic injury for the coming experiments. The effect of NPC-EVs on the regulation of these BBB functional proteins was examined in bEnd.3 cells exposed to OGD/RO treatment (Figure 3.C.). Likewise, the regulation of proteins including NF-κB p65 and IκBα involved in the NF-κB signaling pathway was investigated by Western blotting. To further analyze the NF-κB pathway after EV treatment, the cytoplasmic and nuclear fractions of ECs after OGD/RO were isolated to examine the NF-κB p65 nuclear translocation. To investigate the connection between the NF-κB pathway and ABCB1, I employed the NF-κB p65 nuclear translocation inhibitor (SN50) and ABCB1 inhibitor (Valspodar) during OGD/RO. Thereafter the protein expressions of ABCB1 and p65 were analyzed. The ABCB1 activity was assessed using a Rhodamine 123 accumulation assay. The modulation of the BBB function after NPC-EV treatment was examined in an *in vitro* BBB hypoxia model as described in the next chapter.

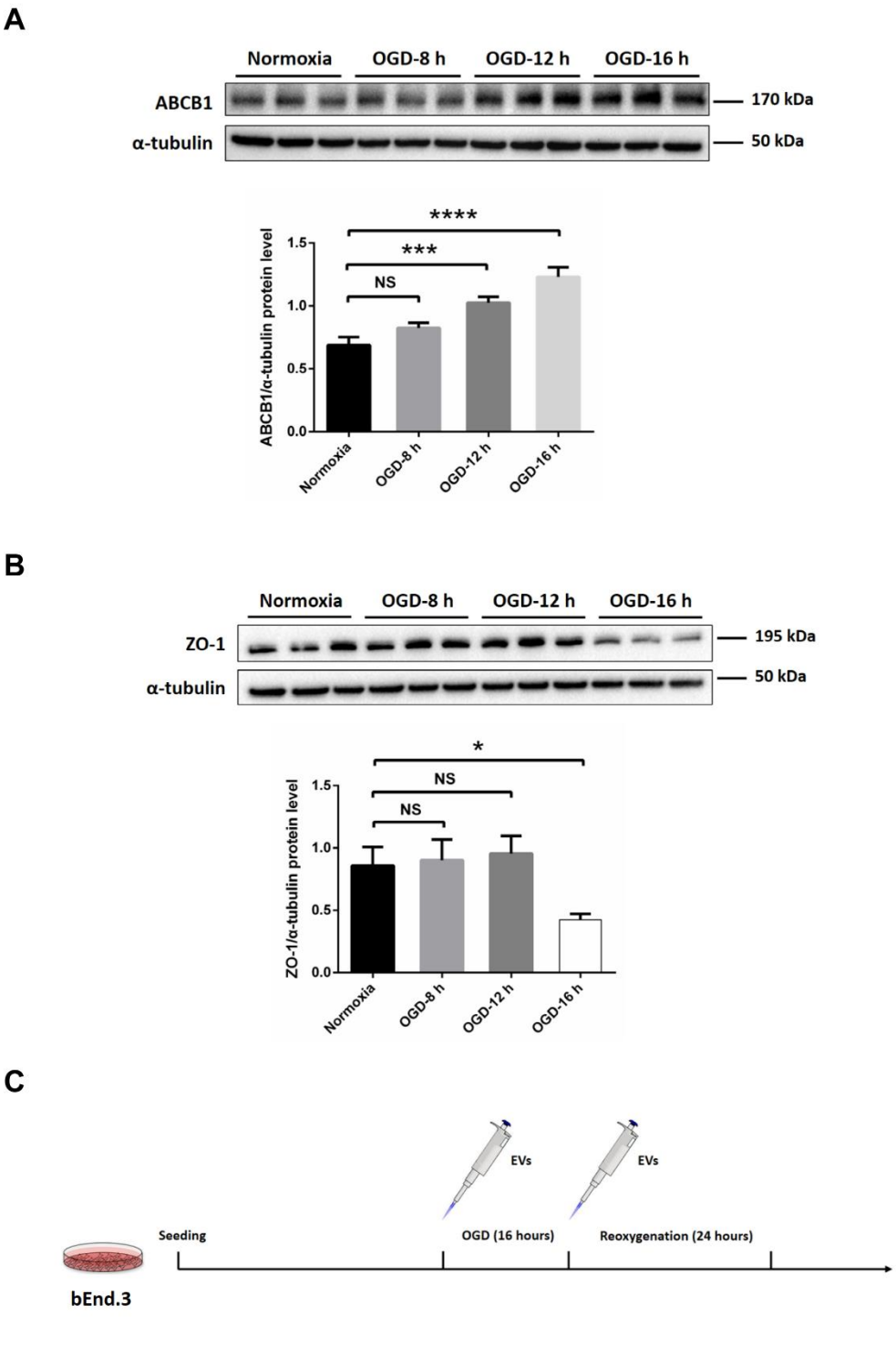

Figure 3: The regulation of ABCB1 and ZO-1 in an *in vitro* hypoxia model. (A-B) Quantitative analysis of ABCB1 and ZO-1 expression under normoxia control, oxygen-glucose deprivation (OGD) for 8, 12, and 16 h by Western blotting normalized to the housekeeping protein α-tubulin in bEnd.3 endothelial cells (n=3; **** $p< 0.0001$, *** $p<0.001$, NS = no significance; ANOVA with Dunnett's multiple comparisons test). (C) Experimental paradigm summarizing the *in vitro* OGD/RO hypoxia model in bEnd.3 cells with 16 h-OGD exposure followed by 24 h-RO and EV treatment during OGD and RO periods. Abbreviations: OGD, oxygen-glucose deprivation; RO, reoxygenation.

2.5 Establishment and functional examination of the BBB co-culture model

To evaluate the effects of EVs on BBB properties including TER, permeability, and transport activity, I established a valid *in vitro* BBB model. Indeed, multiple *in vitro* models of the BBB have been developed, including monolayer, co-culture, triple-culture and even dynamic 3D models (Helms et al. 2016; Miranda-Azpiazu et al. 2018; Naik and Cucullo 2012; Wang JD et al. 2016). Due to different cell types and their combination being key elements for functional BBB models, I compared several different strategies, e.g., monolayer vs. co-culture and cell lines vs. primary cells. Herein, a co-culture BBB system that consisted of primary ECs and primary astrocytes was finally chosen for the remainder of the study.

Briefly, ECs were seeded on a microporous membrane in the upper compartment, whereas astrocytes were put in the bottom compartment, representing the luminal and abluminal sides of the BBB, respectively. According to the timeline in Figure 4.A, the isolation and purification of primary astrocytes were done first, followed by seeding onto Poly-D-lysine (PDL)-coated 24-well plates of the cellZscopeE instrument (nanoAnalytics, Münster, Germany). Three days after seeding of astrocytes, ECs grown on Collagen IV-coated inserts (0.4 μm pore diameter, translucent, Greiner Bio-One GmbH, Frickenhausen, Germany) and primary astrocytes composed the co-culture system (Figure 4.B-C.). Puromycin was added to the full medium during these 2 days in order to remove non-endothelial cells. After the start of the experiment, TER values of the barrier were measured automatically every single hour under different treatment paradigms employing impedance measurement (Kuzmanov et al. 2016; Maherally et al. 2018). The latter was paused during the OGD treatment period itself. As described before, the bEnd.3 cells were exposed to OGD for 16 h in the hypoxia model, whereas the co-culture systems were treated with 24 h of OGD as primary cells possessed robust tolerance. For the *in vitro* experiments, EV treatment was performed during the OGD/RO period.

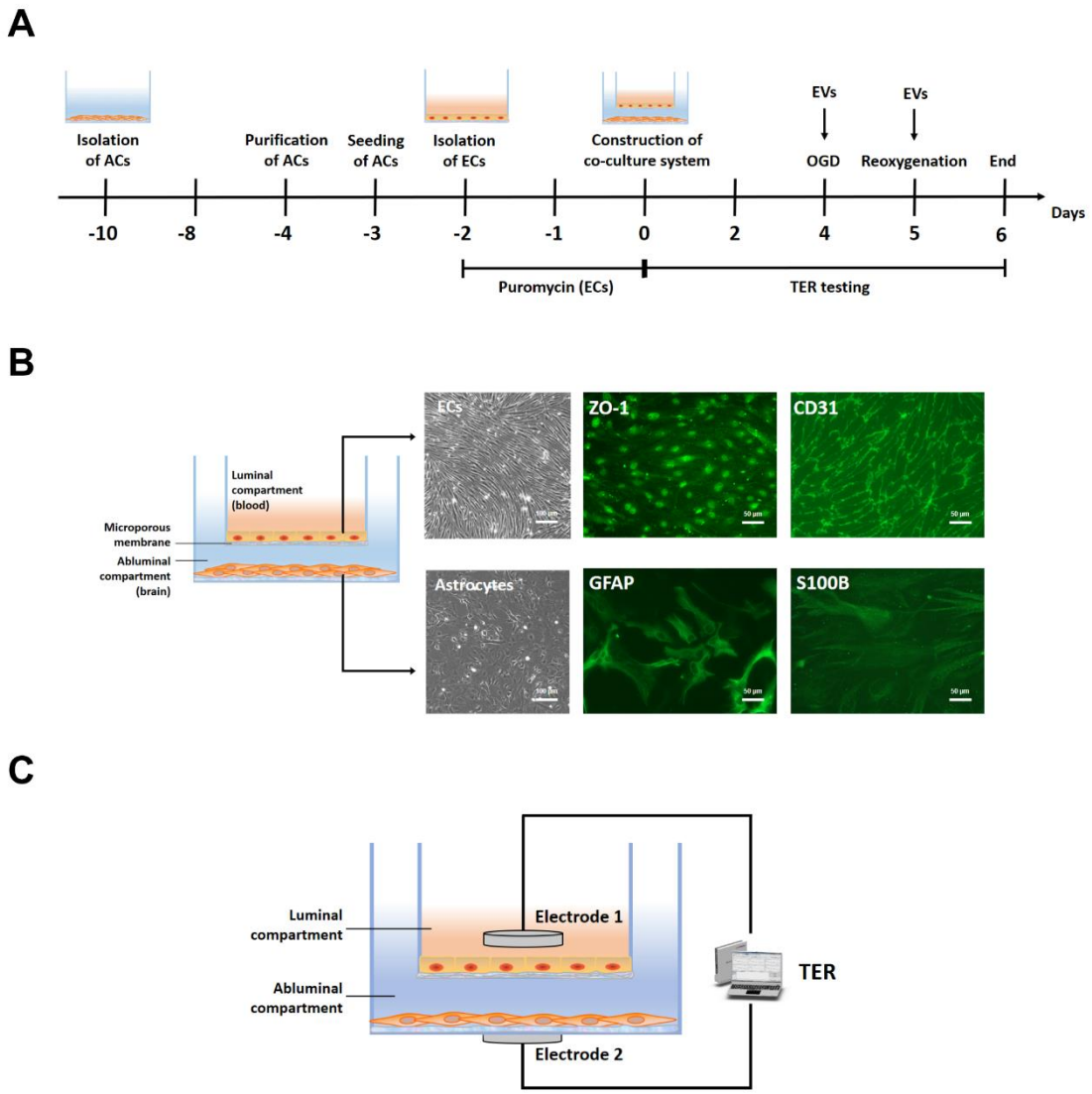

Figure 4: Construction of a BBB co-culture model. (A) Experimental paradigm summarizing the *in vitro* blood-brain barrier (BBB) co-culture model. (B) *In vitro*, the BBB co-culture model consisted of primary endothelial cells (ECs) on a transwell insert with a microporous membrane and astrocytes (ACs) on the other side. Phase-contrast images of ECs and astrocytes under brightfield microscopy are shown. Immunofluorescence staining of their specific markers ZO-1 and CD31 (ECs) as well as GFAP and S100B (ACs) are depicted separately. (C) Electrical circuit diagram on transcellular electrical resistance (TER) recording in the BBB co-culture model with the cellZscopeE apparatus. Abbreviations: BBB, blood-brain barrier; ECs, endothelial cells; ACs, astrocytes; ZO-1, zonula occludens-1; CD31, cluster of differentiation 31; GFAP, glial fibrillary acidic protein; S100B, S100 calcium-binding protein B; TER, transcellular electrical resistance (Zhang et al. 2021).

To examine the paracellular movement of the co-culture BBB model, I performed a barrier functional permeability assay. The flux of different-sized molecules including Lucifer Yellow (LY) and Evans blue-albumin (EBA) across the EC layers of the *in vitro* BBB model was measured as previously described (Takata et al. 2013). Details on the procedures of the permeability assay and the calculation of the permeability coefficient P_{cells} are found in

Supplement Publication 1 Materials and Methods (Zhang et al. 2021). As the target transcellular transporter, ABCB1 activity was determined by measuring the intracellular accumulation of rhodamine 123 (R123), a substrate of the ABCB1 transporter, in bEnd.3 cells or primary ECs in different groups using a previously published protocol with slight modifications (Takata et al. 2013; Watson et al. 2013; Yang S et al. 2018). Since the fluorescent R123 was pumped out via ABCB1 transporter, the accumulation of remained R123 in ECs can in turn indicate the activity of the ABCB1 transporter. The R123 accumulation level was normalized to the protein concentration within the ECs. The details of the R123 accumulation assay can be found in Supplement Publication 1 Materials and Methods (Zhang et al. 2021).

2.6 Middle cerebral artery occlusion (MCAO) model and the *in vivo* experimental paradigm

The induction of transient focal cerebral ischemia in male C57BL/6J mice aged 10 weeks (Janvier Labs, Le Genest-Saint-Isle, France) was performed using the MCAO model. Only male mice were studied in order to avoid the interference of the hormonal disturbances of female mice after MCAO surgery. The details about the procedures of MCAO surgery are described in Supplement Publication 1 Materials and Methods. The mice were induced to ischemia followed by delivery of either the PBS vehicle or EVs (from equivalent 2 x 10^5 NPCs, 10 μg/200 μL) through femoral vein injections at the onset of reperfusion and at 6 h post-MCAO. This optimal EV concentration *in vivo* was chosen according to previous studies from our group (Zheng X et al. 2020). In the sham group, the same procedure was performed except for the insertion of the filament into the middle cerebral artery. The animals in the MCAO control groups were given the vehicle administration at the same time points. All mice were sacrificed at 24 h after MCAO surgery, and brain samples were prepared for Western blotting and immunofluorescence staining. The timeline of the *in vivo* experimental paradigm including MCAO surgery, two EV injections, and single Evans blue injection is shown in Figure 5**.**

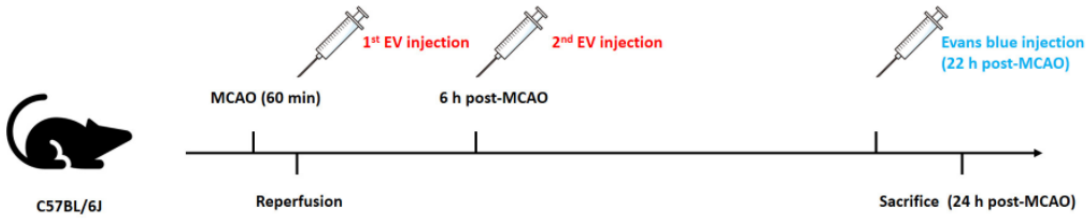

Figure 5: The timeline of *in vivo* experiments. The *in vivo* experimental paradigm including middle cerebral artery occlusion (MCAO), EV treatment, and Evans blue injection.

2.7 *In vivo* BBB functional analysis

The BBB integrity *in vivo* was investigated by the Evans blue extravasation assay (Radu and Chernoff 2013). Briefly, 100 μL of 2 % Evans Blue dye solution in PBS (Sigma-Aldrich,

Darmstadt, Germany) was injected via the femoral vein 2 h before sacrifice. Subsequently, the mice were sacrificed followed by transcardial perfusion with PBS. The Evans Blue dye was extracted with 2 mL of 50 % trichloroacetic acid from the ischemic hemispheres, and the absorbance at 620 nm wavelength of each group (sham, MCAO control, and MCAO with EV infusion) was measured. The Evans Blue concentration was calculated by using a standard curve (2.5 to 500 ng/mL). Evans Blue extravasation from the ischemic hemispheres of each group was evaluated, which is stated as (μg) Evans Blue per (g) tissue.

Beside analyzing the expression of ABCB1 and MMP-9 by using Western blotting, the activity of the MMPs was measured by gelatin zymography as previously described (Hu and Beeton 2010; Zhang JW and Gottschall 1997). After centrifugation of the supernatant obtained from lysed hemispheres, the purified samples were preserved in lysis buffer containing 10 % DMSO. Thereafter, equal amounts of samples were prepared with a non-reducing loading buffer and loaded on 8 % polyacrylamide gel containing 0.1 % gelatin. Electrophoresis was performed for 20 min at 60 V and then for 1.5 h at 125 V. The gel was incubated in a renaturing buffer under gentle agitation for 30 min followed by 48 h of incubation with a developing buffer at 37 °C. Thereafter, the gel was stained with 0.1 % Coomassie Blue solution for 30 min. After destaining, a white band remained behind a dark blue background. The gels were then scanned and densitometrically analyzed. The density of the white band indicated the amount of MMPs in the samples from hemispheres which can decomposite the remained gelatin in the gel. The details of the procedures are described in Supplement Publication 1 Materials and Methods (Zhang et al. 2021).

2.8 Flow cytometry analysis of immune cells in ischemic hemispheres

Since EVs induce BBB protection in the early postischemic brain as shown before, I aimed to investigate whether or not EVs had an impact on very early immune cell recruitment in the postischemic brain. Therefore, the infiltrating immune cells of ischemic hemispheres including leukocytes and their subsets (neutrophils, T-cells, B-cells, monocytes, and macrophages) were analyzed by flow cytometry analysis with a fluorescence-activated cell sorter (Posel et al. 2016) (Figure 6.). Briefly, 24 h after MCAO, the ischemic hemispheres were homogenized in a lysis buffer and centrifuged at 1,600 rpm for 10 min. The pellets were resuspended in a 30 % Percoll solution followed by loading on the Percoll gradients (45 % and 70 % Percoll solution). After centrifugation, the immune cell phases were aspirated and solved in a working solution. Thereafter, the cells of each group were incubated with anti-CD3, anti-CD45, anti-Ly6G, anti-Ly6C, anti-CD19, and anti-CD11b antibodies overnight. The gating and measurements were analyzed with the software FlowJo v. 10.5.3 (BD FACSDiva).

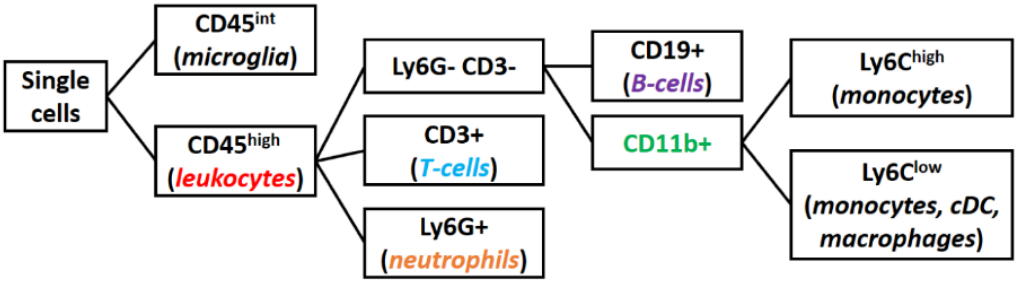

Figure 6: Gating strategy for flow cytometry analysis. The subsets of leukocytes ($CD45^{high}$), T-cells ($CD45^{high}CD3+$), neutrophils ($CD45^{high}Ly6G+$), B-cells ($CD45^{high}CD3\text{-}Ly6G\text{-}CD19+$), macrophages and monocytes ($CD45^{high}CD3\text{-}Ly6G\text{-}CD11b+$) and $Ly6C^{high}$ monocytes ($CD45^{high}CD3\text{-}Ly6G\text{-}CD11b+Ly6C^{high}$) were analyzed by a fluorescence-activated cell sorter.

2.9 Statistical analysis

Results are shown as means ± SD. All data were normally distributed as indicated by the Kolmogorov-Smirnov test. Accordingly, parametric tests were employed. In order to compare two groups, the two-tailed independent Student's t-test was used. The statistical significance of differences between several groups was assessed by a one-way analysis of variance (ANOVA) and a two-way analysis of variance (ANOVA) for factorial comparisons and by Dunnett, Bonferroni or Tukey-Kramer's test for multiple comparisons. A p-value of less than 0.05 was considered to be significantly different. Statistical analysis was obtained using GraphPad Prism 6.0 (GraphPad, CA, USA).

3 Results and Discussion

3.1 Isolation and characterization of NPC-EVs

Previous research from our group showed that transplanted NPCs induce acute postischemic neuroprotection by stabilizing the BBB (Doeppner et al. 2014). Since adult stem cells like NPCs and others mediate their biological effect by secreting EVs, the latter have been reported to enhance neuroregeneration, neurological recovery and to modulate neuroinflammation after stroke (Anderson et al. 2016; Dabrowska et al. 2019; Webb et al. 2018; Zheng X et al. 2020). EVs are a miscellaneous group of lipid bilayer structures that are secreted from virtually all cells, with a diameter between 30-1000 nm (Thery et al. 2018). In the present project, after enriching NPC-EVs by using two well-established methods, i.e., UC and PEG methods, the characterization of such NPC-EVs included Western blot analysis of EV biomarkers, TEM, and NTA according to the ISEV guidelines. Although PEG is often used for the enrichment of EVs, it is considered to yield highly contaminated samples, since it forms a web-like structure in which EVs are trapped. During this process, some co-precipitate organelles and soluble macromolecules of protein may also be precipitated in this process (Ingham 1984; Zhang X et al. 2020). Hence, I compared the PEG method to UC only method, which is still the gold standard for EV enrichment procedures (Thery et al. 2018). Both UC and PEG methods revealed the presence of common EV biomarkers such as Alix, Tsg101, CD63, CD9, and CD81 compared to NPC cell lysate groups (Supplement Publication 1 Figure 2.A.). The TEM analysis suggested that there were no significant morphological differences between UC-EVs and PEG-EVs, with both samples containing smaller and larger vesicles (Supplement Publication 1 Figure 2.B.). NPC-EVs were further quantified and examined in size by using NTA, which displayed an EV-like spectrum in both groups; the most frequently found NPC-EV size was at around 50-150 nm in both groups (Supplement Publication 1 Figure 2.C.). According to these results, I found no statistical difference between these two enriched methods. Therefore, these data provide evidence that the PEG method used in the present experimental paradigm is not inferior to the UC method with regard to sample purity. Given that the PEG method is even faster and improves the efficiency of enriched EVs, I applied the PEG method to collect NPC-EVs for the subsequent study. In parallel, a proteomic analysis on PEG enriched EVs was performed, confirming the presence of the aforementioned EV markers, showing that negative markers (UMOD, APOA1, etc.) were not observed in NPC-EV samples (Supplement Data I).

To further discriminate EVs from non-EV nanoparticles and soluble proteins, I applied an iodixanol gradient centrifugation to subfractionate EVs (Supplement Publication 1 Figure 2.D.). Ten fractions (F1-F10) were recovered and analyzed for the presence of the protein markers Alix, CD63, CD81, Tsg101, and CD9. As shown in the representative Western blots, the EV samples were located mostly in fractions F4 and F5 (1.134-1.149 g/mL). Consistently, protein concentrations indicated an overwhelming majority of protein enriched in the fractions F4 and F5 (Supplement Publication 1 Figure 2.E.). These two fractions were then further quantified

and evaluated for size by NTA, which suggests a quite similar size distribution of these vesicles (Supplement Publication 1 Figure 2.F.). Thereafter, the effect of the fractions F4-F6 on the expression of ABCB1 was studied after OGD/RO treatment. As shown in Supplement Publication 1 Figure 2.G., EVs from F4 and F5 reversed the OGD/RO-induced increase of ABCB1, whereas the samples from F6 did not show this effect. Given the aforementioned similar characterization between F4 and F5 fractions, I collected and pooled fractions F4 and F5 as purified EVs for further experiments.

Since the optimal EV concentration for regulating both ABCB1 and MMP-9 expression patterns were not known, dose-effect experiments were performed using three different NPC-EV concentrations (0.1, 1, and 10 μg/mL of the culture medium or BSS0 solution). Our results show a significantly decreased expression level of ABCB1 and MMP-9 in above three EV concentrations post-OGD. There was no significant difference in the aforementioned effect between the two higher dosages (1 and 10 μg/mL). Thus, for the optimal EV concentration to be used in the *in vitro* experiments, EVs were diluted to $2x10^4$ cell equivalents per milliliter (1 μg/mL) in cell culture medium or BSS0 solution (Figure 7.A-B.).

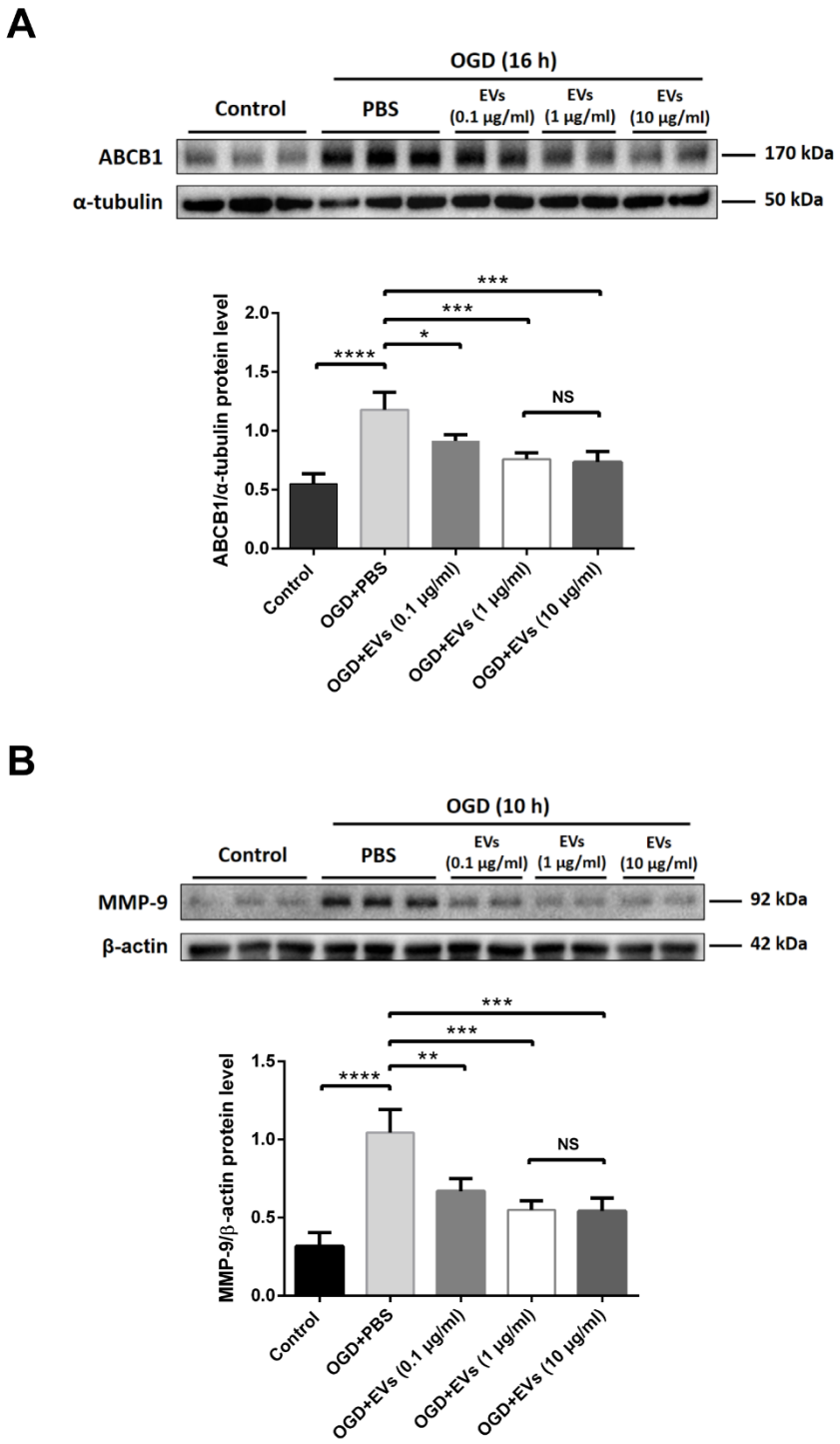

Figure 7: The optimal EV concentration in the *in vitro* experiments. (A) Quantitative analysis of ABCB1 expression under normoxia control and OGD 16 h conditions, using Western blotting normalized to the housekeeping protein α-tubulin in ECs. Within the OGD groups, I tested four different treatment groups (PBS, 0.1, 1, and 10 µg/mL EVs) (n=4). (B) Quantitative analysis of MMP-9 expression of conditioned medium from astrocytes under normoxia control and exposed to OGD 10 h using Western blotting normalized to the housekeeping protein β-actin in astrocytes. Within the OGD groups, I defined the aforementioned groups (PBS, 0.1, 1, and 10 µg/mL EVs) (n=4; **** $p<0.0001$, *** $p<0.001$, ** $p<0.01$, * $p<0.05$, NS = no significance; ANOVA with Dunnett's multiple comparisons test). Abbreviations: OGD, oxygen-glucose deprivation; ECs, endothelial cells; EVs, extracellular vesicles; MMP-9, matrix metalloproteinase-9.

3.2 NPC-EVs suppress OGD/RO-induced upregulation of ABCB1 via inhibiting the NF-κB pathway

Accumulating evidence suggests that early BBB protection promotes neurological recovery in stroke models involving various mechanisms such as immunomodulation (Li Y et al. 2018; Planas 2018; Yang C. et al. 2019). Ischemic stroke changes the microenvironment including oxidative stress, chemokines, and modulation of ECs and astrocytes, which subsequently deteriorates BBB integrity and recruits more immune cells into the brain parenchyma, exacerbating tissue injury (Chamorro et al. 2012; Kamel and Iadecola 2012; Renu et al. 2015; Santos Samary et al. 2016). Meanwhile not only stem cell transplantation, but also the administration of EVs derived from stem cells have been confirmed as potential therapeutic tools against stroke in preclinical studies (Bang and Kim 2019; Moon et al. 2019; Webb et al. 2018; Zheng H et al. 2018; Zheng X et al. 2020). Importantly, our previous studies highlighted that the stabilization of the BBB plays a key role in acute neuroprotection after NPC transplantation in animal stroke models (Doeppner et al. 2011; Doeppner et al. 2014; Doeppner et al. 2015). It is still not fully resolved whether or not the beneficial effects described before on NPC-EVs will hold true compared to NPCs themselves. Hence, it is still elusive, if NPC-EVs are feasible for being a general therapeutic concept in protecting BBB integrity after stroke.

Herein, OGD/RO of ECs triggered a cascade including increased ABCB1 levels, diminished ZO-1 abundance, and an activated NF-κB pathway. Indeed, an activation of the NF-κB pathway is line with previous published work, describing that pathway to contribute to pronounced brain injury after cerebral ischemia (Ridder and Schwaninger 2009). Importantly, both the upregulation of ABCB1 and the activation of the NF-κB pathway were reversed by NPC-EV treatment, albeit the expression patterns of ZO-1 were not significantly affected by that measure (Supplement Publication 1 Figure 3.A-D.). Since OGD/RO triggers cytotoxicity and cell death, I next asked whether or not the regulation of ABCB1 in ECs was merely an indirect consequence of different cell survival rates due to EV treatment. Therefore, survival assays (MTT and LIVE/DEAD) were performed as shown in Supplement Publication 1 Figure 3.E-F. Exposure of ECs to OGD/RO resulted in a significantly increased cell death rate. However, incubation of ECs with EVs did not affect cell survival directly; there was no significant difference between controls and EV-treated cells in this respect. This finding supports the hypothesis that NPC-EVs regulate ABCB1 expression patterns under OGD/RO conditions independent from survival rates of cultured ECs.

Analyzing the NF-κB pathway related protein p65 abundance alone is not sufficient to properly study this signaling pathway. Hence, I next performed a translocation assay under OGD/RO conditions. As shown in the Western blot analysis and the immunofluorescence stainings (Supplement Publication 1 Figure 4.A-B.), OGD/RO-exposure resulted in a pronounced translocation of p65 from the cytoplasm towards the nucleus. On the contrary, incubation of ECs with EVs caused the retention of p65 in the cytoplasm, which further indicated that NPC-EVs suppressed the activation of the NF-κB pathway.

Several studies showed that ABCB1 was upregulated via NF-κB activation in cancer tissues, as well as other neurological diseases such as epilepsy, multiple sclerosis, and amyotrophic lateral sclerosis (Bauer et al. 2007; Katayama et al. 2014; Qosa et al. 2016). Nevertheless, this relationship is unclear in hypoxic ECs. Since OGD/RO-induced activation of the NF-κB pathway promoted p65 translocation and increased transcription of many genes under hypoxic/ischemic conditions (Ridder and Schwaninger 2009), I next elucidated if ABCB1 is a downstream target of the NF-κB pathway in hypoxic ECs. As such, I applied SN50, an NF-κB translocation inhibitor, and Valspodar, an ABCB1 inhibitor, in the OGD/RO system. Both SN50 and Valspodar significantly reduced ABCB1 protein levels in OGD/RO-exposed ECs, as is the case with EVs (Supplement Publication 1 Figure 4.C.). Neither SN50 nor Valspodar affected protein expression of p65 in hypoxic ECs in comparison to ECs treated with EVs (Supplement Publication 1 Figure 4.D.). Since SN50 inhibits only the translocation but not the total protein abundance of p65, the lack of effect of SN50 is in line with these findings (Osorio et al. 2015; Zhu et al. 2011). The latter was confirmed in a proof-of-concept experiment, showing that SN50 indeed inhibits the translocation of p65 in our hypoxia model (Figure 8.A.). Consistently, ABCB1 transporter activity in each treatment group was examined by rhodamine 123 (R123), a known ABCB1 substrate. The cellular accumulation of R123 depends on ABCB1 activity, which can actively transport R123 towards the extracellular compartment. As shown in Supplement Publication 1 Figure 4.E., EVs increased R123 accumulation in ECs by diminishing the ABCB1 transporter activity, which was similar to the SN50 and Valspodar groups. Hence, NPC-EVs regulate post-hypoxic expression patterns of ABCB1 indirectly through the inhibition of the NF-κB pathway.

In order to further back up the aforementioned observations, a second cell injury model was chosen where ECs were treated with the bacterial component lipopolysaccharide (LPS), which has been shown to activate the NF-κB pathway in another scientific context as well (Lee et al. 2017; Li M et al. 2018). To further study the effect of EVs inhibiting the NF-κB pathway in the LPS model, I applied different concentrations of LPS (200, 500, and 1000 ng/mL) to cultured ECs. As shown in Supplement Publication 1 Figure 3.G-H., both the expression of p65 and ABCB1 were increased dose-dependently by the LPS treatment compared to controls. Incubation of ECs with EVs significantly inhibited the LPS-induced (1000 ng/mL) elevation of p65 and ABCB1 (Supplement Publication 1 Figure 3.I-J.). Additionally, EVs also reversed the LPS-induced p65 nuclear translocation, which was similar to the SN50 group (Figure 8.B.). Thus, the impact of NPC-EVs on ABCB1 and NF-κB in ECs is not only restricted to OGD conditions, but can also be found after LPS treatment.

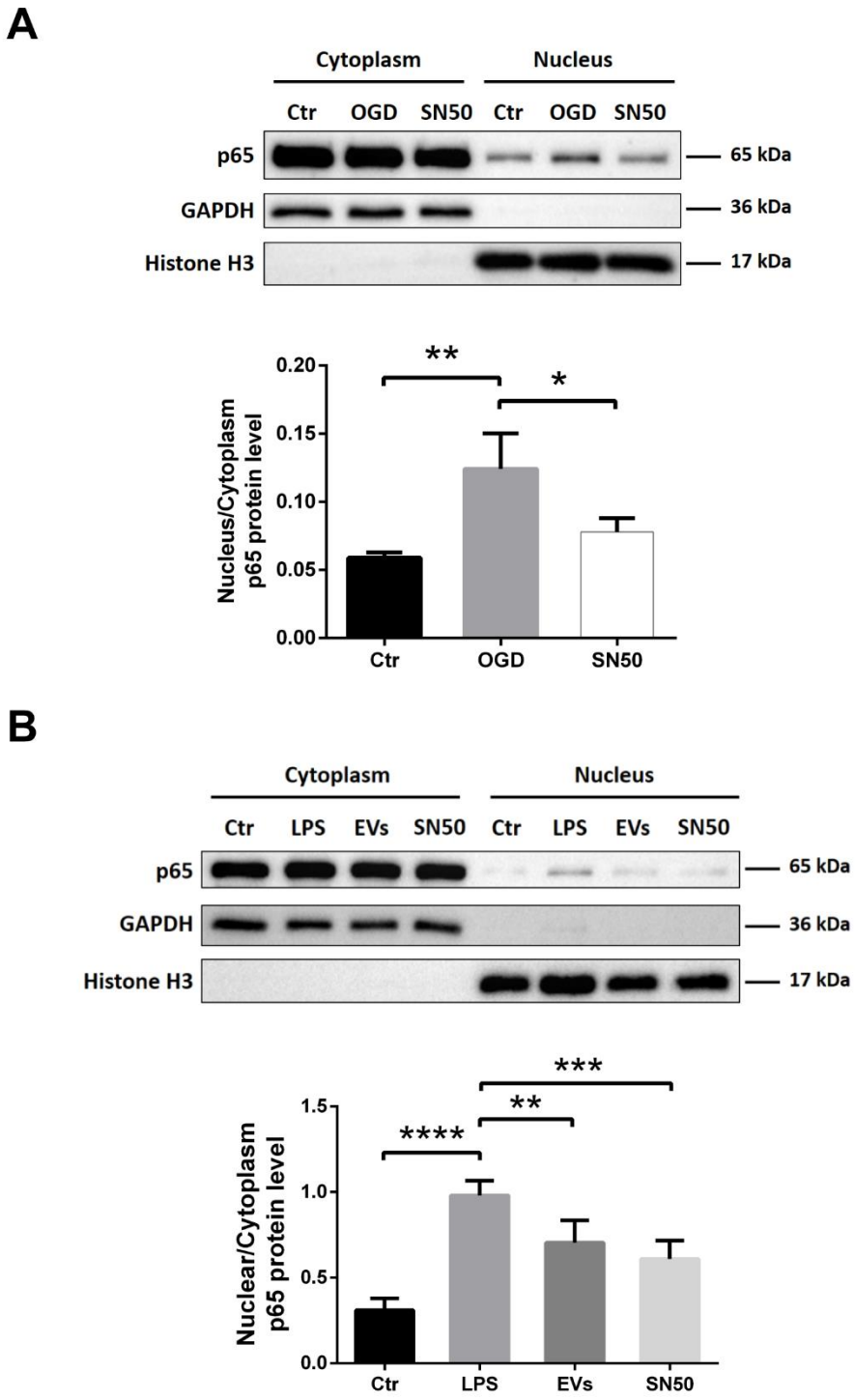

Figure 8: EV effect on the NF-ϰB-related protein p65 nuclear translocation in the LPS model. (A) Quantitative analysis of p65 expression in cytoplasm and nucleus fractions of bEnd.3 cells under normoxia control, OGD and OGD treated with SN50 groups using Western blotting normalized to the housekeeping proteins GAPDH in the cytoplasm fractions and Histone H3 in the nucleus fractions (n=3). Data are expressed as mean ± SD, *p<0.05, **p<0.01; ANOVA with Dunnett's multiple comparisons test. (B) Quantitative analysis of p65 expression in cytoplasmic and nuclear fractions in bEnd.3 cells under control conditions, LPS conditions (1000 ng/mL), LPS-treated with EVs or SN50 using Western blotting normalized to the housekeeping proteins GAPDH in cytoplasm fractions and Histone H3 in the nucleus fractions (n=3). Data are expressed as mean ± SD, *p<0.05, **p<0.01; ANOVA with Dunnett's multiple comparisons test. Abbreviations: EVs, extracellular vesicles; OGD, oxygen-glucose deprivation; LPS, lipopolysaccharide.

Although the precise mechanisms underlying the effect on the NF-κB pathway are not yet completely known, it is likely that EVs transfer cargo including miRNAs or proteins to the respective target cells. Evidence from MSC-EV studies suggest that EVs play a role in immunosuppression. MiRNAs (e.g., miR-146a, miR-182, miR-223 and others) enriched in MSC-EVs can inhibit TLR (toll-like receptor) signaling, which in turn suppresses the NF-κB pathway (Curtale et al. 2019; O'Neill et al. 2011; Qin et al. 2018). Likewise, EVs containing the membrane receptor chemokine (C-C motif) receptor 2 (CCR2) can block CCL2-induced activation of NF-κB signaling pathway (Shen et al. 2016). Some studies also report that EV treatment reduces TNF-α and IL-6, whereas it increases IL-10 and thus subsequently prevents the activation of the NF-κB pathway (Martin-Rufino et al. 2019; Su et al. 2019).

In addition, the proteomic analysis of NPC-EVs as given in Supplement Data I revealed high expression levels of distinct protein candidates such as HSP70 related proteins enriched in NPC-EVs, which might be the biological mediators for the suppression of the NF-κB pathway (Sharp et al. 2013). The HSP70 related proteins are well known to be involved in a plethora of signaling cascades, among which are pathways that help modulate inflammation under hypoxic/ischemic conditions (Giffard and Yenari 2004; Jiang et al. 2020; Wang Y et al. 2005). Under *in vivo* conditions, for instance, HSP70 increases cell viability and improves nervous system recovery by modifying oxidative stress and proteasome activity in brain tissue after ischemic injury (Doeppner et al. 2013; Doeppner et al. 2017). Thus, the inhibition of the NF-κB pathway after OGD/RO injury and treatment with NPC-EVs in bEnd.3 ECs as described in this study, might also be in part HSP70-dependent. These speculations on the regulation of the NF-κB pathway require additional investigation in the future. Collectively, it suggests that EVs may have an impact on the suppression of the NF-κB pathway, possibly via their enriched miRNAs and heat-shock-proteins.

3.3 NPC-EVs regulate the properties of the BBB in a hypoxia co-culture model

To further assess the effect of EVs on the functional properties of the BBB including transcellular electrical resistance, paracellular permeability, and ABCB1 transporter activity, I employed an *in vitro* BBB co-culture model using primary ECs and astrocytes. The isolation, culture, and purification of ECs and astrocytes as well as the construction of the co-culture system are depicted in Figure 4.A. As shown in Figure 4.B., ECs and astrocytes were seeded in the upper and lower chamber, representing the luminal and the abluminal sides of the BBB, respectively. Immunocytochemistry staining was obtained using specific markers to confirm the cell lineage, i.e., ECs (ZO-1, CD31) and astrocytes (GFAP, S100B). Co-culturing of both ECs and astrocytes did not change their biological properties, i.e., both cell types were able to take up EVs under these conditions (Supplement Publication 1 Figure 5.C-D.).

For the detection of the transcellular electrical resistance (TER), the data were recorded every single hour using an automatic cellZscopeE apparatus. As shown in Figure 9.A., TER values

reflected the real-time change of the biological conditions of the BBB in our co-culture system, providing an effective model to mimic BBB disruption. The optimal TER value was reached at 120-180 h in the co-culture system, with values peaking to 14-17 $\Omega \cdot cm^2$ at 120 h. Thereafter, the system was exposed to OGD for 24 h and disconnected from the controller during this period. The recording was restarted after OGD, and the value of each well was reduced to around 50 % of the plateau value at the onset of the RO period (Figure 9.B.). Values for each well and time point were saved and analyzed between groups. However, EV treatment did not significantly rescue TER values after induction of OGD in the BBB co-culture model (Supplement Publication 1 Figure 5.E.).

The permeability studies of the molecules with different molecular weights like Lucifer Yellow (LY, 457.25 Da) and Evans blue-albumin (EBA, 67,000 Da) were performed on inserts after 24 h of RO. The permeability data were plotted as the total number of volumes transported over time in each well. The permeability coefficient P_{cells} analysis for both LY and EBA suggested that EV treatment significantly reduced the BBB permeability in the co-culture system (Supplement Publication 1 Figure 5.F-G.). The representative pictures of the transferred solution on the abluminal side were recorded in OGD and OGD treated with EV groups with an Evans Blue standard curve (Figure 9.C.).

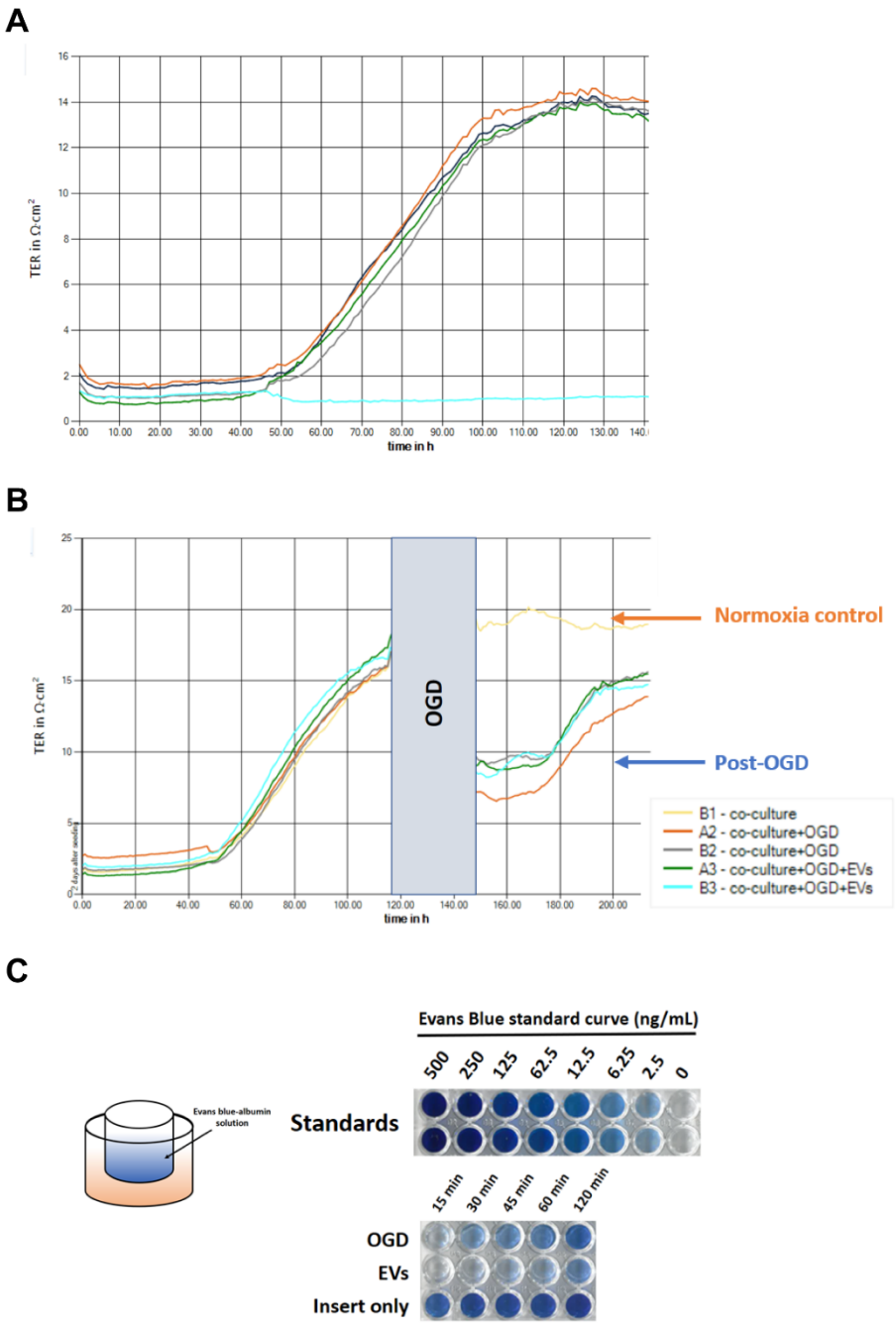

Figure 9: TER testing and permeability assay in the BBB co-culture system. (A) At 45 h after seeding of primary endothelial cells on the transwell inserts, the transcellular electrical resistance (TER) values of 4 wells started to increase from 1 Ω·cm² to 14 Ω·cm² at about 125 h, whereas the TER values of the well without endothelial cells stayed unchanged at about 1 Ω·cm² all the time. (B) When the TER values reached a plateau, the co-culture systems (A2, B2, A3 and B3) were exposed to 24 h of oxygen-glucose deprivation (OGD) compared to the normoxia control group (B1 well, yellow). Two wells (A3, B3) were treated with extracellular vesicles (EVs). The TER values were continuously recorded for 24 hours. (C) In the Evans blue-albumin (EBA) permeability assay, I added EBA solution to the upper well and collected the permeability buffer from the bottom well after 15 min, 30 min, 45 min, 60 min, and 120 min. Then, the transferred speed of each well was calculated to evaluate the permeability of the barrier in OGD and OGD treated with EV groups after normalization to an Evans Blue standard curve (2.5 to 500 ng/mL). For further information, please refer to the materials and methods parts as well as to the result section of **Publication 1**. Abbreviations: TER, transcellular electrical resistance; EVs, extracellular vesicles; OGD, oxygen-glucose deprivation; EBA, Evans blue-albumin.

ECs forming the BBB consist of luminal and abluminal membrane domains. Intercellular tight junction proteins greatly limit both paracellular and transcellular movement of molecules through the EC layer (Luissint et al. 2012; Sandoval and Witt 2008). Regulated bidirectional transport of drugs and metabolites is, however, guaranteed by specific transporters such as ABCB1. ABCB1 knockdown models or pharmacological inhibition of the transporter itself result in reduced brain injury under *in vivo* stroke conditions (Murozono et al. 2009; Spudich et al. 2006). In line with this, neuroinflammation may also increase levels of ABCB1, being associated with exacerbated brain injury (Bauer et al. 2007; Kooij et al. 2009; Kooij et al. 2011). In this context, I aimed to investigate if EVs may also have an impact on modulating ABCB1 expression patterns in hypoxia BBB models. Thus, the ABCB1 transporter activity of ECs was detected by using the aforementioned R123 accumulation assay. As shown in Supplement Publication 1 Figure 5.H., EV treatment significantly reduced the ABCB1 transporter activity on ECs after induction of OGD/RO. EVs not only mitigate the OGD/RO-induced upregulation of ABCB1, but also repress its function and activity.

As shown above, EV treatment did not significantly induce an effect on TER measurement and ZO-1 protein abundance, whereas the permeability of both large and small molecules (EBA, LY) was abolished in the EV groups. Indeed, the TER value is dependent on tight junction proteins between adjacent ECs. Beside tight junction proteins, however, the BBB permeability also—and even more so—relies upon the endothelial basal membrane (Almutairi et al. 2016; Weber 2012). Combining our aforementioned result that EVs did not significantly influence the expression of ZO-1, I postulate that EVs regulate BBB permeability by preventing the degradation of the basal membrane, rather than enhancing tight junction protein patterns in the BBB hypoxia model.

3.4 NPC-EV administration mitigates the MCAO-induced upregulation of ABCB1 and MMP-9 as well as the activation of the NF-κB pathway

To analyze the role of EVs on the regulation of ABCB1 and the NF-κB pathway in ischemic stroke, I studied ABCB1 and p65 expression of ischemic microvessels in mice exposed to 60 min of transient brain ischemia. In the mouse MCAO model, EVs were delivered via femoral vein at the onset and at 6 h after reperfusion. Based on the aforementioned *in vitro* data, systemic injection of NPC-EVs via cannulation of the femoral vein is likely to yield an uptake of DiI labeled EVs by ECs, followed by crossing the basal membrane, entering the end-feet of astrocytes, and reaching the cerebral parenchyma outside of microvessels (Supplement Publication 1 Figure 6.A.). Immunohistochemical stainings of cerebral microvessels and astrocytes located within the infarct core revealed CD31-positive and GFAP-positive cells to be co-localized with DiI-labeled EVs (Supplement Publication 1 Figure 6.B.). Western blot analysis using enriched fractions of brain microvessels of ischemic hemispheres revealed that both ABCB1 and p65 protein levels were increased at 24 h poststroke. These stroke-induced

upregulations were inhibited by EV administration. No significant differences were revealed in the contralateral brain samples (Supplement Publication 1 Figure 6.C-D.). As such, EV infusion significantly inhibited MCAO-induced ABCB1 upregulation and NF-κB activation in the ischemic hemisphere microvessels, which is in accordance with our *in vitro* results.

Additional experiments were conducted to evaluate the effect of EVs on BBB stability *in vivo*. As mentioned before, the induction of cerebral ischemia activates a great number of signaling cascades, among which is the activation of MMP-9 followed by the degradation of the basal lamina, thus facilitating BBB breakdown (Rempe et al. 2016). Whereas within the first hours after stroke onset both MMP-2 and MMP-9 are responsible for BBB impairment, severe disruption of the BBB between poststroke 24-48 h is primarily associated with the activation of MMP-9 only (Fujimura et al. 1999; Park et al. 2009; Suofu et al. 2012). In accordance with these findings, our study shows an extensive upregulation of MMP-9 within the ischemic hemisphere after 24 h, whereas MMP-2 remained at its basal level at that time point. As the present findings suggest that EVs may prevent poststroke degradation of the basal membrane, additional evidence is in favor of MMPs being involved in remodeling of the basal membrane after stroke (Yang Y and Rosenberg 2015). Using Western blotting, zymography and immunofluorescence staining, it could show that EV administration downregulated both the protein level and the activity of MMP-9 compared to the MCAO control groups. However, no significant difference in MMP-2 activities was observed when compared to the sham or the MCAO group, indicating different sensitivity of MMPs to ischemic insult (Supplement Publication 1 Figure 6.E-G.). Interestingly, MMP-9 is known to be modulated by the NF-κB pathway under stroke conditions (Lv et al. 2019; Wang Z et al. 2011), and previous research of ours demonstrated that transplanted NPCs induce postischemic neuroprotection by inhibiting this pathway (Doeppner et al. 2013). Likewise, additional research from oncology and non-stroke related neurologic diseases found an interesting connection between ABCB1 and the NF-κB pathway (Bauer et al. 2007; Katayama et al. 2014; Qosa et al. 2016; Wang Z et al. 2011; Yu et al. 2008; Zhang J et al. 2014), albeit this relationship has not been described for ECs. The NF-κB pathway, therefore, appears to be an interesting target of EVs under stroke conditions.

The Evans Blue extravasation assay was employed to assess the poststroke BBB integrity after ischemia. Evans Blue combined to the albumin in blood can infiltrate into the brain parenchyma from the BBB disruption area, which was analyzed 24 h after MCAO. The result suggested that MCAO exposure significantly increased the Evans Blue extravasation in the brain tissue compared to the sham group. Noteworthy, the Evans Blue concentration of the ischemic hemispheres in the EV treatment group was significantly lower than in the MCAO control group, representing an enhanced poststroke BBB integrity in light of EV infusion (Supplement Publication 1 Figure 6.H.). Herein, EVs enhance the BBB stability as suggested by reduced Evans blue leakage and by mitigated MMP-9 activation in the mouse stroke model.

3.5 NPC-EV administration suppresses early immune cell recruitment in the postischemic brain

As mentioned previously, the cellular immune response is a critical element in the pathophysiology of ischemic stroke, and is it closely associated with BBB impairment. Ischemic stroke initiates BBB disruption, which allows the release of abundant chemokines and increases the expression of endothelial adhesion molecules, facilitating the migration of circulating immune cells towards the ischemic brain parenchyma. Brain-infiltrating leukocytes are responsible for secondary ischemic injury in the early course of stroke, triggering a sustained inflammatory response in the ischemic hemisphere (Courties et al. 2015; Iadecola und Anrather 2011; Posel et al. 2016).

In agreement with the enhanced BBB integrity after EV infusion, I found a dramatically decreased early recruitment of total leukocytes. I further compared the subset composition of these infiltrated leukocytes. In the MCAO groups, increased neutrophils, monocytes, and macrophages were recruited into the infarct area, whereas levels of T-cells and B-cells were decreased. Interestingly, I found that EV treatment reversed these changes, except for the subset of neutrophils (Supplement Publication 1 Figure 7.). Representative flow cytometry measurements of the ischemic hemispheres in the aforementioned groups are shown in Figure 10. Noteworthy, emerging evidence suggests that a large number of monocytes, especially Ly6C^{high} monocytes, are recruited to the injured brain producing pro-inflammatory cytokines that contribute to the early functional impairment after stroke (ElAli and Jean LeBlanc 2016; Hammond et al. 2014). In addition, a plethora of studies claim a role of regulatory T-cells for secreting cytokines like IL-10 and TGF-β, yielding anti-inflammatory actions under conditions of cerebral ischemia (Chamorro et al. 2012; Liesz et al. 2009; Sakaguchi et al. 2008). Hence, our data suggest a role of EVs in mediating the infiltration of Ly6C^{high} monocytes and regulatory T cells to involve the early damage-repairing and remodeling in the ischemic brain. Present data suggests that ABCB1 in ECs is likely to participate in the transport of pro-inflammatory/chemotactic factors into the extracellular space to modulate the subsequent inflammatory responses. By inhibiting ABCB1 transporter activity in ECs, EV treatment is therefore a novel therapeutic approach to attenuate chemokine or cytokine leakage towards the blood side, thus reducing immune cell recruitment into the brain. Furthermore, EVs suppress the secretion of MMP-9 in activated astrocytes, which stabilizes the basal membrane. EVs might hence play a pivotal role in the prevention of immune cell infiltration and subsequent tissue impairment via BBB protection. However, additional studies on the specific substrates of ABCB1 involving these processes remain to be investigated in future studies.

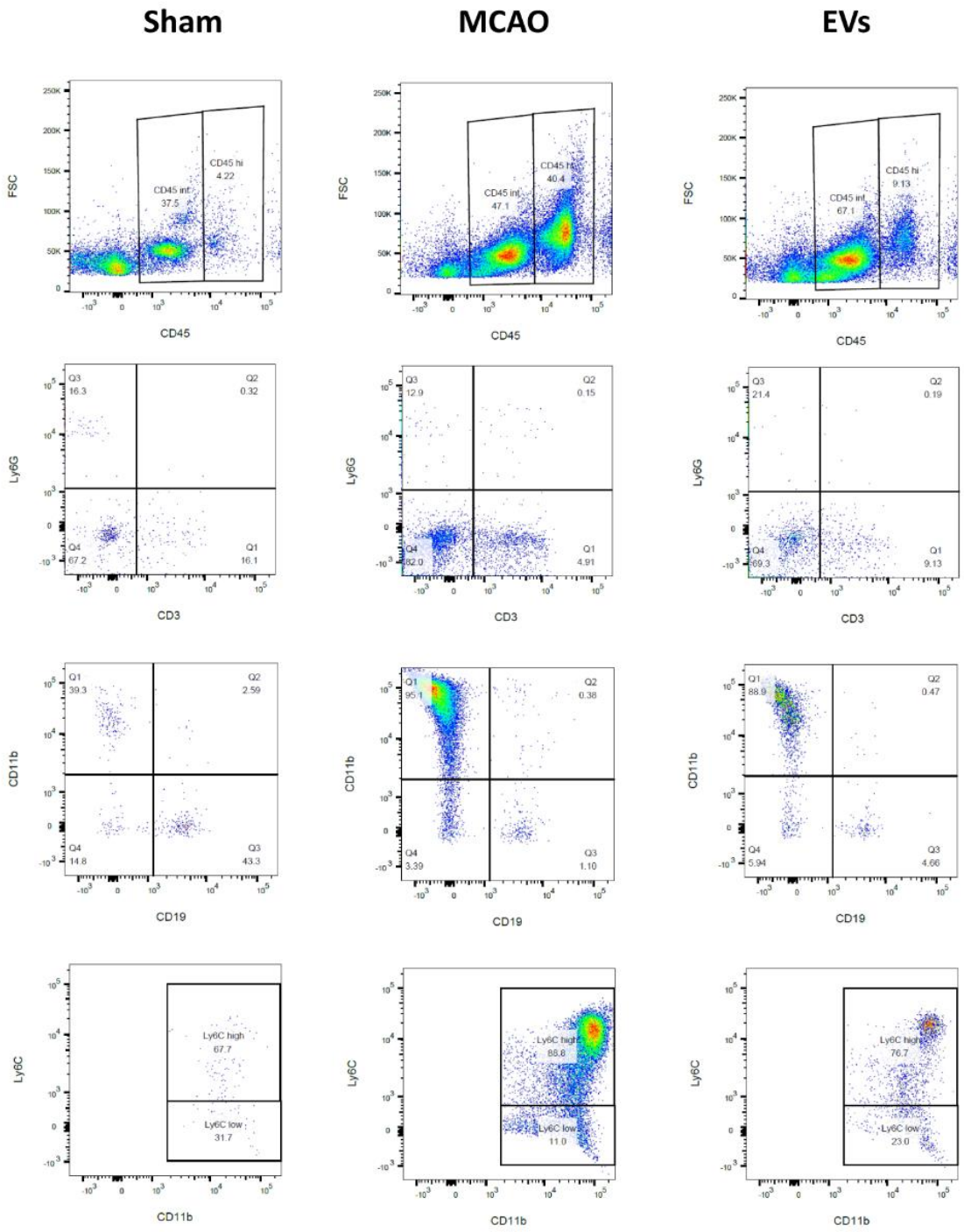

Figure 10: Modulation of early immune cell recruitment in ischemic hemispheres. Representative flow cytometry measurements of ischemic hemispheres in sham mice, MCAO-exposed mice, and MCAO-exposed mice treated with EVs. The latter two groups were exposed to 60 min of MCAO followed by 24 h of survival. For analysis, the cells were stained with antibodies against CD45, Ly6G, CD3, CD19, CD11b, and Ly6C. Abbreviations: EVs, extracellular vesicles; MCAO, middle cerebral artery occlusion.

4 Summary

Novel treatment paradigms of ischemic stroke include the transplantation of subventricular zone-derived neural progenitor cells (NPCs). The latter exert a plethora of effects such as stabilization of the blood-brain barrier (BBB), yielding increased neurological recovery in preclinical stroke studies. However, NPCs mediate their effects through indirect mechanisms, among which is the secretion of extracellular vesicles (EVs). The present study, for the first time, defines the beneficial effects and underlying mechanisms of NPC-EVs in ameliorating BBB damage after cerebral ischemia by using an *in vitro* BBB co-culture model and an *in vivo* mouse stroke model.

EVs were collected from conditioned medium of cultured NPCs and analyzed for EV characterization according to the International Society for Extracellular Vesicles guidelines. Using an *in vitro* oxygen-glucose deprivation setting, the changes of protein levels of ATP-binding cassette subfamily B member 1 transporter (ABCB1) and the involvement of the nuclear factor-kappa B (NF-κB) pathway were detected after EV treatment in endothelial cells exposed to hypoxia. To further investigate the specific BBB properties such as transcellular electrical resistance, permeability, and ABCB1 transporter activity, the impact of EVs on the BBB under hypoxic conditions was evaluated using an *in vitro* co-culture system consisting of primary mouse endothelial cells and astrocytes. Applying an *in vivo* mouse stroke model, the Evans Blue extravasation and the activity of matrix metalloproteinases (MMPs) like MMP-2 and MMP-9 were examined in order to assess the BBB function after EV treatment. In addition, the immune cell recruitment was analyzed by flow cytometry assessment to further evaluate the EV effect on stabilizing the BBB.

As revealed by the results of the present thesis, ischemic stroke activates MMP-9 secretion in astrocytes and increases ABCB1 expression in endothelial cells. These processes are attributed to an activation of the NF-κB pathway, which eventually leads to the breakdown of the basal membrane, an increase in BBB permeability, and an increased recruitment of immune cells towards the ischemic lesion site. The application of EVs, however, reverses the aforementioned process by inhibiting the NF-κB pathway, resulting in reduced ABCB1 and MMP-9 activation levels (Figure 11.). These findings provide novel evidence on the therapeutic potential of EVs under conditions of early ischemic BBB injury, which deserves further scientific investigation. In addition, the robust and effective *in vitro* co-culture BBB model established in this study may prove to be a valuable tool for both neuroprotective drug discovery and for studying the biology of ischemic BBB damage in the future.

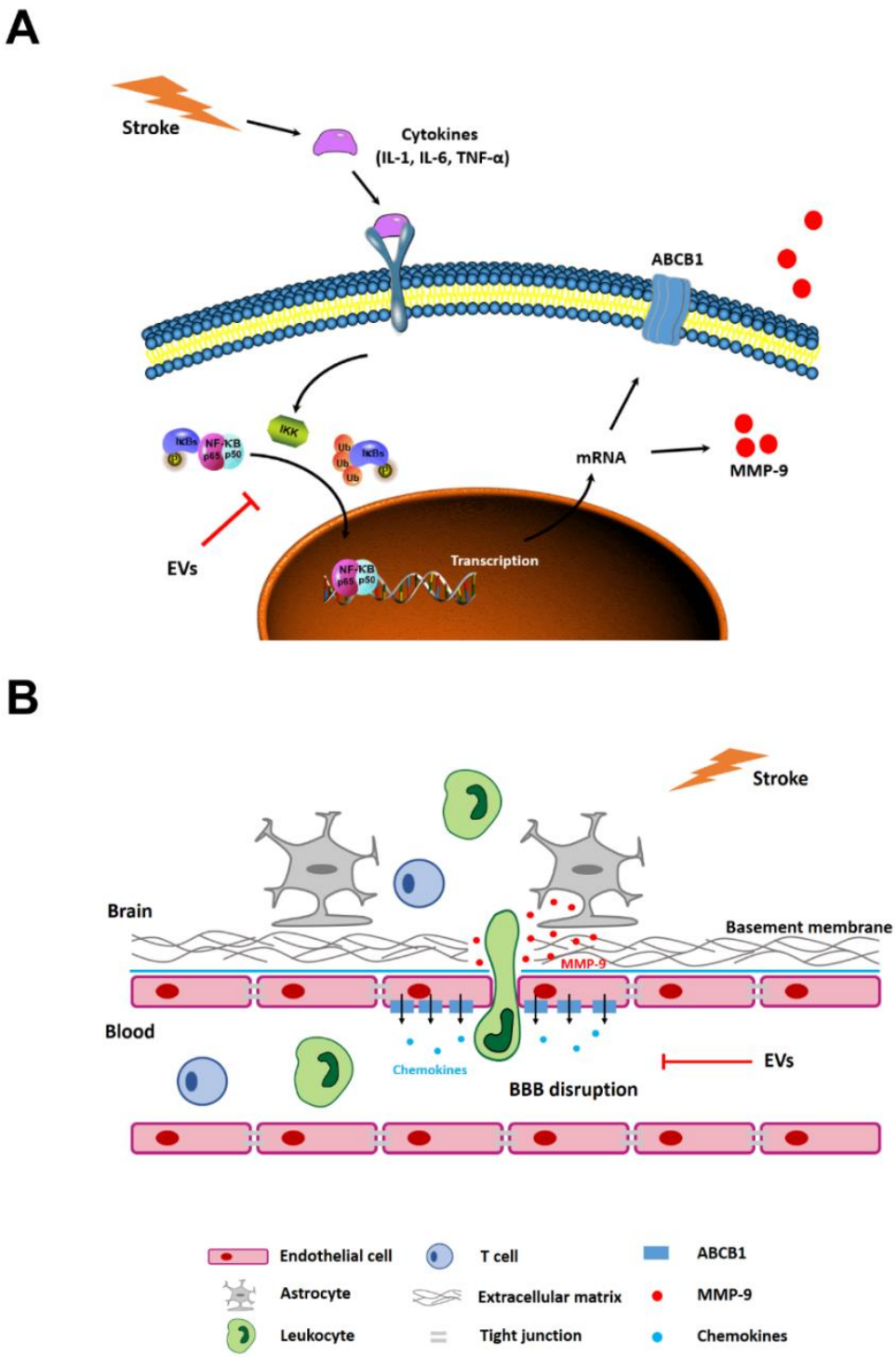

Figure 11: Graphical abstract of the present thesis. EV administration represses poststroke activation of the NF-κB pathway as well as ABCB1 and MMP-9 expression patterns yielding enhanced BBB integrity and decreased early immune cell recruitment. (A) Stroke-triggered signal accumulation in the ischemic brain promotes NF-κB related protein p65 translocation into the nucleus, increasing the transcription of ABCB1 and MMP-9 in endothelial cells or astrocytes. (B) After stroke, activated astrocytes secrete MMP-9 to disrupt the extracellular matrix of the basal membrane. Meanwhile, increased ABCB1 in endothelial cells which transports chemokines to the luminal side, recruits immune cells. As a consequence, these processes stimulate subsequent inflammatory responses in the ischemic brain. The application of EVs in this context, however, mitigates the aforementioned processes stabilizing the BBB (Zhang et al. 2021).

5 Supplement

5.1 Copy of Publication 1

Arteriosclerosis, Thrombosis, and Vascular Biology

BASIC SCIENCES

Neural Progenitor Cell-Derived Extracellular Vesicles Enhance Blood-Brain Barrier Integrity by NF-κB (Nuclear Factor-κB)-Dependent Regulation of ABCB1 (ATP-Binding Cassette Transporter B1) in Stroke Mice

Lin Zhang, Irina Graf, Yaoyun Kuang, Xuan Zheng, Matteo Haupt, Arshad Majid, Ertugrul Kilic, Dirk M. Hermann, Marios-Nikos Psychogios, Martin S. Weber, Jasmin Ochs, Mathias Bähr, Thorsten R. Doeppner

OBJECTIVE: Extracellular vesicles (EVs) derived from neural progenitor cells enhance poststroke neurological recovery, albeit the underlying mechanisms remain elusive. Since previous research described an enhanced poststroke integrity of the blood-brain barrier (BBB) upon systemic transplantation of neural progenitor cells, we examined if neural progenitor cell-derived EVs affect BBB integrity and which cellular mechanisms are involved in the process.

APPROACH AND RESULTS: Using in vitro models of primary brain endothelial cell (EC) cultures as well as co-cultures of brain ECs (ECs) and astrocytes exposed to oxygen glucose deprivation, we examined the effects of EVs or vehicle on microvascular integrity. In vitro data were confirmed using a mouse transient middle cerebral artery occlusion model. Cultured ECs displayed increased ABCB1 (ATP-binding cassette transporter B1) levels when exposed to oxygen glucose deprivation, which was reversed by treatment with EVs. The latter was due to an EV-induced inhibition of the NF-κB (nuclear factor-κB) pathway. Using a BBB co-culture model of ECs and astrocytes exposed to oxygen glucose deprivation, EVs stabilized the BBB and ABCB1 levels without affecting the transcellular electrical resistance of ECs. Likewise, EVs yielded reduced Evans blue extravasation, decreased ABCB1 expression as well as an inhibition of the NF-κB pathway, and downstream matrix metalloproteinase 9 (MMP-9) activity in stroke mice. The EV-induced inhibition of the NF-κB pathway resulted in a poststroke modulation of immune responses.

CONCLUSIONS: Our findings suggest that EVs enhance poststroke BBB integrity via ABCB1 and MMP-9 regulation, attenuating inflammatory cell recruitment by inhibition of the NF-κB pathway.

GRAPHIC ABSTRACT: A graphic abstract is available for this article.

Key Words: astrocytes ■ blood-brain barrier ■ endothelial cells ■ extracellular vesicles ■ matrix metalloproteinase 9

Cerebral ischemia induces blood-brain barrier (BBB) disruption, which allows intravascular molecules and immune cells to penetrate into the extracellular compartment and into the brain parenchyma, resulting in inflammatory responses and brain lesions.[1] The BBB comprises endothelial cells (ECs) connected by tight junctions, astrocytic end-feet, pericytes, perivascular microglia, and an extracellular matrix.[2] Many compounds are extruded through the barrier via ABC (ATP-binding

See accompanying editorial on page 1146

Correspondence to: Thorsten R. Doeppner, MD, MSc, Department of Neurology, University Medical Center Goettingen, Robert-Koch-Str. 40, 37075 Goettingen, Germany. Email thorsten.doeppner@med.uni-goettingen.de

The Data Supplement is available with this article at https://www.ahajournals.org/doi/suppl/10.1161/ATVBAHA.120.315031.

For Sources of Funding and Disclosures, see page 1143.

Nonstandard Abbreviations and Acronyms

ABCB1	ATP-binding cassette subfamily B member 1 transporter
BBB	blood-brain barrier
CM	conditioned medium
EBA	Evans blue-albumin
ECs	endothelial cells
EVs	extracellular vesicles
LY	Lucifer Yellow
MCAO	middle cerebral artery occlusion
MMP-9	matrix metalloproteinase-9
NF-κB	nuclear factor-kappa B
NPCs	neural progenitor cells
NTA	nanoparticle tracking analysis
OGD	oxygen glucose deprivation
PEG	polyethylene glycol 6000
P-gp	P-glycoprotein
R123	rhodamine 123
TER	transcellular electrical resistance
ZO-1	zonula occludens-1

cassette) transporters such as ABCB1, also named P-gp (P-glycoprotein).

ABCB1 binds to a variety of structurally diverse molecules and is mostly located on the luminal side of brain capillary ECs to transport substances towards the blood compartment.[3] Not only is ABCB1 regulated under various pathological conditions like inflammation, oxidative stress, radiation, and heat shock,[4–6] but it is also regulated under stroke conditions. As a matter of fact, ABCB1 is upregulated in cerebral ECs within 3 hours upon stroke induction.[7] Although upregulation of ABCB1 in the ischemic brain lesion is likely a physiological response to export toxic metabolites, both neuroprotective molecules and inflammatory chemokines are also transported towards the luminal side of the endothelium.[8–12] Hence, knockdown of ABCB1 decreases infarct size under experimental stroke conditions in mice.[13]

The stroke-induced regulation of ABCB1 expression patterns is but one element of BBB breakdown, albeit an important one. Other factors such as the degradation of the extracellular matrix by the MMP (matrix metalloproteinases)-2 and MMP-9 play in concert as well.[14] Interestingly, accumulating evidence from cancer research indicates that both ABCB1 and MMP-9 signaling are regulated by the NF-κB (nuclear factor-κB) signaling pathway.[15–18] The role of the latter under stroke conditions has been extensively studied in previous reports.[19–22] A therapeutically feasible tool that interferes with the aforementioned mutual signaling events under stroke conditions, however, does not exist.

Highlights

- Oxygen glucose deprivation induces blood-brain barrier disruption including increased ABCB1 (ATP-binding cassette subfamily B member 1 transporter) and reduced tight junction protein ZO-1 (zonula occludens 1) in endothelial cells.
- Extracellular vesicles derived from neural progenitor cells attenuate oxygen glucose deprivation-induced upregulation of ABCB1 via inhibiting the NF-κB (nuclear factor-κB) pathway in endothelial cells.
- Neural progenitor cells-extracellular vesicles regulate blood-brain barrier properties by diminishing barrier permeability and ABCB1 activity in vitro using a co-culture model.
- Extracellular vesicle administration mitigates upregulation of ABCB1 and MMP-9 (matrix metalloproteinase 9) and activation of the NF-κB pathway after stroke. Additionally, it decreases postischemic infiltration of leukocyte invasion into the ischemic hemisphere.

Extracellular vesicles (EVs) form a heterogeneous group of vesicles ranging in size from 30 to 1000 nm, which contain noncoding RNAs, DNA, and proteins such as heat shock proteins and tetraspanins.[23–25] Previous studies reported that stem cell-derived EVs are not inferior to stem cell transplantation itself. Although EVs derived from mesenchymal stem cells or neural progenitor cells (NPCs) and others partly induce neuroprotection by regulating poststroke immune responses,[26–31] their precise way of action remains uncertain. Interestingly, EVs have recently been described to affect EC function under both physiological and pathological conditions.[32] Studies involving the therapeutic potential of NPC-EVs with regard to poststroke BBB protection, however, do not exist. Using an in vitro BBB co-culture model of ECs and astrocytes as well as an in vivo murine stroke model, the present work analyzes such a potential effect of NPC-EVs and its underlying mechanisms. After demonstration of an EV-dependent impact on the integrity of the hypoxic/ischemic BBB, further analyses will focus on the regulation of ABCB1 protein expression as well as on NF-κB and MMP-9 signaling under these conditions.

MATERIALS AND METHODS

The data that support the findings of this study are available from the corresponding author upon reasonable request.

Cell Cultures

Mouse brain ECs (bEnd.3, CRL-2299, American Type Culture Collection, Manassas, VA) were seeded in tissue culture-plates (Sarstedt, Nuembrecht, Germany) and cultured under confluent conditions at a density of 6×10^4 cells/cm^2. Cells were cultured with 10% fetal bovine serum-containing medium (DMEM/Ham's F-12, Biochrom GmbH, Berlin, Germany).

Primary mouse brain EC were isolated according to a modified version of the method of Assmann et al.[33] Briefly, 4 male C57BL/6J mice were euthanized and whole brains removed and stored in HBSS buffer on ice. Under aseptic conditions, the brain stem, cerebellum, and meninges were removed in turn. The cortical tissue homogenate was pelleted by centrifugation at 1350*g* for 5 minutes at 4 °C. The pellet was resuspended in 10 mL dextran solution and vortexed extensively (2 minutes). The mixture was pelleted by centrifugation at 3900*g* for 10 minutes at 4 °C. The pellet was resuspended in prewarmed digestion medium and incubated at 37 °C for 1 hour with gentle shaking. After digestion, the microvessel fragments were pelleted by centrifugation at 1350*g* for 5 minutes at room temperature and washed once in PBS. The resulting microvessel fragments were resuspended in full medium (DMEM/F12 with 20% plasma-derived serum, L-glutamine, heparin, puromycin, antibiotic/antimycotic, and EC growth supplement). ECs were cultivated on 10 μg/cm^2 collagen IV-coated flasks, plates, or Transwell systems at 37 °C.

Primary mouse brain astrocytes were prepared using a protocol based on the method of Schildge et al.[34] Four C57BL/6J mouse pups at postnatal day 0 to 2 were decapitated and whole brains removed and placed in HBSS on ice. From each brain, both the cerebellum and the olfactory bulbs were removed with a sterile blade. The meninges were dissected from the cortex hemispheres by pulling with forceps. Pooled cortical tissue was digested with 0.25% trypsin at 37 °C for 30 minutes. Then the cell suspension was centrifuged at 300*g* for 5 minutes. The resulting pellet was suspended in 20 mL of astrocyte full medium (DMEM supplemented with 10% FBS and 1% penicillin/streptomycin) and cultivated on Poly-D-lysine-coated T75 flask. The astrocytes were cultured for 1 week (37 °C, 5% CO_2) before a full medium change to remove nonadherent cell debris. The astrocytes were passaged with 0.25% trypsin and resuspended in full medium at a density of 6×10^4 cells/cm^2 for the upcoming experiments.

EV Enrichment From Cultured NPCs

The NPC preparation and EV enrichment were based on the method of Zheng et al.[31] Briefly, C57BL/6J mouse pups at postnatal day 0 to 2 were decapitated and whole brains removed and placed in HBSS on ice. Thereafter, the subventricular zone was dissected in cold PBS under microscopic control, followed by spinning down tissue chunks at 200*g* for 1 minute at 4 °C. The pellet was suspended and incubated with 0.05% trypsin for 15 minutes. Each cell pellet was resuspended with NPC culture medium (DMEM/F12 with B27, L-glutamine, 1% penicillin/streptomycin, 20 ng/mL of FGF-2 [fibroblast growth factor-2], and 20 ng/mL EGF [epidermal growth factor]). The mixture was pelleted by centrifugation at 400*g* for 15 minutes at room temperature followed by washing steps 3× with NPC medium. The resulting pellet was resuspended with NPC medium, and the cells were plated onto the cell culture dish. The neurospheres were observed within 72 hours. The cell passage period of NPCs was 5 to 6 days.

After passage 3, NPCs were transferred to T75 flasks with 30 mL NPCs culture medium without growth factors. NPC-conditioned medium (NPC-CM) was collected after 24 hours of incubation under standard cell culture conditions. Large vesicles and debris were removed by filtration through 220 nm pore filters (TPP Techno Plastic Products AG, Trasadingen, Switzerland). EVs were enriched from the NPC-CM using the polyethylene glycol (PEG) precipitation method as previously described.[24,35] In brief, PEG precipitation was performed at a final concentration of 10% PEG 6000 (50% wt/vol; Merck Group, Darmstadt, Germany) and 75 mmol/L NaCl. After incubation for 12 hours at 4°C, the EVs were concentrated by centrifugation for 45 minutes at 4500*g*. EVs pellets were dissolved in PBS and precipitated by ultracentrifugation for 2 hours at 110000*g* (Optima XPN-80 Ultracentrifuge, Beckman Coulter, Brea). The EV pellets were resuspended in PBS to a concentration of 500 μL containing EVs obtained from CM of 432×10^6 NPCs. Aliquots of 500 μL each were stored at −80°C until usage. For the ultracentrifugation method, the NPC-CM was centrifuged for 2 hours at 110000*g* to pellet EVs and washed with PBS by a centrifugation at 110000*g* subsequently (Figure IIIA in the Data Supplement).

EV Characterization and Purification of NPC-EVs

Details about transmission electron microscopy, nanoparticle tracking analysis (NTA), Western blotting of EV markers, proteomic analysis, and iodixanol gradient centrifugation can be found in Materials and Methods I in the Data Supplement.

Importantly, the amount of NPC-EVs applied to cells was calculated by the following process. The EVs from 432×10^6 NPCs were diluted in 500 μL of PBS, each microliter contained 8.64×10^5 cell equivalent EVs (8.64×10^5 cell equivalent/μL, 43.2 μg/μL). In our previous experiments, several different NPC-EV concentrations (0.1, 1, and 10 μg/mL of the culture medium or BSS0 [glucose-free balanced salt solution] solution) were chosen to investigate the optimal EV dosage of the experiment. For the optimal EV concentration in vitro, we suggested EVs to be diluted to 2×10^4 cell equivalents per milliliter (1 μg/mL) in cell culture medium or BSS0 solution (Figure IC and ID in the Data Supplement).

When fluorescent EVs were needed, the supernatant was incubated with 10 μmol/L DiI, a lipophilic membrane dye, for 1 hour at 37°C in the dark. DiI-labeled EVs were separated from extra DiI dye in the light fraction and protein aggregates in the dense fractions by the aforementioned iodixanol gradient centrifugation. Different fractions were washed with PBS and recentrifuged. Pellets with DiI-labeled EVs were applied for EV tracking, and the pellets from F9-10 fractions lacking EVs were used as negative controls for the following in vitro and in vivo experiments.

Oxygen Glucose Deprivation

The cells were exposed to oxygen glucose deprivation (OGD) when they reached 90% confluence. For OGD, the cells were incubated in BSS0 solution (116 mmol/L NaCl, 5.4 mmol/L KCl, 0.8 mmol/L $MgSO_4$, 1 mmol/L $NaH_2PO_4H_2O$, 26.2 mmol/L $NaHCO_3$, 10 mmol/L HEPES, 0.01 mmol/L glycine, and 1.8 mmol/L $CaCl_2$, pH 7.2–7.4) and transferred to a hypoxia incubator chamber containing 0.2% O_2, 5% CO_2, and 70% humidity (Toepffer Lab Systems, Göppingen, Germany). For reoxygenation after removing the BSS0 solution, the cells were incubated in the cell culture medium for 24 hours in the 5% CO_2 incubator at 37°C. Thereafter, the cells were treated for the next experiments. bEnd.3 cells were exposed to 16 hours of OGD, whereas the co-culture systems were treated with 24 hours of OGD as primary cells possessed robust tolerance. For in vitro experiments, EV treatment was performed during OGD and during reoxygenation periods.

Cell Survival Assay

Cell viability was measured by a colorimetric assay by using the MTT (methylthiazolyldiphenyl-tetrazolium bromide; Thiazolyl Blue Tetrazolium Bromide, Sigma-Aldrich, St. Louis, MO) viability assay according to the protocol.[36] Cell viability data are presented as relative changes in percent compared with untreated controls. Furthermore, the cell death rate was also determined via fluorescence microscopy by using a LIVE/DEAD Viability kit (Lonza, Basel, Switzerland) as directed by the manufacturer's instructions. Living cells were identified with calcein AM (acetoxymethyl; 4 µmol/L, green fluorescence), and dead cells were identified with ethidium homodimer 1 (2 µmol/L, red fluorescence). Three independent experiments were conducted and ≥200 cells were evaluated for each condition.

In Vitro Co-Culture BBB Model and TER Measurement

To establish a valid in vitro co-culture BBB model, the system consisted of primary ECs and astrocytes as described before. ECs were seeded on a microporous membrane in the upper compartment, whereas astrocytes were put in the bottom compartment, representing luminal and abluminal sides of the BBB, respectively. According to the timeline in Figure 4B, the isolation and purification of astrocytes was done first. When astrocytes were grown to 90% confluence, astrocytes were passaged with 0.25% trypsin, and seeded into Poly-D-lysine-coated 24-well metal plates of the cellZscopeE instrument (nanoAnalytics, Münster, Germany). These were prepared at least 3 days before the inserts with ECs were placed to the 24-well plate. ECs grown on collagen IV-coated inserts (0.4 µm pore diameter, translucent, Greiner Bio-One GmbH, Frickenhausen, Germany) were transferred to the cellZscopeE instrument to establish a co-culture system 2 days after isolation of ECs. Puromycin was added to the full medium during these 2 days to remove non-ECs. After the start of the experiment, transcellular electrical resistance (TER) values of the barrier were measured automatically every single hour under different treatment paradigms by means of impedance measurement.[37–40] The latter was paused during the OGD treatment period itself.

BBB Permeability Studies With EBA and LY

The flux of different sized molecules such as Lucifer Yellow (LY) and Evans blue-albumin (EBA) across the EC layers of the in vitro BBB model was determined as previously described.[41] Cell culture inserts were transferred to 24-well tissue culture plates containing a 0.8 mL permeability assay buffer (141 mmol/L NaCl, 2.8 mmol/L $CaCl_2$, 1 mmol/L $MgSO_4$, 4 mmol/L KCl, 1 mmol/L NaH_2PO_4, 10 mmol/L glucose, and 10 mmol/L HEPES, pH 7.4) in the bottom or abluminal compartment. In the inserts (luminal compartment), the culture medium was replaced by 0.2 mL buffer containing 50 µmol/L LY (molecular weight: 457.25 Da) or 4% BSA mixed with 0.67 mg/mL Evans blue dye (EBA; molecular weight: 67 000 Da). Samples (200 µL) were collected from each bottom well at 15, 30, 45, 60, and 120 minutes to a 96-well plate for next detection. After removing the samples, we immediately replaced with fresh permeability assay buffer of each well. The concentrations of LY at different time points were determined with a POLARstar Omega Multimode Plate Reader (BMG LABTECH GmbH, Ortenberg, Germany) using a fluorescein filter pair (Ex[λ] 485±10 nm; Em[λ] 530±10 nm). The EBA concentration of the abluminal chamber at different time points were measured by determining the absorbance of samples at 630 nm photometrically.[37,38,41–43] The transendothelial permeability coefficient P_{cells} was calculated as described in analysis of in vitro permeability data.

Analysis of In Vitro Permeability Data

The permeability coefficient was calculated according to the method described by Dehouck et al.[44] The transferred volume (µL) of the tracer diffusing from the abluminal to the luminal chamber was calculated for each tracer using the following equation: transferred volume (µL)=$[C]_{Abluminal} \times V_{Abluminal}/[C]_{Luminal}$, where $[C]_{Luminal}$ is the tracer concentration on the side of the chamber, $[C]_{Abluminal}$ is the tracer concentration on the opposite side of the chamber, and $V_{Abluminal}$ is the volume of the opposite side of the chamber loaded with the tracer. During the experiment, the transferred volume increased linearly with time, and the slope was estimated by linear regression analysis. The clearance slopes of the transferred volume curves for the barriers were denoted by $PS_{cells+membrane}$ where PS is the permeability-surface area product (in µL/min). The slope of the transferred volume curve with the control membrane was denoted by $PS_{membrane}$. The control membrane was the cell free transwell insert membrane. The permeability clearance for the in vitro BBB models (PS_{cells}) was calculated from $1/PS_{cells+membrane}=1/PS_{membrane}+1/PS_{cells}$. The PS_{cells} values were divided by the surface area of the transwell inserts to generate the permeability coefficient (P_{cells}, in cm/min).[38,41,43]

Rhodamine 123 Accumulation Assay

ABCB1 activity was determined by measuring intracellular accumulation of rhodamine 123 (R123) in bEND.3 cells or primary ECs in different groups as previously reported.[41–43] Briefly, the ECs were incubated at 37°C for 60 minutes with R123 (5 µmol/L) after different treatment paradigms. After washing with PBS, the cells were lysed at 37°C for 15 minutes with 0.8% Triton X-100 in PBS. The protein concentrations of cell lysates were determined by the BCA assay. The concentration of R123 was measured using a POLARstar Omega Multimode Plate Reader (Ex[λ] 485±10 nm; Em[λ] 530±10 nm; BMG LABTECH GmbH, Ortenberg, Germany). The R123 accumulation level was normalized to the protein concentration within the ECs.

MCAO and EV Administration

All animal studies were performed with governmental approval according to the National Institutes of Health guidelines for the care and use of laboratory animals. The induction of transient focal cerebral ischemia in male C57BL/6J mice aged 10 weeks (Janvier Labs, Le Genest-Saint-Isle, France) was obtained using the middle cerebral artery occlusion (MCAO) model as previously described. Only male mice were studied to avoid the interference of the hormonal disturbances of female mice after MCAO surgery. In short, under anesthesia with 2% isoflurane and 0.8 L/min O_2 the right common carotid artery was isolated and a 6-0 nylon silicon-coated monofilament (Doccol Corporation, MA) inserted. The filament was gently pushed forward towards the MCA where it was placed for 60 minutes. After filament removal, the wounds were carefully

sutured. The occlusion and reperfusion were monitored under constant laser doppler flow. The mice were exposed to MCAO followed by administration of normal saline and EVs (from equivalent 2×10^5 NPCs, 10 µg/200 µL) via femoral vein injections at the onset of reperfusion and at 6 hours post-MCAO. This optimal EV concentration in vivo was chosen according to previous studies from our group.[31] For the sham group, animals underwent the very same procedure except for insertion of the nylon filament and were given the saline administration at the same time points. All mice were euthanized at 24 hours post-MCAO, and brain samples were prepared for the Western blotting and immunofluorescence staining.

Preparation of Brain Microvessel Fractions

Enriched microvessel fractions were obtained from brain samples of C57BL/6J mice submitted to sham surgery, MCAO and MCAO treated with EV injection. According to the method of Spudich et al,[7] brain samples from animals belonging to the same group were pooled, weighed, and homogenized in cold Ringer solution containing 1% BSA, 10 mmol/L N-2-hydroxyethylpiperazine-N-2-ethanesulfonic acid, and 5% protease inhibitor (pH 7.4). The homogenate was centrifuged at 1500*g* for 15 minutes. Thereafter, the pellet was resuspended and again centrifuged (10 minutes, 1500*g*). The pellet was suspended in 0.25 mol/L sucrose at pH 7.0, layered over a 1.0 to 1.5 mol/L sucrose gradient, and centrifuged for 30 minutes at 58000*g* using a Beckmann ultracentrifuge. This ultracentrifugation produced 3 distinct fractions of which the pellet represents the enriched cerebral microvessel fraction. The latter was prepared for Western blotting.

Evans Blue Extravasation

BBB integrity was evaluated by Evans blue extravasation, which was performed as previously described.[45,46] Briefly, 100 µL of 2% Evans Blue dye (Sigma-Aldrich, Darmstadt, Germany) was administered via the femoral vein 2 hours before euthanize. Subsequently, the mice were euthanized and transcardially perfused with PBS. The ischemic hemispheres were weighed, homogenized in 2 mL of 50% trichloroacetic acid, and centrifuged at 10000 rpm for 20 minutes. The extracted Evans Blue dye was further diluted with ethanol, and the absorbance at 620 nm wavelength was measured photometrically. The Evans Blue concentration was based on a standard curve (2.5 to 500 ng/mL) calculated. Evans blue extravasation of each group was evaluated, which is given as (µg) Evans Blue per (g) tissue.

Gelatin Zymography

The gelatin zymography measurement was performed with affinity-support purification as previously described.[47,48] In short, hemispheres were lysed in a nonreducing lysis puffer containing 50 mmol/L Tris-HCl (pH 7.6), 150 mmol/L NaCl, 5 mmol/L $CaCl_2$, 0.05% BRIJ-35, 0.02% NaN_3, and 1% Triton X-100 and afterwards centrifuged at 12000 rpm for 5 minutes. After collecting the supernatant, the protein concentration was measured (Pierce BCA Protein Assay Kit, Thermo Fisher Scientific), and the samples were incubated with 1:10 volume of sepharose 4B (Sigma-Aldrich, Darmstadt, Germany) for 60 minutes at 4°C. After incubation and centrifugation, the purified pellet was resuspended in lysis buffer containing 10% DMSO. Equal amounts of volume were then incubated with nonreducing sample buffer (Carl Roth, Karlsruhe, Germany) and loaded on 8% polyacrylamide containing 0.1% gelatin. After electrophoresis, the gel was incubated in renaturing buffer containing 2.5% Triton X-100 under gentle agitation for 30 minutes. Then, the gel was washed twice and incubated for 48 hours at 37°C with developing buffer (Novex). After incubation, the gel was stained with 0.1% Coomassie Blue for 30 minutes and then distained in washing solution containing 40% methanol and 10% acetic acid. After distaining, a white band remained behind a dark blue background. Thereafter, the gels were scanned and densitometrically analyzed.

Western Blot and NF-κB p65 Activation Assay

The brain microvessel fractions and the cell samples were lysed in a buffer containing 50 mmol/L Tris, 1% Triton X 100, 131 mmol/L sodium chloride, 1 mmol/L sodium diphosphate, 1 mmol/L sodium fluoride, 1 mmol/L EDTA, 1% protease inhibitor, and 1% phosphatase inhibitor with a homogenisator for 10 minutes and subsequently centrifuged at 4°C with 16000 rpm for 10 minutes. The supernatant was collected, and quantification of the protein concentration was photometrically accomplished (Pierce BCA Protein Assay Kit, Thermo Fisher Scientific). Reducing sample buffer (Carl Roth, Karlsruhe, Germany) was added, and the samples were heated for 5 minutes at 95°C. The samples were not recommended to be heated for ABCB1 blots according to the antibody datasheet provided by Abcam. Equal amounts of protein were separated on 8% to 12% SDS-PAGE and transferred onto nitrocellulose membranes (Bio-Rad, CA). Following transfer, the membranes were blocked for 1 hour and incubated with the primary antibodies ZO-1, ABCB1, NF-κB p65, IκBα (inhibitor of nuclear factor-κB), Histone H3, β-actin, α-tubulin, and GAPDH overnight. After washing with tris-buffered saline supplemented with 0.1% Tween 20 detergent 3×, the blots were incubated with horseradish peroxidase coupled secondary anti-mouse-antibody and anti-rabbit-antibody (1:10000) for 1 hour. The specific antibody working dilutions are given in the resource table I in the Data Supplement. The membranes were bathed in ECL (enhanced chemiluminescence) reagent and developed with the imaging system ChemiDoc XRS+ (Bio-Rad). For assessment of NF-κB translocation, an NF-κB activation kit (FIVEphoton Biochemicals, CA) was used, thus discriminating between both cytoplasm and nuclear fractions of NF-κB p65.

Immunohistochemistry and Immunocytochemistry Staining

Brain samples from C57BL/6J mice after perfusion were fixed in 4% paraformaldehyde overnight, dehydrated with 30% sucrose, and prepared in 16 µmol/L cryostat sections. The brain sections were blocked with buffer containing 2% BSA, 10% donkey serum, 0.25% Triton X-100 in PBST (phosphate-buffered saline solution with Tween detergent). Then, the sections were incubated overnight with the following primary antibodies: ZO-1, CD31, GFAP (glial fibrillary acidic protein), S100B, NF-κB p65, and MMP-9. Thereafter, the sections were incubated for 1 hour with the following appropriate Cy-3-labeled or Alexa Fluor 488-labeled secondary antibodies (1:10000, Jackson ImmunoResearch, Ely, United Kingdom) followed by 4′,6-Diamidin-2-phenylindol (DAPI, 1:10000; AppliChem, Darmstadt, Germany) staining. For cells, the slides or wells

were fixed with 4% paraformaldehyde and blocked using 10% DS, 1% BSA in PBST before incubation with the primary antibody. Five pictures per hemisphere were taken in the striatum as our region of interest, and 5 pictures per well of cells were taken with the Axioplan 2 fluorescence microscope (Carl Zeiss, Jena, Germany). The software ImageJ (National Institutes of Health) was used for cell counting and intensity quantification.

Flow Cytometry Analysis

Infiltrating leukocytes and the subset of T cells, B cells, neutrophils, macrophages, and monocytes were determined by flow cytometry with a fluorescence-activated cell sorter as described previously.[49] Briefly, the ischemic hemispheres were mechanically homogenized in lysis buffer (0.5% BSA, 5% glucose, DNase [10 mg/mL], PBS) and centrifuged at 1600 rpm for 10 minutes. Thereafter, the pellet was solved in 30% Percoll solution (GE Healthcare) and loaded on the Percoll gradient containing 45% and 70% Percoll phases. Following centrifugation, the leukocytes between the phases were aspirated and solved in working solution (3% fetal bovine serum in PBS). After washing, the cells were incubated with anti-CD3 (Becton Dickinson), anti-CD45, anti-Ly6G, anti-Ly6C, anti-CD19, and anti-CD11b antibodies (BioLegend, San Diego, CA) overnight. Gating and quantification were obtained with the software FlowJo v. 10.5.3 (BD FACSDiva).

Statistical Analysis

Results are shown as means±SD. All data were normally distributed as indicated by the Kolmogorov-Smirnov test. Accordingly, parametric tests were applied. Statistical analysis was performed using the Student *t* test to compare 2 groups. The statistical significance of differences between several groups were assessed by a 1-way ANOVA and a 2-way ANOVA for factorial comparisons and by Bonferroni or Tukey-Kramer test for multiple comparisons. Differences were considered significant when *P* values were <0.05, using GraphPad Prism 6.0 (GraphPad, San Diego, CA).

RESULTS

OGD-Induced Regulation of ABCB1 and ZO-1 in ECs

Protein levels of the efflux transporter ABCB1, one of the most important transporters of the BBB, were increased in ECs exposed to 16 hours of OGD (Figure 1A). On the contrary, both immunofluorescence staining and Western blotting revealed reduced expression of the tight junction protein ZO-1 in the OGD in vitro model (Figure 1B and 1C). These results suggest that the endothelium OGD model chosen is associated with an upregulation of ABCB1 and the loss of tight junction proteins, mimicking the BBB breakdown in vitro.

Purification, Isolation, and Characterization of NPC-EVs

Primary NPCs were isolated from the mouse subventricular zone, and NPC-EVs were enriched by using 2 well established methods, that is, ultracentrifugation and PEG. The subsequent characterization of such enriched NPC-EVs included Western blot of EV biomarkers, transmission electron microscopy, and NTA. EV enrichment using either ultracentrifugation or PEG revealed the presence of commonly reported EV biomarkers such as Alix, Tsg101, CD63, CD9, and CD81 compared with NPC cell lysate groups (Figure 2A). Transmission electron microscopy analysis showed no significant morphological differences between ultracentrifugation-EVs and PEG-EVs, as both preparations contained smaller and larger vesicles (Figure 2B). NPC-EVs were further quantified and evaluated for size using NTA, which displayed an EV-like spectrum in both groups. The distribution patterns from the NTA results revealed the majority of NPC-EVs to be at about 50 to 150 nm in size in both groups (Figure 2C). According to the above results, we found that there is no significant difference between these 2 enriched methods from CM of NPCs. Given that the PEG method can greatly reduce the amount of work and improve the enriched efficiency, we applied the PEG method to enrich NPC-EVs for the remainder of the study. In parallel, we performed a proteomic analysis on PEG enriched EVs, confirming the presence of the aforementioned EV markers (Data Supplement II). To further discriminate EVs from non-EV nanoparticles and protein, we applied an iodixanol gradient centrifugation to subfractionate EVs (Figure 2D). Ten fractions (F1-F10) were recovered and analyzed for the presence of protein markers like Alix, CD63, CD81, Tsg101, and CD9. As shown in the representative Western blots, the samples floated mostly in fractions F4 and F5 (1.134–1.149 g/mL). Consistently, protein concentrations revealed a vast majority of protein to be in fractions F4 and F5 (Figure 2E). These 2 fractions were further quantified and evaluated for size by NTA, which reflects a similar size distribution pattern in these vesicles (Figure 2F). Thereafter, the effect of fractions F4 to F6 were studied with regard to the expression of ABCB1 after OGD treatment. As shown in Figure 2G, EVs from F4 and F5 reversed the OGD-induced increase of ABCB1, whereas the samples from F6 had no effect in that respect. Given the aforementioned similar characterization between F4 and F5 fractions, we collected and pooled fractions F4 and F5 as purified EVs for further experiments.

NPC-EVs Reverse the OGD-Induced Upregulation of ABCB1 and Inhibit the Activation of the NF-κB Without Affecting Cell Survival Directly

As shown in Figure 1, ABCB1 protein abundance is increased upon induction of OGD. The application of NPC-EVs, however, reversed the OGD-induced increase of ABCB1. Of note, expression patterns of ZO-1 were not affected by EV treatment (Figure 3A and 3B). Analysis of the NF-κB pathway, which is known to be activated in cerebral ischemia contributing to pronounced brain injury,[22]

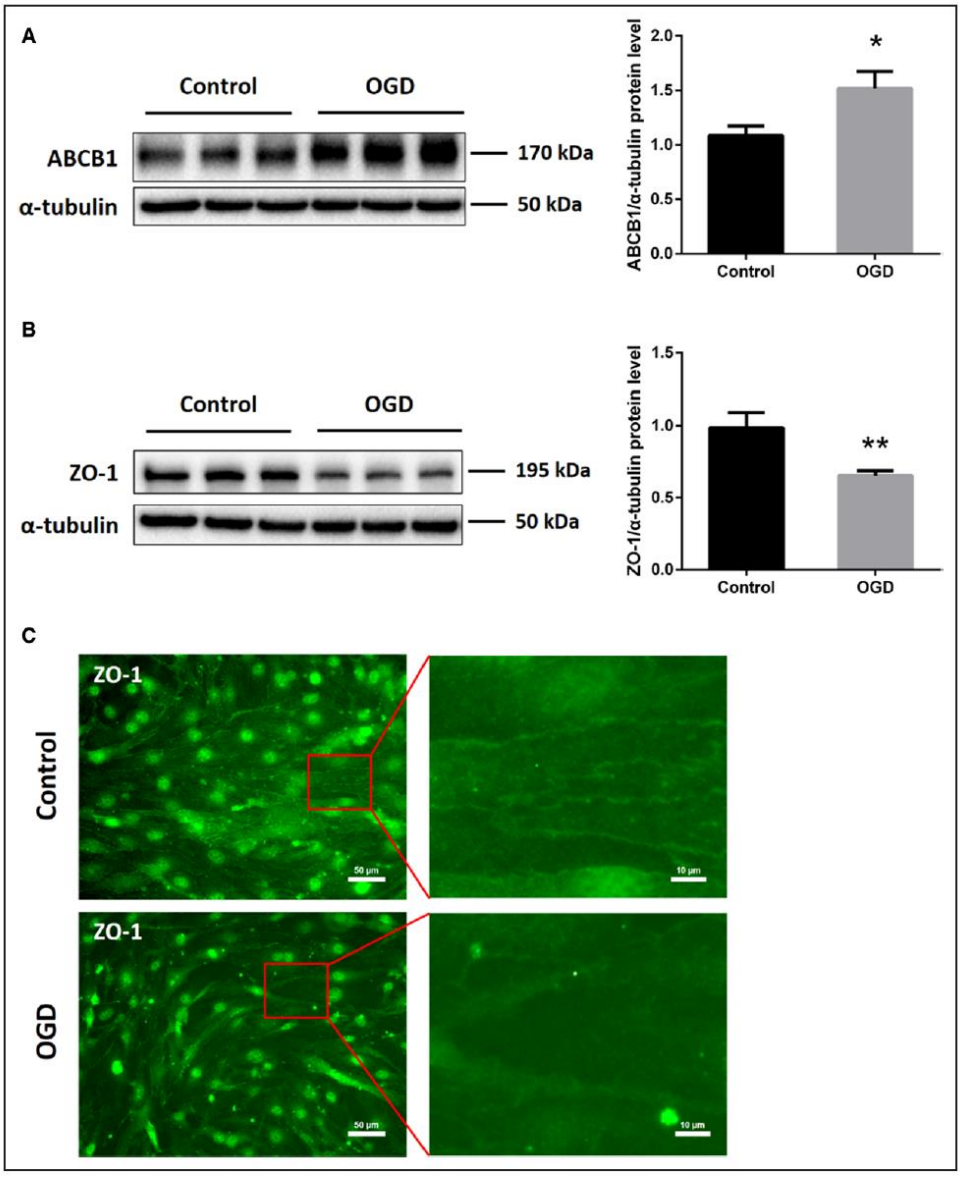

Figure 1. In vitro oxygen glucose deprivation (OGD) induces upregulation of ABCB1 (ATP-binding cassette subfamily B member 1 transporter) and reduces tight junction protein ZO-1 (zonula occludens 1) expression in endothelial cells (ECs; bEnd.3). bEnd.3 were exposed to 16 h of OGD followed by 24 h of reoxygenation with normal cell culture medium. **A** and **B**, Quantitative measurement of ABCB1 and ZO-1 protein expression using Western blot analysis normalized with the housekeeping protein α-tubulin (n=5 per group). Data are expressed as mean±SD; *$P<0.05$, **$P<0.01$. **C**, Nonquantitative immunofluorescence staining of ZO-1 in adjacent ECs, depicting representative staining areas. Scale bars: 50 μm. Red squares show magnifications of indicated areas. Scale bars: 10 μm.

demonstrated that induction of OGD resulted in an activation of that pathway. In detail, NF-κB p65 protein abundance was increased whereas IκBα protein expression was decreased. This OGD-induced activation was abolished by EV treatment (Figure 3C and 3D). Since OGD triggers cytotoxicity and cell death, we next asked the question whether

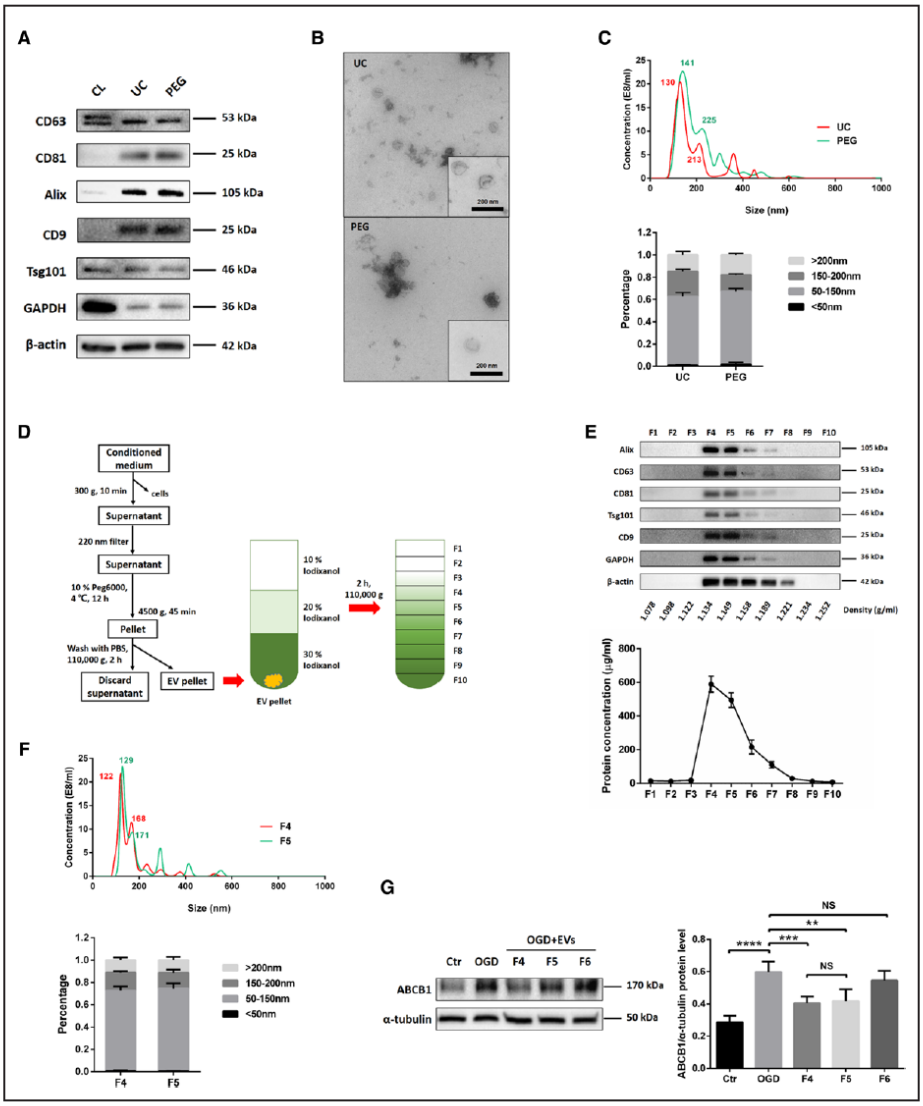

Figure 2. Purification, isolation, and characterization of extracellular vesicles (EVs) derived from NPCs (NPC-EVs). EVs were enriched from conditioned medium of NPCs by ultracentrifugation (UC) and by polyethylene glycol (PEG) precipitation. **A**, Western blot analysis of EVs against exosomal markers such as CD9, CD63, CD81, Tsg101, and Alix, with β-actin serving as a loading control. Western blots were performed on total cell lysates (CL) and EV lysates obtained using either UC or PEG. **B**, Representative transmission electron microscopy (TEM) analysis from EVs enriched by either UC or PEG. Scale bar: 200 nm. **C**, Nanoparticle tracking analysis (NTA) from enriched EVs (UC and PEG) depicting size distribution patterns. **D**, Resuspended EVs enriched by PEG were allowed to float into an overlayed iodixanol gradient to purify and separate different EV populations. **E**, The iodixanol gradient fractions for PEG were analyzed by Western blotting (fraction F1–10) using exosomal markers. Equivalent volumes of each fraction were loaded per lane. Representative images are shown for CD9, CD63, CD81, Tsg101, and alix which were enriched in fraction F4 and F5. The protein concentration of each fraction was calculated by the BCA assay, indicating a vast majority of protein to be in fraction F4 and F5 (n=3 per group). **F**, NTA was used to analyze enriched EVs in fraction F4 and F5 depicting size distribution patterns. **G**, Quantitative analysis of ABCB1 (ATP-binding cassette subfamily B member 1 transporter) expression in ECs under normoxic conditions (Ctr) as well as under OGD conditions and under conditions of OGD-exposed ECs treated with EV fractions F4–F6 using Western blot analysis (n=3 per group). Data are expressed as mean±SD. NS: no significance, $^{**}P<0.01$, $^{***}P<0.001$, and $^{****}P<0.0001$.

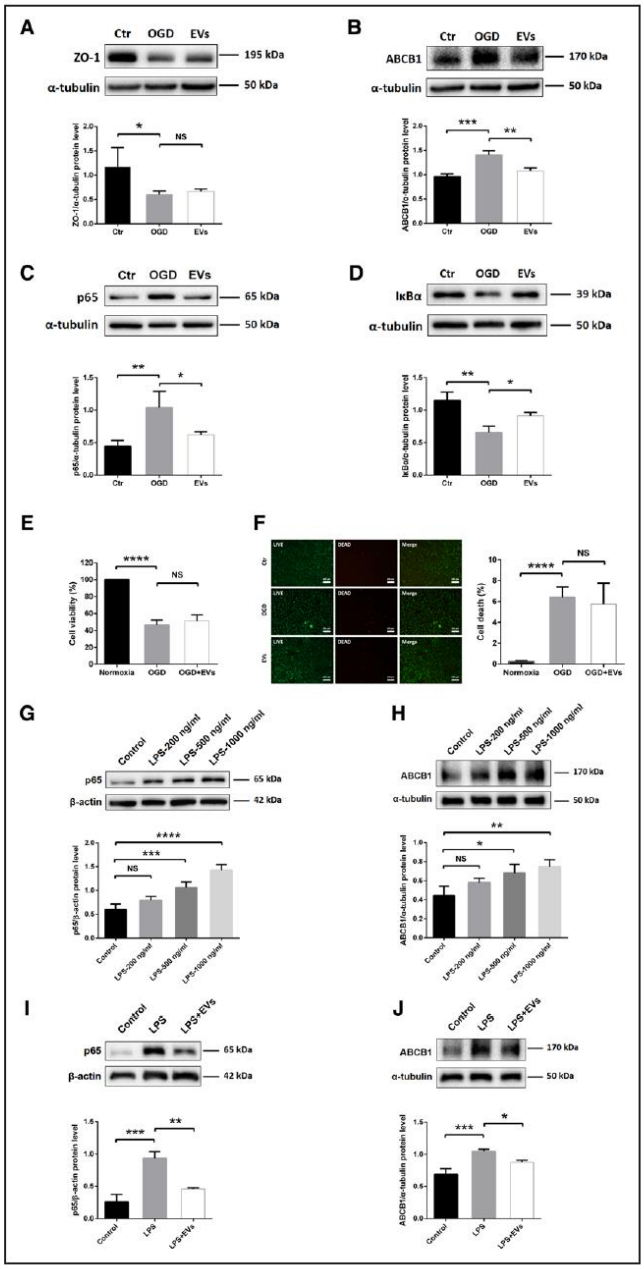

Figure 3. Neural progenitor cell (NPC)-extracellular vesicles (EVs) reverse upregulation of ABCB1 (ATP-binding cassette subfamily B member 1 transporter) and activation of NF-κB (nuclear factor-κB) in endothelial cell (ECs) under both oxygen glucose deprivation (OGD) and lipopolysaccharide (LPS) conditions. **A** and **B**, Quantitative analysis of ZO-1 (zonula occludens 1) and ABCB1 expression in normoxia control, OGD and OGD treated with EVs using Western blot analysis normalized with the housekeeping protein α-tubulin (n=4 per group). **C** and **D**, Quantitative analysis of p65 and IκBα (inhibitor of nuclear factor-κB) expression associated with the NF-κB pathway in the same three groups using Western blot analysis normalized with the housekeeping protein α-tubulin (n=4 per group). **E**, Cell viability was analyzed in ECs exposed to 16 h of OGD followed by 24 h of reoxygenation using the MTT (methylthiazolyldiphenyl-tetrazolium bromide) assay (n=5 per group). Cells incubated under normoxic conditions were defined as 100% cell survival. **F**, The LIVE/DEAD assay uses the same conditions as mentioned for the MTT assay. The photos display representative immunofluorescence stainings of calcein AM (acetoxymethyl; LIVE cells, green) and ethidium homodimer-1 (DEAD cells, red). Scale bars: 200 μm (n=5 per group). **G** and **H**, Quantitative analysis of p65 and ABCB1 expression under control conditions and in ECs exposed to LPS 200, 500, or 1000 ng/mL using Western blot analysis normalized with the housekeeping protein β-actin or α-tubulin (n=4 per group). **I** and **J**, Quantitative analysis of p65 and ABCB1 expression in normoxia control, LPS (1000 ng/mL) and LPS-treated ECs in the presence of EVs using Western blot analysis normalized with the housekeeping protein β-actin or α-tubulin (n=4 per group). Data are expressed as mean±SD. **P*<0.05, ***P*<0.01, ****P*<0.001, and *****P*<0.0001.

or not the regulation of ABCB1 in ECs is merely an indirect consequence of different cell survival rates due to EV treatment. We, therefore, performed survival assays (MTT and LIVE/DEAD) as shown in Figure 3E and 3F. Exposure of ECs to OGD resulted in a significant cell death rate. However, incubation of ECs with EVs did not affect cell survival directly; there was no significant difference between controls and EV-treated cells in this respect. This finding

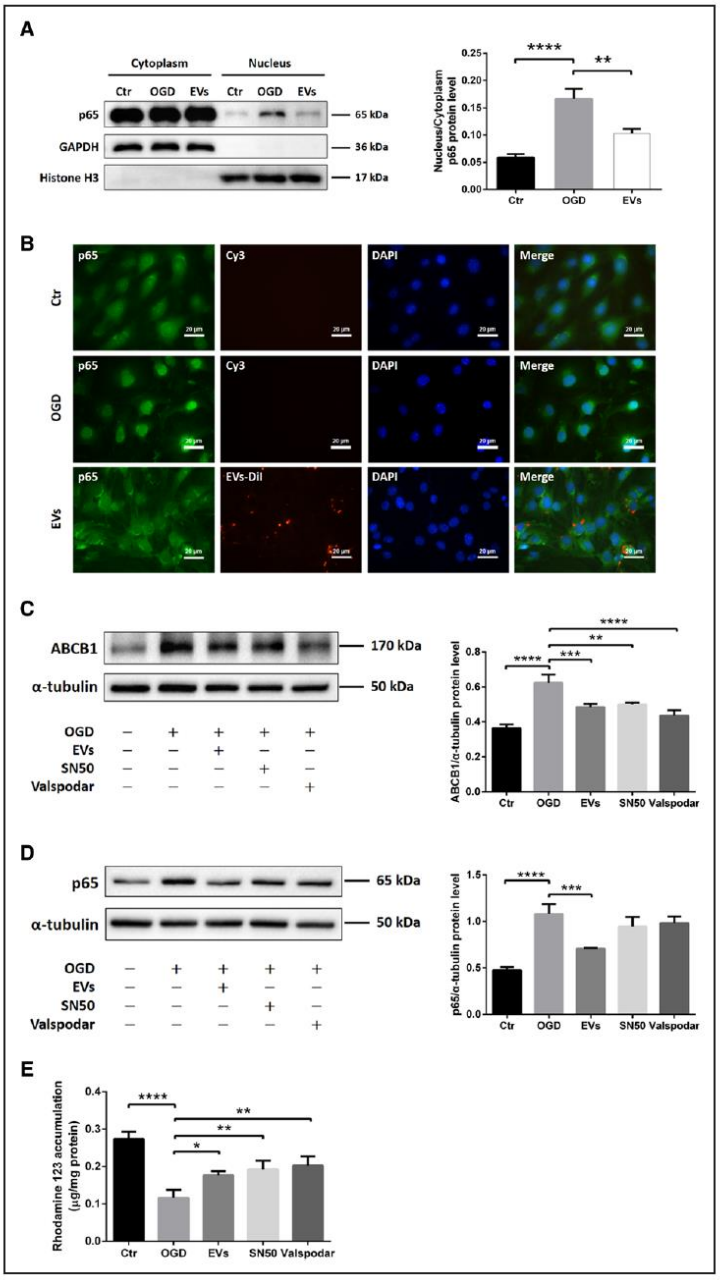

Figure 4. Extracellular vesicles (EVs) attenuate oxygen glucose deprivation (OGD)-induced upregulation of ABCB1 (ATP-binding cassette subfamily B member 1 transporter) via inhibiting the NF-κB (nuclear factor-κB) pathway.
A, Quantitative analysis of p65 expression of cytoplasm and nucleus fractions in normoxia control, OGD, and OGD treated with EVs groups using Western blot analysis normalized with the housekeeping proteins GAPDH in the cytoplasm fractions and Histone H3 in the nucleus fractions. **B**, Nonquantitative immunofluorescence staining of p65 (green), EVs-DiI (red), and DAPI (blue) in 3 groups (*Continued*)

supports the hypothesis that NPC-EVs regulate ABCB1 expression patterns under OGD conditions independent from survival rates of cultured ECs.

NPC-EVs Reverse Lipopolysaccharide-Induced Activation of NF-κB and Increase of ABCB1

Evidence suggests that treatment with the bacterial component lipopolysaccharide can activate the NF-κB pathway in ECs.[50,51] To further study an effect of EVs inhibiting the NF-κB pathway, we applied different concentrations of lipopolysaccharide (200, 500, and 1000 ng/mL) in cultured ECs. As shown in Figure 3G and 3H, both the expression of p65 and ABCB1 were increased by the dose-dependent lipopolysaccharide treatment compared with controls. Incubation of ECs with EVs significantly inhibited the lipopolysaccharide-induced (1000 ng/mL) elevation of p65 and ABCB1 (Figure 3I and 3J). Additionally, EVs also reversed the lipopolysaccharide-induced p65 nuclear translocation of the NF-κB pathway, which was similar to the SN50 group (Figure IF in the Data Supplement). Thus, the impact of NPC-EVs on ABCB1 and NF-κB in ECs is not restricted to OGD conditions but can also be found in the lipopolysaccharide model.

NPC-EVs Mitigate the p65 Nuclear Translocation and Downregulate the Expression and Activity of a Downstream Target ABCB1

Analyzing NF-κB p65 protein abundance is not sufficient to properly study this signaling pathway. Hence, we next performed a translocation assay under OGD conditions. Western blotting and immunofluorescence staining demonstrated that EC exposure to OGD resulted in a pronounced translocation of p65 from the cytoplasm towards the nucleus. Incubation of ECs with EVs inhibited the p65 nuclear translocation (Figure 4A and 4B). Since OGD-induced activation of the NF-κB pathway promoted p65 translocation, known to increase transcription of a number of genes under hypoxic/ischemic conditions,[22] we next elucidated if ABCB1 is a downstream target of the NF-κB pathway. As such, we applied SN50, an NF-κB translocation inhibitor, and Valspodar, an ABCB1 inhibitor, in the OGD system. Both SN50 and Valspodar significantly reduced ABCB1 protein abundance in OGD-exposed ECs, as is the case with EVs (Figure 4C). Neither SN50 nor Valspodar affected protein expression of NF-κB p65 in hypoxic ECs in comparison to ECs treated with EVs (Figure 4D). Since SN50 inhibits the translocation but not the total protein abundance of NF-κB p65, the lack of effect of SN50 is in line. The latter was confirmed in a proof-of-concept experiment, showing that SN50 indeed inhibits the translocation of NF-κB p65 in our OGD model (Figure IE in the Data Supplement). Consistently, ABCB1 transporter activity in each group was examined by R123, a known ABCB1 substrate. The cellular accumulation of R123 depends on ABCB1 activity, which can actively transport R123 towards the extracellular compartment. As shown in Figure 4E, EVs increased R123 accumulation in ECs by diminishing the ABCB1 transporter activity, which was similar to the SN50 and Valspodar groups. Hence, NPC-EVs regulate posthypoxic expression patterns of ABCB1 indirectly through the inhibition of the NF-κB pathway.

NPC-EVs Regulate Properties of the BBB in an In Vitro OGD Co-Culture Model

To further assess the effect of EVs on the functional properties of the BBB, we employed an in vitro BBB co-culture model using primary ECs and astrocytes. The isolation, culture, and purification of ECs and astrocytes, as well as the construction of the co-culture system, is depicted in Figure 5A. As shown in Figure 5B, ECs and astrocytes were seeded on the upper and lower chamber, representing the luminal and the abluminal sides of the BBB, respectively. Immunocytochemistry staining was conducted using specific known markers to confirm the cell lineage, that is, ECs (ZO-1, CD31) and astrocytes (GFAP, S100B). Co-culturing of both ECs (CD31 positive) and astrocytes (GFAP positive) did not change their biological properties, that is, both cell types were able to take up EVs under these conditions (Figure 5C and 5D).

For the detection of the TER, the values were recorded every single hour using an automatic cellZscopeE apparatus. The optimal TER value was reached between 120 and 180 hours in the co-culture system, with values peaking to 14 to 17 $\Omega \cdot cm^2$ at 120 hours. Thereafter, the system was exposed to OGD for 24 hours and disconnected to the controller during this period. The recording was restarted after OGD and the value of each well reduced to around 50% of the plateau value at the onset of the reoxygenation period (Figure IIA and IIB in the Data Supplement). Values for each well and time point were saved and analyzed between groups. However, EV treatment did not significantly rescue TER values after induction of OGD in the BBB co-culture model (Figure 5E).

The permeability studies with different molecules of different sizes like LY (457.25 Da) and EBA (67 000 Da)

Figure 4 Continued. showed p65 nuclear translocation of the NF-κB pathway. Scale bars: 20 μm. **C** and **D**, Quantitative analysis of ABCB1 and p65 expression by Western blot analysis in normoxia control, OGD, OGD treated with EVs, OGD with SN50 (NF-κB translocation inhibitor) and OGD with valspodar (ABCB1 inhibitor) groups. Western blots were normalized with the housekeeping protein α-tubulin (n=3 per group). **E**, Statistical analysis of rhodamine 123 accumulation in ECs representing ABCB1 transporter activity were done in the same groups (n=6 per groups). DAPI indicates 4',6-diamidino-2-phenylindole. Data are expressed as mean±SD, *P<0.05, **P<0.01, ***P<0.001, ****P<0.0001.

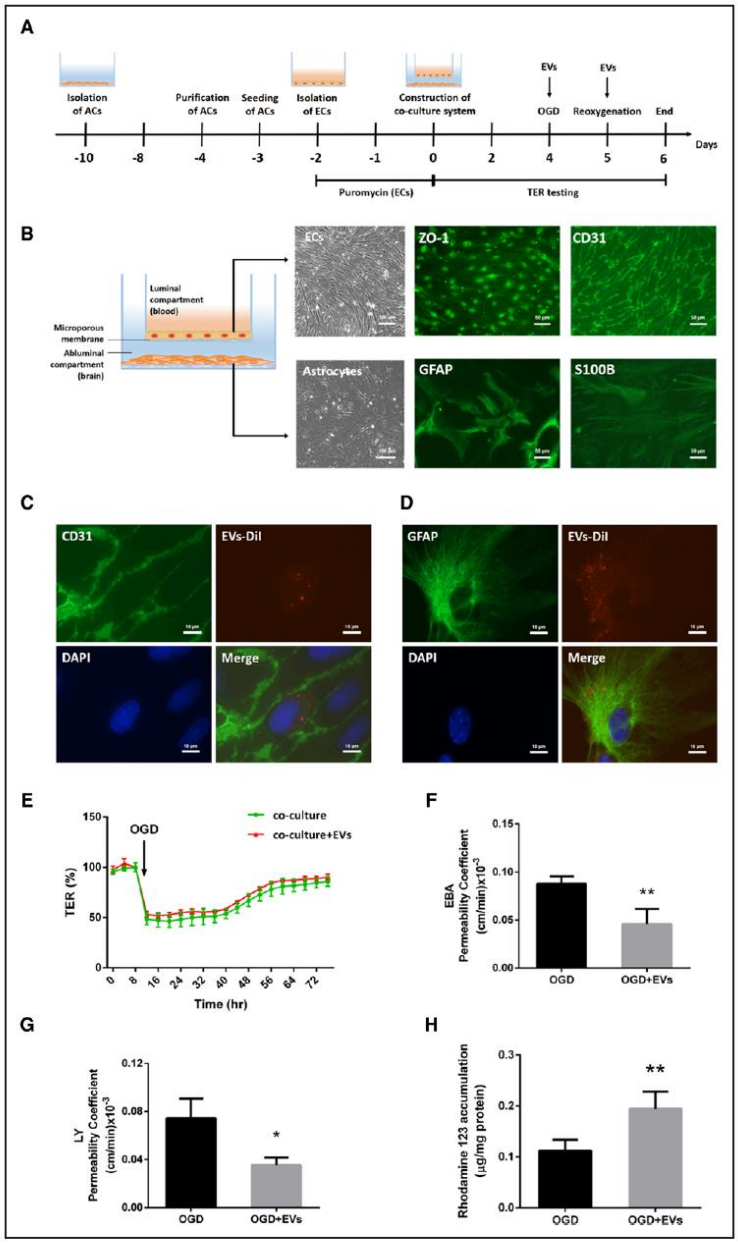

Figure 5. Extracellular vesicles (EVs) regulate blood-brain barrier (BBB) properties in vitro using a co-culture model.
A, Experimental paradigm summarizing the in vitro BBB co-culture model. **B**, In vitro, the BBB co-culture model consisted of primary ECs on a transwell insert with a microporous membrane and astrocytes (ACs) on the other side. Phase-contrast images of endothelial cells (ECs) and astrocytes under brightfield microscopy are shown. Scale bars: 100 μm. Immunofluorescence staining of their specific markers ZO-1 (zonula occludens 1), CD31 (ECs), and GFAP (glial fibrillary acidic protein), and S100B (astrocytes) are depicted separately. Scale bars: 50 μm. **C** and **D**, EVs labeled with DiI (red) were taken up into the cytoplasm of ECs and astrocytes. CD31 and GFAP (green) represent markers of ECs and astrocytes separately. Scale bars: 10 μm. **E**, In the co-culture system, real-time transcellular electrical resistance (TER) values were (*Continued*)

were performed on inserts after 24 hours of reoxygenation. The permeability data were plotted as the total number of volume transported over time in each well. The permeability coefficient P_{cells} analysis for both LY and EBA suggested that EV treatment significantly reduced the BBB permeability in the co-culture system (Figure 5F and 5G).

Next, ABCB1 transporter activity of ECs was detected by using the aforementioned R123 accumulation assay. As shown in Figure 5H, EV treatment significantly reduced the ABCB1 transporter activity on ECs after induction of OGD. Collectively, EVs not only mitigate the OGD-induced upregulation of ABCB1, but also repress its function and activity.

NPC-EV Administration Mitigates the MCAO-Induced Upregulation of ABCB1 and the Activation of the NF-κB Pathway In Vivo

To analyze the role of EVs on regulation of ABCB1 and the NF-κB pathway in ischemic stroke, we studied ABCB1 and p65 expression in mice submitted to 60 minutes of MCAO. Based on the aforementioned in vitro data, systemic injection of NPC-EVs via cannulation of the femoral vein is likely to yield an uptake of DiI-labeled EVs by ECs, followed by crossing the basal membrane, entering the end-feet of astrocytes, and reaching the cerebral parenchyma outside of microvessels (Figure 6A). Immunohistochemistry staining of cerebral microvessels and astrocytes located within the infarct core revealed CD31-positive and GFAP-positive cells to be co-localized with DiI-labeled EVs (Figure 6B). Western blots using enriched fractions of brain microvessels of ischemic hemispheres revealed that both ABCB1 and p65 protein levels were increased at 24 hours poststroke (Figure 6C and 6D). These stroke-induced upregulations were inhibited by EV administration. No significant differences were observed in the contralateral hemispheres. Sham group mice underwent the surgery procedure without MCA occlusion. And mice were treated with PBS vehicle in MCAO control groups intravenously at the beginning of reperfusion and 6 hours later after MCAO.

NPC-EV Administration Attenuates MCAO-Induced MMP-9 Elevation and Evans Blue-Albumin Leakage

Additional experiments were conducted to evaluate the effect of EVs on BBB stability in vivo. As mentioned before, the induction of cerebral ischemia activates a great deal of signaling cascades, among which is the activation of MMP-9 followed by the degradation of the basal lamina.[52] Using Western blotting, zymography and immunofluorescence staining, the results indicated that EV administration significantly reduced both the protein expression and the activity of MMP-9 compared with the MCAO group. However, there was no significant difference of MMP-2 activities when compared with the sham or the MCAO group (Figure 6E through 6G).

The Evans blue extravasation assay was employed to assess the integrity of the poststroke BBB after EV administration. Evans Blue-Albumin leakage in the brain tissue of the ischemic hemisphere of both stroke mice and nonischemic sham mice was analyzed 24 hours after MCAO. Spectrophotometric analysis revealed a significant increase of Evans Blue concentration in the brain parenchyma of the MCAO group compared with the sham group (Figure 6H). Noteworthy, the Evans Blue concentration in the EV group was significantly lower than in the MCAO group, suggesting an enhanced level of BBB stability due to EV administration. Taken together, EV treatment significantly suppresses MMP-9 activation resulting in reduced BBB leakage in the rodent stroke model.

NPC-EV Administration Represses Early Inflammatory Cell Recruitment in the Postischemic Brain

As mentioned previously, the cellular immune response is a key element in the pathophysiology of ischemic stroke which is closely linked to the opening of the BBB. Since EVs induce BBB protection in the early postischemic brain as shown before, we wondered whether or not EVs had an impact on very early inflammatory cell recruitment in the postischemic brain. Therefore, the brain tissue of the ischemic hemisphere was analyzed by flow cytometry 24 hours after MCAO. The subsets of leukocytes ($CD45^{high}$), T cells ($CD45^{high}CD3^+$), neutrophils ($CD45^{high}Ly6G^+$), B cells ($CD45^{high}CD3^-Ly6G^-CD19^+$), macrophages, monocytes ($CD45^{high}CD3^-Ly6G^-CD11b^+$), and $Ly6C^{high}$ monocytes ($CD45^{high}CD3^-Ly6G^-CD11b^+Ly6C^{high}$) were analyzed. The analysis showed a significantly higher ratio of leukocytes and $Ly6C^{high}$ monocytes as well as a relatively lower ratio of T cells and B cells in the MCAO group in comparison to the sham group. On the contrary, EV treatment significantly reversed the augment of leukocytes and the suppression of T cells and B cells in the MCAO groups. EV administration showed

Figure 5 Continued. recorded by the cellZscopeE apparatus as given in Figure SIIA and SIIB in the Data Supplement. The real-time percentage of maximum TER values after the plateau period were calculated in oxygen glucose deprivation (OGD) and OGD-treated with EVs groups. **F** and **G**, In the co-culture system, statistical analysis of Evans blue-albumin (EBA; large molecule) and Lucifer Yellow (LY; small molecule) permeability coefficients in OGD and OGD-treated with EVs groups were performed. **H**, Statistical analysis of rhodamine 123 accumulation in ECs representing ABCB1 transporter activity was examined in OGD and OGD-treated with EVs groups (n=5 per group). Data are expressed as mean±SD; *P<0.05 and **P<0.01.

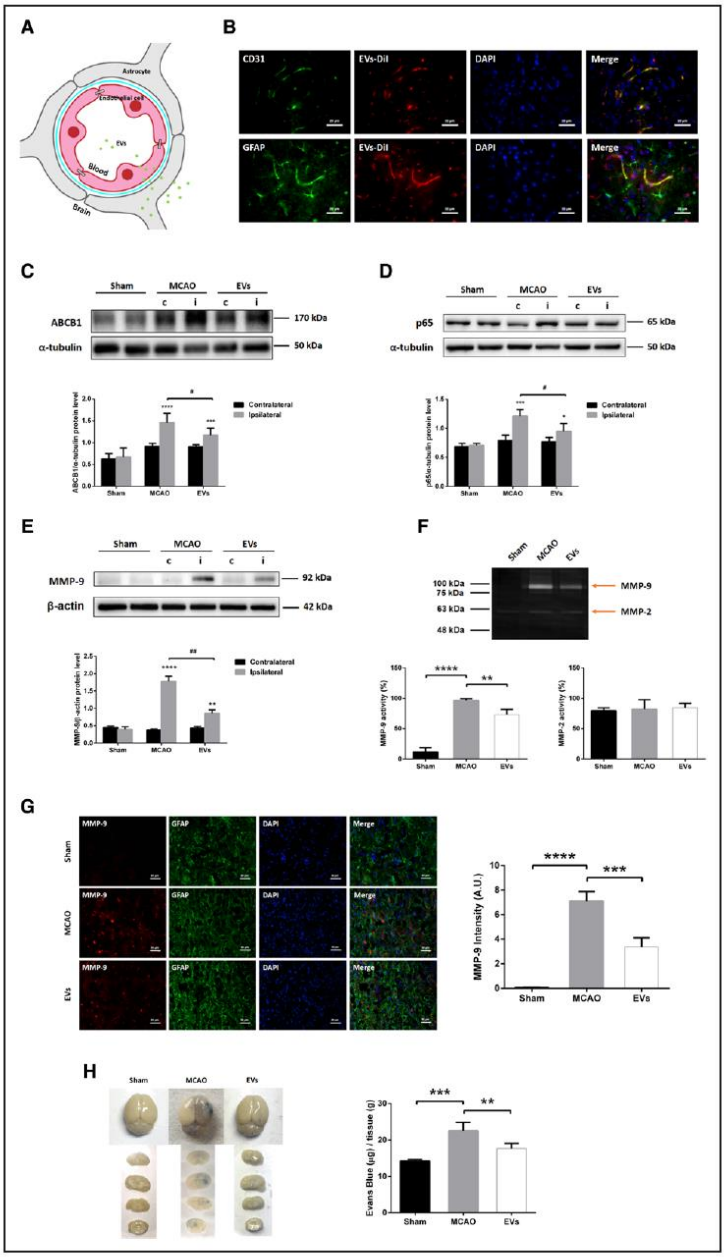

Figure 6. Extracellular vesicle (EV) administration mitigates middle cerebral artery occlusion (MCAO)-induced upregulation of ABCB1 (ATP-binding cassette subfamily B member 1 transporter) and MMP-9 (matrix metalloproteinase 9) as well as activation of NF-κB (nuclear factor-κB) in ischemic microvessels.

Mice were exposed to 60 min of middle cerebral artery (MCA) occlusion followed by 24 h of survival. Sham group mice underwent the surgery procedure without MCA occlusion. Mice were treated with PBS (control and sham) or intravenously treated at the beginning of reperfusion and 6 h later with another EV administration. **A**, In the schematic diagram, EVs reach endothelial cells (ECs), cross (*Continued*)

no effect on the subset of neutrophils (Figure 7). Taken together, these results indicate that EV treatment significantly decreased the infiltration of leukocytes and especially the Ly6C^{high} monocyte invasion into the brain tissue at 24 hours poststroke. On the contrary, the ratio of T cells and B cells in leukocytes were significantly elevated at this early stage due to EV treatment.

DISCUSSION

Using both an in vitro and an in vivo stroke model, the present study analyzed the therapeutic value of NPC-EVs with regard to the stability of the BBB. Focusing on the ABCB1 transporter, our data demonstrate that ABCB1 is upregulated upon induction of hypoxia in the BBB co-culture model and in stroke mice as well. The application of EVs reverses these effects. ABCB1 protein expression is, however, not directly affected by NPC-EVs. Rather, EVs modify the aforementioned protein expression by inhibiting the proinflammatory NF-κB pathway, all of which resulting in reduced activation of MMP-9 and enhanced BBB integrity.

ECs forming the BBB consist of luminal (blood side) and abluminal (brain side) membrane domains. Intercellular tight junction proteins greatly limit both paracellular and transcellular movement of molecules through the EC layer.[53,54] Regulated bidirectional transport of drugs and metabolites is, however, guaranteed by specific transporters such as ABCB1 (P-gp, Mdr-1 [multidrug resistance protein-1]). As a matter of fact, up to 50% of pharmaceutical compounds currently tested are likely to be ABCB1 substrates,[55] and ABCB1 has been repeatedly reported to be regulated under stroke conditions.[7,11,56–58] ABCB1 knockdown models or pharmacological inhibition of the transporter itself result in reduced brain injury under in vivo stroke conditions.[7,13] In line with this, other disease models such as neuroinflammation find increased levels of ABCB1 to be associated with exacerbated brain injury,[8,59,60] emphasizing the role of ABCB1 under pathological brain conditions. The present data of our study, however, do not only further stress the role of ABCB1 but also show a potential means to pharmacologically modulate ABCB1 expression patterns in patients with stroke as well.

Previous research from our group showed that transplanted NPCs induce acute postischemic neuroprotection by stabilizing the BBB.[61] Since adult stem cells like NPCs and others mediate their biological effect by secreting EVs, the latter have been reported to enhance neuroregeneration, neurological recovery, and to modulate neuroinflammation after stroke.[27,29–31] Herein, EVs enhance the BBB stability as suggested by reduced Evans blue leakage and by reduced MMP activity in a rodent stroke model. As such, EV infusion decreases the expression of ABCB1 in the ischemic brain, which is in accordance with our in vitro results.

When stimulated by ischemic stroke, activated astrocytes are an important source of MMP secretion which contributes to the degradation of the basal membrane, thus facilitating BBB breakdown.[52,62–64] Whereas within the first hours after stroke onset both MMP-2 and MMP-9 are responsible for BBB opening, severe disruption of the BBB between 24 hours to 48 hours is primarily associated with an activation of MMP-9 only.[65–67] In accordance with these findings, our study shows an extensive upregulation of MMP-9 within the ischemic hemisphere after 24 hours, whereas MMP-2 remained at its basal level at that time point. Of note, EVs do not significantly modify TER measurements in our in vitro BBB model, nor do they affect ZO-1 protein abundance. Indeed, the TER value depends on tight junction proteins between adjacent ECs. Beside tight junctions, however, the BBB permeability also––and even more so––relies on the endothelial basal membrane.[68,69] Hence, our in vitro data suggest that EVs regulate the permeability of the posthypoxic BBB by preventing the degradation of the basal membrane, rather than enhancing tight junction protein patterns.

Interestingly, MMP-9 is known to be modulated by the NF-κB pathway under stroke conditions[21,70] and previous research of ours demonstrate that transplanted NPCs induce postischemic neuroprotection by inhibiting this pathway.[19] Likewise, additional research from oncology and nonstroke related neurosciences found an interesting connection between ABCB1 and the NF-κB pathway,[17,60,70–73] albeit this relationship has not been described for ECs. The NF-κB pathway, therefore, appears to be an interesting target of EVs under stroke conditions. Whereas OGD exposure yields NF-κB p65 nuclear translocation, EV treatment results in retention of p65 within the cytoplasm. Thus, NPC-EVs indeed suppress the activation of the NF-κB pathway in ECs exposed to OGD, thus repressing the transcription of downstream ABCB1 genes in ECs.

Figure 6 Continued. the blood-brain barrier (BBB), enter end-feet of astrocytes, and arrive in the brain parenchyma outside of microvessels. **B**, EVs labeled with DiI (red) reached ECs of the brain tissue as shown by immunofluorescence staining against CD31 (green). Furthermore, EVs-DiI (red spots) were also detected in the brain parenchyma outside of the microvessels with some positive signaling in astrocytes (GFAP [glial fibrillary acidic protein], green). Scale bars: 20 μm. **C** and **E**, Quantitative analysis of ABCB1, p65, and MMP-9 expression in sham, MCAO, and MCAO treated with EVs by Western blot analysis of the hemisphere microvessels. Western blot was normalized with the housekeeping protein α-tubulin or β-actin (n=5 per group). **F**, Analysis of MMP-9 and MMP-2 activity using gelatin zymography of the ischemic hemisphere or sham hemisphere. **G**, Quantitative analysis of MMP-9 (red) expression by immunofluorescence staining and measurement of fluorescence intensity of the ischemic striatum in the 3 groups. GFAP (green) represents a specific maker of astrocytes. Scale bars: 50 μm. **H**, Analysis of the blood-brain barrier integrity using the Evans blue extravasation assay in ischemic hemispheres of the three groups (n=5 per group). Data are expressed as mean±SD, *P<0.05, **P<0.01, ***P<0.001, ****P<0.0001, #P<0.05 and ##P<0.001.

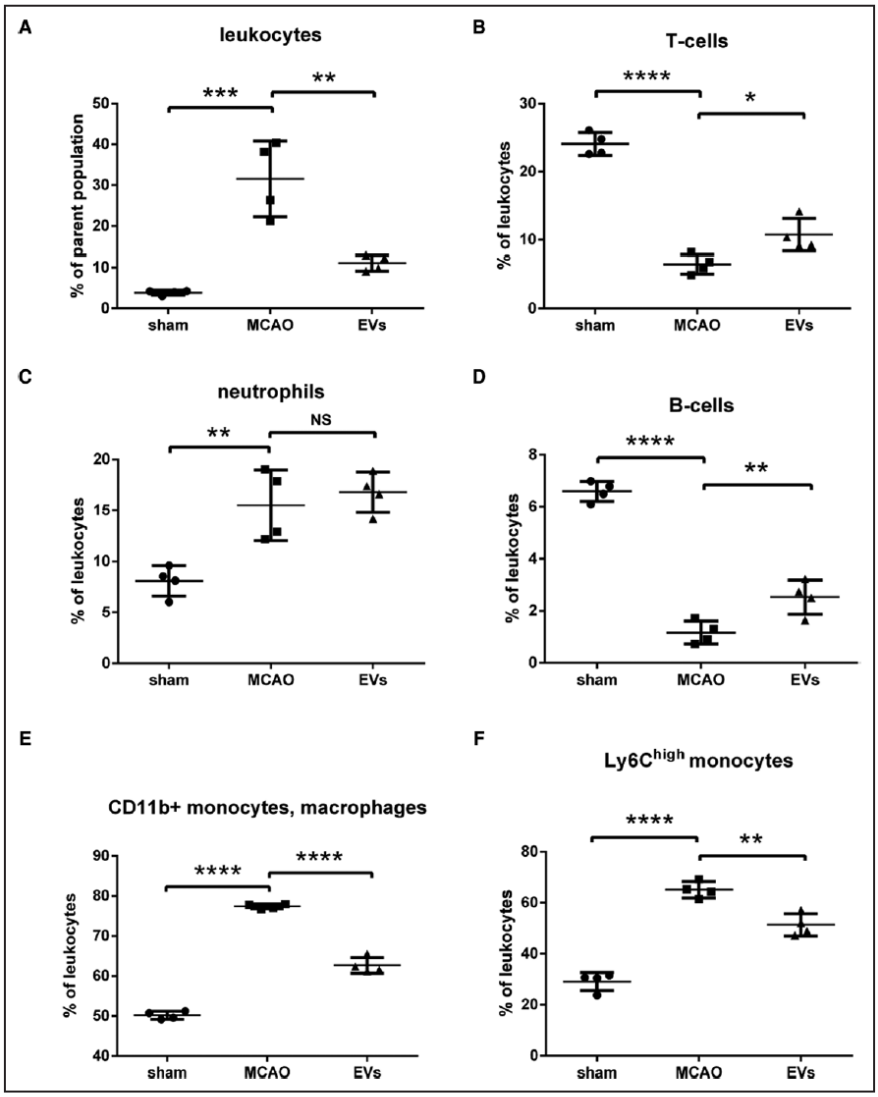

Figure 7. Extracellular vesicles (EVs) decrease postischemic infiltration of leukocyte invasion into the ischemic hemisphere. Flow cytometry of ischemic hemispheres showed a significant decrease of infiltrated total number of leukocytes (**A**), a relative increase of T cells (**B**), a relative increase of B cells (**D**), and a relative decrease of monocytes (**E** and **F**) in the EV treatment group compared with the middle cerebral artery occlusion (MCAO) control group. EVs did not affect the subset of neutrophils (**C**). Data are expressed as mean±SD (n=4 per group). **P*<0.05, ***P*<0.01, ****P*<0.001, and *****P*<0.0001.

Brain-invading leukocytes significantly contribute to early phase secondary ischemic injury after breakdown of the BBB, triggering a sustained inflammatory response.[49,74–76] Consistent with the observed stabilization of the BBB by EV infusion, we report a decreased early infiltration of total numbers of leukocytes, for which significant changes of higher ratios of T cells and B cells as well as a lower ratio of Ly6C^{high} monocytes are found. In this context, emerging evidence suggests that a large number of infiltrated monocytes, especially Ly6C^{high} monocytes, produce proinflammatory cytokines contributing to the early functional impairment after stroke.[77–79]

Likewise, a plethora of studies claim a role of regulatory T cells for secreting cytokines like IL-10 and TGF-β, yielding anti-inflammatory actions under conditions of cerebral ischemia.[80–82] Hence, our data suggest a role of EVs in mediating the infiltration of Ly6C^{high} monocytes and T cells into the ischemic brain. Since previous work suggests ABCB1 in ECs to be involved in the secretion of proinflammatory and chemotactic factors into the extracellular space, inhibiting ABCB1 transporter activity due to EV treatment is an elegant tool to attenuate immune cell recruitment into the brain.

The present study, for the first time, defines a novel way of action for EVs under conditions of cerebral ischemia, demonstrating enhanced BBB integrity due to EV application. We propose that ischemic stroke activates MMP-9 secretion by astrocytes and increases ABCB1 expression in ECs, which are attributed to the activation of the NF-κB signaling pathway. The latter eventually leads to the disruption of the basal membrane and to increased BBB permeability. The application of EVs, however, reverses the aforementioned process by inhibiting the NF-κB pathway, resulting in reduced ABCB1 and MMP-9 activation. These findings provide novel evidence on the therapeutic potential of EVs under conditions of early ischemic BBB injury, which deserve further scientific investigation.

ARTICLE INFORMATION

Received July 12, 2020; accepted December 7, 2020.

Affiliations

Department of Neurology (L.Z., I.G., Y.K., X.Z., M.H., M.S.W., M.B., T.R.D.) and Department of Neuropathology (M.S.W., J.O.), University Medical Center Göttingen, Germany. Sheffield Institute for Translational Neuroscience, University of Sheffield, United Kingdom (A.M.). Istanbul Medipol University, Regenerative and Restorative Medical Research Center, Turkey (E.K., T.R.D.). Department of Neurology, University Hospital Essen, University of Duisburg-Essen, Germany (D.M.H.). Department of Neuroradiology, University Hospital Basel, Switzerland (M.-N.P.).

Acknowledgments

We thank Regine Kruse for excellent technical assistance. This article does not contain any studies with human participants performed by any of the authors. All animal experiments were performed with governmental approval according to the National Institutes of Health guidelines for the care and use of laboratory animals. Both the STAIR (Stroke Therapy Academic Industry Roundtable) criteria and the ARRIVE (Animal Research: Reporting of In Vivo Experiments) guidelines have been followed.

Sources of Funding

L. Zhang thanks the China Scholarship Council for the financial support (No. 201706230260).

Disclosures

None.

REFERENCES

1. Dirnagl U, Iadecola C, Moskowitz MA. Pathobiology of ischaemic stroke: an integrated view. *Trends Neurosci*. 1999;22:391–397. doi: 10.1016/s0166-2236(99)01401-0
2. Abbott NJ, Rönnbäck L, Hansson E. Astrocyte-endothelial interactions at the blood-brain barrier. *Nat Rev Neurosci*. 2006;7:41–53. doi: 10.1038/nrn1824
3. Miller DS. Regulation of ABC transporters blood-brain barrier: the good, the bad, and the ugly. *Adv Cancer Res*. 2015;125:43–70. doi: 10.1016/bs.acr.2014.10.002
4. Felix RA, Barrand MA. P-glycoprotein expression in rat brain endothelial cells: evidence for regulation by transient oxidative stress. *J Neurochem*. 2002;80:64–72. doi: 10.1046/j.0022-3042.2001.00660.x
5. Zhou SF. Structure, function and regulation of P-glycoprotein and its clinical relevance in drug disposition. *Xenobiotica*. 2008;38:802–832. doi: 10.1080/00498250701867889
6. Sanchez-Covarrubias L, Slosky LM, Thompson BJ, Davis TP, Ronaldson PT. Transporters at CNS barrier sites: obstacles or opportunities for drug delivery? *Curr Pharm Des*. 2014;20:1422–1449. doi: 10.2174/13816128113199990463
7. Spudich A, Kilic E, Xing H, Kilic U, Rentsch KM, Wunderli-Allenspach H, Bassetti CL, Hermann DM. Inhibition of multidrug resistance transporter-1 facilitates neuroprotective therapies after focal cerebral ischemia. *Nat Neurosci*. 2006;9:487–488. doi: 10.1038/nn1676
8. Kooij G, Mizee MR, van Horssen J, Reijerkerk A, Witte ME, Drexhage JA, van der Pol SM, van Het Hof B, Scheffer G, Scheper R, et al. Adenosine triphosphate-binding cassette transporters mediate chemokine (C-C motif) ligand 2 secretion from reactive astrocytes: relevance to multiple sclerosis pathogenesis. *Brain*. 2011;134(pt 2):555–570. doi: 10.1093/brain/awq330
9. Patak P, Hermann DM. ATP-binding cassette transporters at the blood-brain barrier in ischaemic stroke. *Curr Pharm Des*. 2011;17:2787–2792. doi: 10.2174/138161211797440195
10. DeMars KM, Yang C, Hawkins KE, McCrea AO, Siwarski DM, Candelario-Jalil E. Spatiotemporal changes in P-glycoprotein levels in brain and peripheral tissues following ischemic stroke in rats. *J Exp Neurosci*. 2017;11:1179069517701741. doi: 10.1177/1179069517701741
11. ElAli A, Hermann DM. Liver X receptor activation enhances blood-brain barrier integrity in the ischemic brain and increases the abundance of ATP-binding cassette transporters ABCB1 and ABCC1 on brain capillary cells. *Brain Pathol*. 2012;22:175–187. doi: 10.1111/j.1750-3639.2011.00517.x
12. Hermann DM. Future Perspectives for brain pharmacotherapies: implications of drug transport processes at the blood-brain barrier. *Ther Adv Neurol Disord*. 2008;1:167–179. doi: 10.1177/1756285608097775
13. Murozono M, Matsumoto S, Okada S, Nagaoka D, Isshiki A, Watanabe Y. Reduction of brain infarction induced by a transient brain ischemia in mdr1a knockout mice. *Neurochem Res*. 2009;34:1555–1561. doi: 10.1007/s11064-009-9943-6
14. Lakhan SE, Kirchgessner A, Tepper D, Leonard A. Matrix metalloproteinases and blood-brain barrier disruption in acute ischemic stroke. *Front Neurol*. 2013;4:32. doi: 10.3389/fneur.2013.00032
15. Andersson P, Yang Y, Hosaka K, Zhang Y, Fischer C, Braun H, Liu S, Yu G, Liu S, Beyaert R, et al. Molecular mechanisms of IL-33-mediated stromal interactions in cancer metastasis. *JCI Insight*. 2018;3:e122375. doi: 10.1172/jci.insight.122375
16. Chiu CT, Chen JH, Chou FP, Lin HH. Hibiscus sabdariffa leaf extract inhibits human prostate cancer cell invasion via down-regulation of Akt/NF-kB/MMP-9 pathway. *Nutrients*. 2015;7:5065–5087. doi: 10.3390/nu7075065
17. Katayama K, Noguchi K, Sugimoto Y. Regulations of P-glycoprotein/ABCB1/MDR1in human cancer cells. *N J Sci*. 2014;2014:1–10. doi: 10.1042/BCJ20190736
18. Nakanishi C, Toi M. Nuclear factor-kappaB inhibitors as sensitizers to anticancer drugs. *Nat Rev Cancer*. 2005;5:297–309. doi: 10.1038/nrc1588
19. Doeppner TR, Kaltwasser B, Fengyan J, Hermann DM, Bähr M. TAT-Hsp70 induces neuroprotection against stroke via anti-inflammatory actions providing appropriate cellular microenvironment for transplantation of neural precursor cells. *J Cereb Blood Flow Metab*. 2013;33:1778–1788. doi: 10.1038/jcbfm.2013.126
20. Harari OA, Liao JK. NF-κB and innate immunity in ischemic stroke. *Ann N Y Acad Sci*. 2010;1207:32–40. doi: 10.1111/j.1749-6632.2010.05735.x
21. Lv Y, Liu W, Ruan Z, Xu Z, Fu L. Myosin IIA regulated tight junction in oxygen glucose-deprived brain endothelial cells via activation of TLR4/PI3K/Akt/JNK1/2/14-3-3ε/NF-κB/MMP9 signal transduction pathway. *Cell Mol Neurobiol*. 2019;39:301–319. doi: 10.1007/s10571-019-00654-y
22. Ridder DA, Schwaninger M. NF-kappaB signaling in cerebral ischemia. *Neuroscience*. 2009;158:995–1006. doi: 10.1016/j.neuroscience.2008.07.007
23. Mathivanan S, Fahner CJ, Reid GE, Simpson RJ. ExoCarta 2012: database of exosomal proteins, RNA and lipids. *Nucleic Acids Res*. 2012;40(Database issue):D1241–D1244. doi: 10.1093/nar/gkr828
24. Théry C, Witwer KW, Aikawa E, Alcaraz MJ, Anderson JD, Andriantsitohaina R, Antoniou A, Arab T, Archer F, Atkin-Smith GK, et al. Minimal information for studies of extracellular vesicles 2018 (MISEV2018): a position

statement of the International Society for Extracellular Vesicles and update of the MISEV2014 guidelines. *J Extracell Vesicles*. 2018;7:1535750. doi: 10.1080/20013078.2018.1535750
25. Kim DK, Kang B, Kim OY, Choi DS, Lee J, Kim SR, Go G, Yoon YJ, Kim JH, Jang SC, et al. EVpedia: an integrated database of high-throughput data for systemic analyses of extracellular vesicles. *J Extracell Vesicles*. 2013;2:1–7. doi: 10.3402/jev.v2i0.20384
26. Go V, Bowley BGE, Pessina MA, Zhang ZG, Chopp M, Finklestein SP, Rosene DL, Medalla M, Buller B, Moore TL. Extracellular vesicles from mesenchymal stem cells reduce microglial-mediated neuroinflammation after cortical injury in aged Rhesus monkeys. *Geroscience*. 2020;42:1–17. doi: 10.1007/s11357-019-00115-w
27. Dabrowska S, Andrzejewska A, Strzemecki D, Muraca M, Janowski M, Lukomska B. Human bone marrow mesenchymal stem cell-derived extracellular vesicles attenuate neuroinflammation evoked by focal brain injury in rats. *J Neuroinflammation*. 2019;16:216. doi: 10.1186/s12974-019-1602-5
28. Bang OY, Kim EH. Mesenchymal stem cell-derived extracellular vesicle therapy for stroke: challenges and progress. *Front Neurol*. 2019;10:211. doi: 10.3389/fneur.2019.00211
29. Webb RL, Kaiser EE, Scoville SL, Thompson TA, Fatima S, Pandya C, Sriram K, Swetenburg RL, Vaibhav K, Arbab AS, et al. Human neural stem cell extracellular vesicles improve tissue and functional recovery in the murine thromboembolic stroke model. *Transl Stroke Res*. 2018;9:530–539. doi: 10.1007/s12975-017-0599-2
30. Anderson JD, Johansson HJ, Graham CS, Vesterlund M, Pham MT, Bramlett CS, Montgomery EN, Mellema MS, Bardini RL, Contreras Z, et al. Comprehensive proteomic analysis of mesenchymal stem cell exosomes reveals modulation of angiogenesis via nuclear factor-kappaB signaling. *Stem Cells*. 2016;34:601–613. doi: 10.1002/stem.2298
31. Zheng X, Zhang L, Kuang Y, Venkataramani V, Jin F, Hein K, Zafeiriou MP, Lenz C, Moebius W, Kilic E, et al. Extracellular vesicles derived from neural progenitor cells--a preclinical evaluation for stroke treatment in mice [published online May 2, 2020]. *Transl Stroke Res*. doi: 10.1007/s12975-020-00814-z
32. Maacha S, Sidahmed H, Jacob S, Gentilcore G, Calzone R, Grivel JC, Cugno C. Paracrine mechanisms of mesenchymal stromal cells in angiogenesis. *Stem Cells Int*. 2020;2020:4356359. doi: 10.1155/2020/4356359
33. Assmann JC, Muller K, Wenzel J, Walther T, Brands J, Thornton P, Allan SM, Schwaninger M. Isolation and cultivation of primary brain endothelial cells from adult mice. *Bio Protoc*. 2017;7:e2294. doi: 10.21769/BioProtoc.2294
34. Schildge S, Bohrer C, Beck K, Schachtrup C. Isolation and culture of mouse cortical astrocytes. *J Vis Exp*. 2013;71:50079. doi: 10.3791/50079
35. Ludwig AK, De Miroschedji K, Doeppner TR, Börger V, Ruesing J, Rebmann V, Durst S, Jansen S, Bremer M, Behrmann E, et al. Precipitation with polyethylene glycol followed by washing and pelleting by ultracentrifugation enriches extracellular vesicles from tissue culture supernatants in small and large scales. *J Extracell Vesicles*. 2018;7:1528109. doi: 10.1080/20013078.2018.1528109
36. Riss TL, Moravec RA, Niles AL, Duellman S, Benink HA, Worzella TJ, Minor L. *Assay Guidance Manual*. Eli Lilly & Company and the National Center for Advancing Translational Sciences; 2004.
37. Maherally Z, Fillmore HL, Tan SL, Tan SF, Jassam SA, Quack FI, Hatherell KE, Pilkington GJ. Real-time acquisition of transendothelial electrical resistance in an all-human, *in vitro*, 3-dimensional, blood-brain barrier model exemplifies tight-junction integrity. *FASEB J*. 2018;32:168–182. doi: 10.1096/fj.201700162R
38. Eigenmann DE, Xue G, Kim KS, Moses AV, Hamburger M, Oufir M. Comparative study of four immortalized human brain capillary endothelial cell lines, hCMEC/D3, hBMEC, TY10, and BB19, and optimization of culture conditions, for an *in vitro* blood-brain barrier model for drug permeability studies. *Fluids Barriers CNS*. 2013;10:33. doi: 10.1186/2045-8118-10-33
39. Czupalla CJ, Liebner S, Devraj K. *In vitro* models of the blood-brain barrier. *Methods Mol Biol*. 2014;1135:415–437. doi: 10.1007/978-1-4939-0320-7_34
40. Kuzmanov I, Herrmann AM, Galla HJ, Meuth SG, Wiendl H, Klotz L. An in vitro model of the blood-brain barrier using impedance spectroscopy: a focus on T cell-endothelial cell interaction. *J Vis Exp*. 2016;118:54592. doi: 10.3791/54592
41. Takata F, Dohgu S, Yamauchi A, Matsumoto J, Machida T, Fujishita K, Shibata K, Shinozaki Y, Sato K, Kataoka Y, et al. *In vitro* blood-brain barrier models using brain capillary endothelial cells isolated from neonatal and adult rats retain age-related barrier properties. *PLoS One*. 2013;8:e55166. doi: 10.1371/journal.pone.0055166
42. Yang S, Jin H, Zhao Z. Paracellular tightness and the functional expression of efflux transporters P-gp and BCRP in bEnd3 cells. *Neurol Res*. 2018;40:644–649. doi: 10.1080/01616412.2018.1460701
43. Watson PM, Paterson JC, Thom G, Ginman U, Lundquist S, Webster CI. Modelling the endothelial blood-CNS barriers: a method for the production of robust *in vitro* models of the rat blood-brain barrier and blood-spinal cord barrier. *BMC Neurosci*. 2013;14:59. doi: 10.1186/1471-2202-14-59
44. Dehouck MP, Jolliet-Riant P, Brée F, Fruchart JC, Cecchelli R, Tillement JP. Drug transfer across the blood-brain barrier: correlation between *in vitro* and *in vivo* models. *J Neurochem*. 1992;58:1790–1797. doi: 10.1111/j.1471-4159.1992.tb10055.x
45. Radu M, Chernoff J. An in vivo assay to test blood vessel permeability. *J Vis Exp*. 2013;73:e50062. doi: 10.3791/50062
46. Doeppner TR, Kaltwasser B, ElAli A, Zechariah A, Hermann DM, Bähr M. Acute hepatocyte growth factor treatment induces long-term neuroprotection and stroke recovery via mechanisms involving neural precursor cell proliferation and differentiation. *J Cereb Blood Flow Metab*. 2011;31:1251–1262. doi: 10.1038/jcbfm.2010.211
47. Hu X, Beeton C. Detection of functional matrix metalloproteinases by zymography. *J Vis Exp*. 2010;45:2445. doi: 10.3791/2445
48. Zhang JW, Gottschall PE. Zymographic measurement of gelatinase activity in brain tissue after detergent extraction and affinity-support purification. *J Neurosci Methods*. 1997;76:15–20. doi: 10.1016/s0165-0270(97)00065-4
49. Posel C, Moller K, Boltze J, Wagner DC, Weise G. Isolation and flow cytometric analysis of immune cells from the ischemic mouse brain. *J Vis Exp*. 2016;108:53658. doi: 10.3791/53658
50. Li M, van Esch BCAM, Wagenaar GTM, Garssen J, Folkerts G, Henricks PAJ. Pro- and anti-inflammatory effects of short chain fatty acids on immune and endothelial cells. *Eur J Pharmacol*. 2018;831:52–59. doi: 10.1016/j.ejphar.2018.05.003
51. Lee BK, Lee WJ, Jung YS. Chrysin attenuates VCAM-1 expression and monocyte adhesion in lipopolysaccharide-stimulated brain endothelial cells by preventing NF-kappaB signaling. *Int J Mol Sci*. 2017;18:1424. doi: 10.3390/ijms18071424
52. Rempe RG, Hartz AMS, Bauer B. Matrix metalloproteinases in the brain and blood-brain barrier: versatile breakers and makers. *J Cereb Blood Flow Metab*. 2016;36:1481–1507. doi: 10.1177/0271678X16655551
53. Luissint AC, Artus C, Glacial F, Ganeshamoorthy K, Couraud PO. Tight junctions at the blood brain barrier: physiological architecture and disease-associated dysregulation. *Fluids Barriers CNS*. 2012;9:23. doi: 10.1186/2045-8118-9-23
54. Sandoval KE, Witt KA. Blood-brain barrier tight junction permeability and ischemic stroke. *Neurobiol Dis*. 2008;32:200–219. doi: 10.1016/j.nbd.2008.08.005
55. Abbott NJ, Khan EU, Rollinson CM, Reichel A, Janigro D, Dombrowski SM, Dobbie MS, Begley DJ. Drug resistance in epilepsy: the role of the blood-brain barrier. *Novartis Found Symp*. 2002;243:38–47.
56. Cen J, Liu L, Li MS, He L, Wang LJ, Liu YQ, Liu M, Ji BS. Alteration in P-glycoprotein at the blood-brain barrier in the early period of MCAO in rats. *J Pharm Pharmacol*. 2013;65:665–672. doi: 10.1111/jphp.12033
57. Qosa H, Miller DS, Pasinelli P, Trotti D. Regulation of ABC efflux transporters at blood-brain barrier in health and neurological disorders. *Brain Res*. 2015;1628(Pt B):298–316. doi: 10.1016/j.brainres.2015.07.005
58. Ji BS, Cen J, He L, Liu M, Liu YQ, Liu L. Modulation of P-glycoprotein in rat brain microvessel endothelial cells under oxygen glucose deprivation. *J Pharm Pharmacol*. 2013;65:1508–1517. doi: 10.1111/jphp.12122
59. Kooij G, Backer R, Koning JJ, Reijerkerk A, van Horssen J, van der Pol SM, Drexhage J, Schinkel A, Dijkstra CD, den Haan JM, et al. P-glycoprotein acts as an immunomodulator during neuroinflammation. *PLoS One*. 2009;4:e8212. doi: 10.1371/journal.pone.0008212
60. Bauer B, Hartz AM, Miller DS. Tumor necrosis factor alpha and endothelin-1 increase P-glycoprotein expression and transport activity at the blood-brain barrier. *Mol Pharmacol*. 2007;71:667–675. doi: 10.1124/mol.106.029512
61. Doeppner TR, Kaltwasser B, Teli MK, Bretschneider E, Bähr M, Hermann DM. Effects of acute versus post-acute systemic delivery of neural progenitor cells on neurological recovery and brain remodeling after focal cerebral ischemia in mice. *Cell Death Dis*. 2014;5:e1386. doi: 10.1038/cddis.2014.359
62. Turner RJ, Sharp FR. Implications of MMP9 for blood brain barrier disruption and hemorrhagic transformation following ischemic stroke. *Front Cell Neurosci*. 2016;10:56. doi: 10.3389/fncel.2016.00056
63. Yang C, Candelario-Jalil E. Role of matrix metalloproteinases in brain edema. *Brain Edema*. 2017:199–215.
64. Song J, Wu C, Korpos E, Zhang X, Agrawal SM, Wang Y, Faber C, Schäfers M, Körner H, Opdenakker G, et al. Focal MMP-2 and MMP-9 activity at the blood-brain barrier promotes chemokine-induced leukocyte migration. *Cell Rep*. 2015;10:1040–1054. doi: 10.1016/j.celrep.2015.01.037

65. Suofu Y, Clark JF, Broderick JP, Kurosawa Y, Wagner KR, Lu A. Matrix metalloproteinase-2 or -9 deletions protect against hemorrhagic transformation during early stage of cerebral ischemia and reperfusion. *Neuroscience*. 2012;212:180–189. doi: 10.1016/j.neuroscience.2012.03.036
66. Fujimura M, Gasche Y, Morita-Fujimura Y, Massengale J, Kawase M, Chan PH. Early appearance of activated matrix metalloproteinase-9 and blood-brain barrier disruption in mice after focal cerebral ischemia and reperfusion. *Brain Res*. 1999;842:92–100. doi: 10.1016/s0006-8993(99)01843-0
67. Park KP, Rosell A, Foerch C, Xing C, Kim WJ, Lee S, Opdenakker G, Furie KL, Lo EH. Plasma and brain matrix metalloproteinase-9 after acute focal cerebral ischemia in rats. *Stroke*. 2009;40:2836–2842. doi: 10.1161/STROKEAHA.109.554824
68. Weber CR. Dynamic properties of the tight junction barrier. *Ann N Y Acad Sci*. 2012;1257:77–84. doi: 10.1111/j.1749-6632.2012.06528.x
69. Almutairi MM, Gong C, Xu YG, Chang Y, Shi H. Factors controlling permeability of the blood-brain barrier. *Cell Mol Life Sci*. 2016;73:57–77. doi: 10.1007/s00018-015-2050-8
70. Wang Z, Leng Y, Tsai LK, Leeds P, Chuang DM. Valproic acid attenuates blood-brain barrier disruption in a rat model of transient focal cerebral ischemia: the roles of HDAC and MMP-9 inhibition. *J Cereb Blood Flow Metab*. 2011;31:52–57. doi: 10.1038/jcbfm.2010.195
71. Qosa H, Lichter J, Sarlo M, Markandaiah SS, McAvoy K, Richard JP, Jablonski MR, Maragakis NJ, Pasinelli P, Trotti D. Astrocytes drive upregulation of the multidrug resistance transporter ABCB1 (P-glycoprotein) in endothelial cells of the blood-brain barrier in mutant superoxide dismutase 1-linked amyotrophic lateral sclerosis. *Glia*. 2016;64:1298–1313. doi: 10.1002/glia.23003
72. Zhang J, Zhang M, Sun B, Li Y, Xu P, Liu C, Liu L, Liu X. Hyperammonemia enhances the function and expression of P-glycoprotein and Mrp2 at the blood-brain barrier through NF-κB. *J Neurochem*. 2014;131:791–802. doi: 10.1111/jnc.12944
73. Yu C, Argyropoulos G, Zhang Y, Kastin AJ, Hsuchou H, Pan W. Neuroinflammation activates Mdr1b efflux transport through NFkappaB: promoter analysis in BBB endothelia. *Cell Physiol Biochem*. 2008;22:745–756. doi: 10.1159/000185558
74. Iadecola C, Anrather J. The immunology of stroke: from mechanisms to translation. *Nat Med*. 2011;17:796–808. doi: 10.1038/nm.2399
75. Courties G, Herisson F, Sager HB, Heidt T, Ye Y, Wei Y, Sun Y, Severe N, Dutta P, Scharff J, et al. Ischemic stroke activates hematopoietic bone marrow stem cells. *Circ Res*. 2015;116:407–417. doi: 10.1161/CIRCRESAHA.116.305207
76. Möller K, Boltze J, Pösel C, Seeger J, Stahl T, Wagner DC. Sterile inflammation after permanent distal MCA occlusion in hypertensive rats. *J Cereb Blood Flow Metab*. 2014;34:307–315. doi: 10.1038/jcbfm.2013.199
77. Gliem M, Mausberg AK, Lee JI, Simiantonakis I, van Rooijen N, Hartung HP, Jander S. Macrophages prevent hemorrhagic infarct transformation in murine stroke models. *Ann Neurol*. 2012;71:743–752. doi: 10.1002/ana.23529
78. Hammond MD, Taylor RA, Mullen MT, Ai Y, Aguila HL, Mack M, Kasner SE, McCullough LD, Sansing LH. CCR2+ Ly6C(hi) inflammatory monocyte recruitment exacerbates acute disability following intracerebral hemorrhage. *J Neurosci*. 2014;34:3901–3909. doi: 10.1523/JNEUROSCI.4070-13.2014
79. ElAli A, Jean LeBlanc N. The role of monocytes in ischemic stroke pathobiology: new avenues to explore. *Front Aging Neurosci*. 2016;8:29. doi: 10.3389/fnagi.2016.00029
80. Chamorro Á, Meisel A, Planas AM, Urra X, van de Beek D, Veltkamp R. The immunology of acute stroke. *Nat Rev Neurol*. 2012;8:401–410. doi: 10.1038/nrneurol.2012.98
81. Sakaguchi S, Yamaguchi T, Nomura T, Ono M. Regulatory T cells and immune tolerance. *Cell*. 2008;133:775–787. doi: 10.1016/j.cell.2008.05.009
82. Liesz A, Suri-Payer E, Veltkamp C, Doerr H, Sommer C, Rivest S, Giese T, Veltkamp R. Regulatory T cells are key cerebroprotective immunomodulators in acute experimental stroke. *Nat Med*. 2009;15:192–199. doi: 10.1038/nm.1927

5.2 Supplement Materials and Methods

EV characterization and purification of NPC-EVs

Transmission electron microscopy (TEM) was used to investigate the microstructure of NPC-EVs. Briefly, formvar-coated TEM grids (copper, 150 hexagonal mesh, Science Services, Munich, Germany) were put on the top of a droplet of the respective EV fraction and incubated for 10 min. Then, the grids were washed and incubated with ultrapure water. For contrast, the grids were incubated for 5 min on droplets of uranylacetate-oxalate, followed by a 5-min incubation on droplets of a 1:9 dilution of 4 % uranylacetate in 2 % methylcellulose. After draining the methylcellulose from the grids using a filter paper and drying of the methylcellulose film as previously described, samples were imaged with a LEO912 transmission electron microscope (Carl Zeiss Microscopy, Oberkochen, Germany) and images were taken using an onaxis 2k CCD camera (TRS-STAR, Stutensee, Germany).

The characterization of EVs was confirmed by measuring expression of specific markers Alix and Tsg101, and EV-associated protein markers CD63, CD81 and CD9 by Western blot analysis. For both size determination and quantification analysis of enriched NPC-EVs, a nanoparticle tracking analysis (NTA) was performed using the Nanosight platform (NanoSight LM10, Malvern Panalytical, Kassel, Germany). As shown previously (Sokolova et al. 2011), 1:1,000 PBS-diluted samples were measured in duplicate, and 400 µl of the diluted sample were injected into the measurement chamber. Each sample was measured three times, and the length of the video of each measurement was set to 30 s.

In addition, we further examined the characteristics of EVs using iodixanol gradient centrifugation as reported by Kowal et al. (2016). The discontinuous iodixanol gradients were prepared by diluting a stock solution of OptiPrepTM (60 % w/v; STEMCELL Technologies, Vancouver, Canada) with 0.25 M sucrose/10 mM Tris, pH 7.5 to generate 30 %, 20 % and 10 % (wt/vol) iodixanol solutions. The EV pellets were resuspended in the 30 % iodixanol solution, and the overlaid gradient solution (20 % and 10 % iodixanol solution) were loaded on the top subsequently. After ultracentrifugation, ten fractions (F1-F10) were recovered, washed with PBS and recentrifuged at 110,000 g for 2 h. The resulting pellets were resuspended in PBS and analyzed for protein concentration and the presence of EV markers in both pellets.

Quantitative Proteomic Analysis of NPC-EVs

Mass spectrometric analyses were performed by the Core Facility Proteomics at the University Medical Center Göttingen. Samples were reconstituted in 1x NuPAGE LDS Sample Buffer (Invitrogen) and run into 4-12 % NuPAGE Novex Bis-Tris Minigels (Invitrogen) for 1 cm distance. Gels were stained with Coomassie Blue for visualization purposes, and each sample cut out as a whole and diced. After washing, gel slices were reduced with dithiothreitol (DTT), alkylated with 2-iodoacetamide and digested with Endopeptidase Trypsin (sequencing grade, Promega) overnight. The resulting peptide mixtures were then extracted, dried in a SpeedVac,

reconstituted in 2 % acetonitrile/0.1 % formic acid/ (v:v) and prepared for nanoLC-MS/MS as described previously (Atanassov and Urlaub 2013).

For mass spectrometric analysis samples were enriched on a self-packed reversed phase-C18 precolumn (0.15 mm ID x 20 mm, Reprosil-Pur120 C18-AQ 5 µm, Dr. Maisch, Ammerbuch-Entringen, Germany) and separated on an analytical reversed phase-C18 column (0.075 mm ID x 200 mm, Reprosil-Pur 120 C18-AQ, 3 µm, Dr. Maisch) using a 30 min linear gradient of 5-35 % acetonitrile/0.1 % formic acid (v:v) at 300 nl min-1). The eluent was analyzed on a Q Exactive hybrid quadrupole/orbitrap mass spectrometer (ThermoFisher Scientific, Dreieich, Germany) equipped with a FlexIon nanoSpray source and operated under Excalibur 2.4 software using a data-dependent acquisition method. Each experimental cycle was of the following form: one full MS scan across the 350-1600 m/z range was acquired at a resolution setting of 70,000 FWHM, and AGC target of 1*10e6 and a maximum fill time of 60 ms. Up to the 12 most abundant peptide precursors of charge states 2 to 5 above a 2*10e4 intensity threshold were then sequentially isolated at 2.0 FWHM isolation width, fragmented with nitrogen at a normalized collision energy setting of 25 %, and the resulting product ion spectra recorded at a resolution setting of 17,500 FWHM, and AGC target of 2*10e5 and a maximum fill time of 60 ms. Selected precursor m/z values were then excluded for the following 15 s. Two technical replicates per sample were acquired.

Raw data were processed using MaxQuant Software version 1.5.7.4 (Max Planck Institute for Biochemistry, Martinsried, Germany). Proteins were identified against the UniProtKB mouse reference proteome (v2020.10, 55.466 protein entries) along with a set of common lab contaminants. The search was performed with trypsine (excluding proline-proximal cleavage sites) as enzyme and iodoacetamide as cysteine blocking agent. Up to two missed tryptic cleavages were allowed for, and methionine oxidation and protein N-terminal acetylation variable modifications. Instrument type 'Orbitrap' was selected to adjust for MS acquisition specifics. Following an initial internal recalibration, this translated into an MS mass tolerance of 4.5 ppm and an MS/MS mass tolerance of 20 ppm. Protein and peptide results lists were thresholded at False Discovery Rates (FDR) of 0.01, respectively, using a forward-and-reverse decoy database approach. The Arginine R10 and Lysine K8 labels including the 'Re-quantify' option were specified for relative protein quantitation. Perseus Software version 1.5.6.0 (Max Planck Institute for Biochemistry, Martinsried, Germany) was used to obtain relative protein intensity values from the MaxQuant Software results.

5.3 Resources Tables

Table 1: Antibodies

Reagent	Source	Identifier	Application
ZO1	Abcam, UK	ab96587	0.5 µg/ml (for western blot, WB) 2 µg/ml (for immunofluorescence staining, IF)
ABCB1	Abcam, UK	ab170904	0.5 µg/ml (for WB)
NF-kB p65	Abcam, UK	ab16502	0.5 µg/ml (for WB) 2 µg/ml (for IF)
α-tubulin	GeneTex, USA	GTX628802	0.1 µg/ml (for WB)
IκBα	Cell Signaling Technology, USA	#9242	0.5 µg/ml (for WB)
GAPDH	GeneTex, USA	GTX627408	0.1 µg/ml (for WB)
Histone H3	Cell Signaling Technology, USA	#4499	0.5 µg/ml (for WB)
β-actin	Abcam, UK	ab6276	0.2 µg/ml (for WB)
Alix	BD Biosciences, USA	611620	0.5 µg/ml (for WB)
CD63	Biorbyt, UK	orb11317	0.5 µg/ml (for WB)
CD81	Abcam, UK	ab155760	0.5 µg/ml (for WB)
CD9	Abcam, UK	ab92726	0.5 µg/ml (for WB)
Tsg101	GeneTex, USA	GTX70255	1 µg/ml (for WB)
MMP-9	Abcam, UK	ab38898	0.5 µg/ml (for WB) 5 µg/ml (for IF)
CD31	Santa Cruz Biotechnology, USA	SC-18916	0.5 µg/ml (for WB) 5 µg/ml (for IF)
GFAP	Sigma-Aldrich, USA	G9269	0.5 µg/ml (for WB)
GFAP	Thermo Fisher Scientific, USA	13-0300	5 µg/ml (for IF)
S100B	Abcam, UK	ab52642	5 µg/ml (for IF)
CD3	BD Biosciences, USA	555275	20 µg/ml (for fluorescence-activated cell sorting, FACS)
Ly6C	BD Biosciences, USA	560594	20 µg/ml (for FACS)
CD45	BD Biosciences, USA	563891	20 µg/ml (for FACS)

Reagent	Source	Identifier	Application
Ly6G	BioLegend, USA	127606	20 µg/ml (for FACS)
CD19	BD Biosciences, USA	550992	20 µg/ml (for FACS)
CD11b	BD Biosciences, USA	552850	20 µg/ml (for FACS)

WB: Western Blot

IF: Immunofluorescence Staining

FACS: Fluorescence-activated Cell Sorting

Table 2: Chemicals and Recombinant Proteins

Reagent	Source	Identifier	Application
Collagen IV	Corning, USA	354233	56 µl collagen IV + 944 µl 0.05 N HCl
Dextran MW 60,000-90,000	Alfa Aesar, USA	J14495	5.4 g dextran in 30 ml PBS
Plasma-derived bovine serum (PDS)	First Link, UK	60-00-810	10 ml PDS in 50 ml medium
L-glutamine	Thermo Fisher Scientific, USA	25030024	100 µl L-glutamine in 10 ml medium
Heparin-sodium	Ratiopharm, Germany	PZN 003029843	150 µl heparin in 50 ml medium
Puromycin	Sigma-Aldrich, USA	P8833	32 µl puromycin in 1 ml medium
Antibiotic/antimycotic (100x)	Thermo Fisher Scientific, USA	15240062	100 µl AA in 10 ml medium
Nα-Tosyl-L-lysine chloromethyl ketone hydrochloride (TLCK)	Sigma-Aldrich, USA	90182	100 µl TLCK in 10 ml medium
Endothelial cell growth supplement (ECGS)	Sigma-Aldrich, USA	E2759	500 µl ECGS in 50 ml medium
Trypsin-EDTA 0.25%	Thermo Fisher Scientific, USA	25200-056	undiluted
Poly-D-lysine	Sigma-Aldrich, USA	P6407	5mg PDL in 50 ml H_2O (0.1 mg/mL)
Coomassie Blue	Sigma-Aldrich, USA	B0770	0.1 % Coomassie Blue with 40 % methanol and 10 % acetic acid

Reagent	Source	Identifier	Application
Penicillin/streptomycin	Thermo Fisher Scientific, USA	15140122	500 µl pen/strep in 50 ml medium
B27	Thermo Fisher Scientific, USA	17504001	1ml B27 in 50 ml medium
EGF	PeproTech, USA	AF-100-15	100 µg EGF in 50ml PBS with 0.1 % BSA
FGF-2	PeproTech, USA	100-18B	100 µg FGF-2 in 50ml PBS with 0.1 % BSA
Polyethylene glycol 6000	Sigma-Aldrich, USA	8074911000	20g Peg6000 in 200 ml H_2O with 75 mM NaCl
DiI	Thermo Fisher Scientific, USA	D3911	10 µM in DMSO
Evans blue dye	Sigma-Aldrich, USA	E2129	0.67 mg/ml in permeability assay buffer with 4 % BSA
Lucifer Yellow	Sigma-Aldrich, USA	L0259	50 µM LY in permeability assay buffer
Rhodamine 123	Sigma-Aldrich, USA	83702	5 mM R123 in the permeability assay buffer
Sepharose 4B	Merck KGaA, Germany	GE17-0956-01	100 µl Sepharose 4B in 1 ml lysis buffer
Gelatin	Sigma-Aldrich, USA	G9391	0.1 % gelatin in 8 % polyacrylamide gel
DAPI	AppliChem, Germany	A1001	1 µg/ml in PBS/TBS

5.4 Supplement Data I

The results about quantitative proteomic analysis results of NPC-EVs in a xlsx. file can be reached at: https://www.ahajournals.org/doi/suppl/10.1161/ATVBAHA.120.315031.

6 References

Abbott NJ, Ronnback L, Hansson E (2006): Astrocyte-endothelial interactions at the blood-brain barrier. Nat Rev Neurosci 7, 41-53

Abbott NJ, Patabendige AA, Dolman DE, Yusof SR, Begley DJ (2010): Structure and function of the blood-brain barrier. Neurobiol Dis 37, 13-25

Abbott NJ, Khan EU, Rollinson CM, Reichel A, Janigro D, Dombrowski SM, Dobbie MS, Begley DJ (2002): Drug resistance in epilepsy: the role of the blood-brain barrier. Novartis Found Symp 243, 38-53

Almutairi MM, Gong C, Xu YG, Chang Y, Shi H (2016): Factors controlling permeability of the blood-brain barrier. Cell Mol Life Sci 73, 57-77

Anderson JD, Johansson HJ, Graham CS, Vesterlund M, Pham MT, Bramlett CS, Montgomery EN, Mellema MS, Bardini RL, Contreras Z, et al. (2016): Comprehensive Proteomic Analysis of Mesenchymal Stem Cell Exosomes Reveals Modulation of Angiogenesis via Nuclear Factor-KappaB Signaling. Stem Cells 34, 601-613

Andres RH, Horie N, Slikker W, Keren-Gill H, Zhan K, Sun G, Manley NC, Pereira MP, Sheikh LA, McMillan EL, et al. (2011): Human neural stem cells enhance structural plasticity and axonal transport in the ischaemic brain. Brain 134, 1777-1789

Atanassov I, Urlaub H (2013): Increased proteome coverage by combining PAGE and peptide isoelectric focusing: comparative study of gel-based separation approaches. Proteomics 13, 2947-2955

Bang OY, Kim EH (2019): Mesenchymal Stem Cell-Derived Extracellular Vesicle Therapy for Stroke: Challenges and Progress. Front Neurol 10, 211

Bauer B, Hartz AM, Miller DS (2007): Tumor necrosis factor alpha and endothelin-1 increase P-glycoprotein expression and transport activity at the blood-brain barrier. Mol Pharmacol 71, 667-675

Buschmann D, Kirchner B, Hermann S, Marte M, Wurmser C, Brandes F, Kotschote S, Bonin M, Steinlein OK, Pfaffl MW, et al. (2018): Evaluation of serum extracellular vesicle isolation methods for profiling miRNAs by next-generation sequencing. J Extracell Vesicles 7, 1481321

Cen J, Liu L, Li MS, He L, Wang LJ, Liu YQ, Liu M, Ji BS (2013): Alteration in P-glycoprotein at the blood-brain barrier in the early period of MCAO in rats. J Pharm Pharmacol 65, 665-672

Chamorro A, Meisel A, Planas AM, Urra X, van de Beek D, Veltkamp R (2012): The immunology of acute stroke. Nat Rev Neurol 8, 401-410

Chiu CT, Chen JH, Chou FP, Lin HH (2015): Hibiscus sabdariffa Leaf Extract Inhibits Human Prostate Cancer Cell Invasion via Down-Regulation of Akt/NF-kB/MMP-9 Pathway. Nutrients 7, 5065-5087

Courties G, Herisson F, Sager HB, Heidt T, Ye Y, Wei Y, Sun Y, Severe N, Dutta P, Scharff J, et al. (2015): Ischemic stroke activates hematopoietic bone marrow stem cells. Circ Res 116, 407-417

Curtale G, Rubino M, Locati M (2019): MicroRNAs as Molecular Switches in Macrophage Activation. Front Immunol 10, 799

Dabrowska S, Andrzejewska A, Strzemecki D, Muraca M, Janowski M, Lukomska B (2019): Human bone marrow mesenchymal stem cell-derived extracellular vesicles attenuate neuroinflammation evoked by focal brain injury in rats. J Neuroinflammation 16, 216

DeMars KM, Yang C, Hawkins KE, McCrea AO, Siwarski DM, Candelario-Jalil E (2017): Spatiotemporal Changes in P-glycoprotein Levels in Brain and Peripheral Tissues Following Ischemic Stroke in Rats. J Exp Neurosci 11, 1-9

Dirnagl U, Iadecola C, Moskowitz MA (1999): Pathobiology of ischaemic stroke: an integrated view. Trends Neurosci 22, 391-397

Doeppner TR, Kaltwasser B, Fengyan J, Hermann DM, Bahr M (2013): TAT-Hsp70 induces neuroprotection against stroke via anti-inflammatory actions providing appropriate cellular microenvironment for transplantation of neural precursor cells. J Cereb Blood Flow Metab 33, 1778-1788

Doeppner TR, Kaltwasser B, ElAli A, Zechariah A, Hermann DM, Bahr M (2011): Acute hepatocyte growth factor treatment induces long-term neuroprotection and stroke recovery via mechanisms involving neural precursor cell proliferation and differentiation. J Cereb Blood Flow Metab 31, 1251-1262

Doeppner TR, Kaltwasser B, Teli MK, Bretschneider E, Bahr M, Hermann DM (2014): Effects of acute versus post-acute systemic delivery of neural progenitor cells on neurological recovery and brain remodeling after focal cerebral ischemia in mice. Cell Death Dis 5, e1386

Doeppner TR, Kaltwasser B, Teli MK, Sanchez-Mendoza EH, Kilic E, Bahr M, Hermann DM (2015): Post-stroke transplantation of adult subventricular zone derived neural progenitor cells--A comprehensive analysis of cell delivery routes and their underlying mechanisms. Exp Neurol 273, 45-56

Doeppner TR, Doehring M, Kaltwasser B, Majid A, Lin F, Bahr M, Kilic E, Hermann DM (2017): Ischemic Post-Conditioning Induces Post-Stroke Neuroprotection via Hsp70-Mediated Proteasome Inhibition and Facilitates Neural Progenitor Cell Transplantation. Mol Neurobiol 54, 6061-6073

Doyle LM, Wang MZ (2019): Overview of Extracellular Vesicles, Their Origin, Composition, Purpose, and Methods for Exosome Isolation and Analysis. Cells 8, 727

ElAli A, Hermann DM (2012): Liver X Receptor Activation Enhances Blood-Brain Barrier Integrity in the Ischemic Brain and Increases the Abundance of ATP-Binding Cassette Transporters ABCB1 and ABCC1 on Brain Capillary Cells. Brain Pathol 22, 175-187

ElAli A, Jean LeBlanc N (2016): The Role of Monocytes in Ischemic Stroke Pathobiology: New Avenues to Explore. Front Aging Neurosci 8, 29

Felix RA, Barrand MA (2002): P-glycoprotein expression in rat brain endothelial cells: evidence for regulation by transient oxidative stress. J Neurochem 80, 64-72

Fujimura M, Gasche Y, Morita-Fujimura Y, Massengale J, Kawase M, Chan PH (1999): Early appearance of activated matrix metalloproteinase-9 and blood-brain barrier disruption in mice after focal cerebral ischemia and reperfusion. Brain Res 842, 92-100

Giffard RG, Yenari MA (2004): Many mechanisms for hsp70 protection from cerebral ischemia. J Neurosurg Anesthesiol 16, 53-61

Gladstone DJ, Black SE, Hakim AM, Heart, Stroke Foundation of Ontario Centre of Excellence in Stroke R (2002): Toward wisdom from failure: lessons from neuroprotective stroke trials and new therapeutic directions. Stroke 33, 2123-2136

Goyal M, Menon BK, van Zwam WH, Dippel DW, Mitchell PJ, Demchuk AM, Dávalos A, Majoie CB, van der Lugt A, de Miquel MA, et al. (2016): Endovascular thrombectomy after large-vessel ischaemic stroke: a meta-analysis of individual patient data from five randomised trials. Lancet 387, 1723-1731

Green AR, Shuaib A (2006): Therapeutic strategies for the treatment of stroke. Drug Discov Today 11, 681-693

Hammond MD, Taylor RA, Mullen MT, Ai Y, Aguila HL, Mack M, Kasner SE, McCullough LD, Sansing LH (2014): CCR2+ Ly6C(hi) inflammatory monocyte recruitment exacerbates acute disability following intracerebral hemorrhage. J Neurosci 34, 3901-3909

Helms HC, Abbott NJ, Burek M, Cecchelli R, Couraud PO, Deli MA, Forster C, Galla HJ, Romero IA, Shusta EV, et al. (2016): In vitro models of the blood-brain barrier: An overview of commonly used brain endothelial cell culture models and guidelines for their use. Journal of Cerebral Blood Flow and Metabolism 36, 862-890

Hermann DM (2008): Future Perspectives for Brain Pharmacotherapies: Implications of Drug Transport Processes at the Blood-brain Barrier. Ther Adv Neurol Disord 1, 167-179

Hu X, Beeton C (2010): Detection of functional matrix metalloproteinases by zymography. J Vis Exp 45, 2445

Iadecola C, Anrather J (2011): The immunology of stroke: from mechanisms to translation. Nat Med 17, 796-808

Ingham KC (1984): Protein precipitation with polyethylene glycol. Methods Enzymol 104, 351-356

Ji BS, Cen J, He L, Liu M, Liu YQ, Liu L (2013): Modulation of P-glycoprotein in rat brain microvessel endothelial cells under oxygen glucose deprivation. J Pharm Pharmacol 65, 1508-1517

Jiang Y, He R, Shi Y, Liang J, Zhao L (2020): Plasma exosomes protect against cerebral ischemia/reperfusion injury via exosomal HSP70 mediated suppression of ROS. Life Sci 256, 117987

Kamel H, Iadecola C (2012): Brain-immune interactions and ischemic stroke: clinical implications. Arch Neurol 69, 576-581

Kaneko N, Kako E, Sawamoto K (2011): Prospects and limitations of using endogenous neural stem cells for brain regeneration. Genes (Basel) 2, 107-130

Katayama K, Noguchi K, Sugimoto Y (2014): Regulations of P-Glycoprotein/ABCB1/MDR1in Human Cancer Cells. New J Sci 2014, 1-10

Kim DK, Kang B, Kim OY, Choi DS, Lee J, Kim SR, Go G, Yoon YJ, Kim JH, Jang SC, et al. (2013): EVpedia: an integrated database of high-throughput data for systemic analyses of extracellular vesicles. J Extracell Vesicles 2, 1-7

Kooij G, Backer R, Koning JJ, Reijerkerk A, van Horssen J, van der Pol SM, Drexhage J, Schinkel A, Dijkstra CD, den Haan JM, et al. (2009): P-glycoprotein acts as an immunomodulator during neuroinflammation. PLoS One 4, e8212

Kooij G, Mizee MR, van Horssen J, Reijerkerk A, Witte ME, Drexhage JA, van der Pol SM, van Het Hof B, Scheffer G, Scheper R, et al. (2011): Adenosine triphosphate-binding cassette transporters mediate chemokine (C-C motif) ligand 2 secretion from reactive astrocytes: relevance to multiple sclerosis pathogenesis. Brain 134, 555-570

Kowal J, Arras G, Colombo M, Jouve M, Morath JP, Primdal-Bengtson B, Dingli F, Loew D, Tkach M, Thery C (2016): Proteomic comparison defines novel markers to characterize heterogeneous populations of extracellular vesicle subtypes. Proc Natl Acad Sci U S A 113, E968-977

Kuzmanov I, Herrmann AM, Galla HJ, Meuth SG, Wiendl H, Klotz L (2016): An In Vitro Model of the Blood-brain Barrier Using Impedance Spectroscopy: A Focus on T Cell-endothelial Cell Interaction. J Vis Exp 118, 54592

Lakhan SE, Kirchgessner A, Tepper D, Leonard A (2013): Matrix metalloproteinases and blood-brain barrier disruption in acute ischemic stroke. Front Neurol 4, 32

Lee BK, Lee WJ, Jung YS (2017): Chrysin Attenuates VCAM-1 Expression and Monocyte Adhesion in Lipopolysaccharide-Stimulated Brain Endothelial Cells by Preventing NF-kappaB Signaling. Int J Mol Sci 18, 1424

Li M, van Esch B, Wagenaar GTM, Garssen J, Folkerts G, Henricks PAJ (2018): Pro- and anti-inflammatory effects of short chain fatty acids on immune and endothelial cells. Eur J Pharmacol 831, 52-59

Li Y, Zhu ZY, Huang TT, Zhou YX, Wang X, Yang LQ, Chen ZA, Yu WF, Li PY (2018): The peripheral immune response after stroke-A double edge sword for blood-brain barrier integrity. CNS Neurosci Ther 24, 1115-1128

Liesz A, Suri-Payer E, Veltkamp C, Doerr H, Sommer C, Rivest S, Giese T, Veltkamp R (2009): Regulatory T cells are key cerebroprotective immunomodulators in acute experimental stroke. Nat Med 15, 192-199

Liu X, Ye R, Yan T, Yu SP, Wei L, Xu G, Fan X, Jiang Y, Stetler RA, Liu G, et al. (2014): Cell based therapies for ischemic stroke: from basic science to bedside. Prog Neurobiol 115, 92-115

Ludwig AK, De Miroschedji K, Doeppner TR, Borger V, Ruesing J, Rebmann V, Durst S, Jansen S, Bremer M, Behrmann E, et al. (2018): Precipitation with polyethylene glycol followed by washing and pelleting by ultracentrifugation enriches extracellular vesicles from tissue culture supernatants in small and large scales. J Extracell Vesicles 7, 1528109

Luissint AC, Artus C, Glacial F, Ganeshamoorthy K, Couraud PO (2012): Tight junctions at the blood brain barrier: physiological architecture and disease-associated dysregulation. Fluids Barriers CNS 9, 23

Lv Y, Liu W, Ruan Z, Xu Z, Fu L (2019): Myosin IIA Regulated Tight Junction in Oxygen Glucose-Deprived Brain Endothelial Cells Via Activation of TLR4/PI3K/Akt/JNK1/2/14-3-3epsilon/NF-kappaB/MMP9 Signal Transduction Pathway. Cell Mol Neurobiol 39, 301-319

Maherally Z, Fillmore HL, Tan SL, Tan SF, Jassam SA, Quack FI, Hatherell KE, Pilkington GJ (2018): Real-time acquisition of transendothelial electrical resistance in an all-human, in vitro, 3-dimensional, blood-brain barrier model exemplifies tight-junction integrity. FASEB J 32, 168-182

Martin-Rufino JD, Espinosa-Lara N, Osugui L, Sanchez-Guijo F (2019): Targeting the Immune System With Mesenchymal Stromal Cell-Derived Extracellular Vesicles: What Is the Cargo's Mechanism of Action? Front Bioeng Biotechnol 7, 308

Mathivanan S, Fahner CJ, Reid GE, Simpson RJ (2012): ExoCarta 2012: database of exosomal proteins, RNA and lipids. Nucleic Acids Res 40, D1241-1244

Miller DS (2015): Regulation of ABC transporters blood-brain barrier: the good, the bad, and the ugly. Adv Cancer Res 125, 43-70

Miranda-Azpiazu P, Panagiotou S, Jose G, Saha S (2018): A novel dynamic multicellular co-culture system for studying individual blood-brain barrier cell types in brain diseases and cytotoxicity testing. Sci Rep 8, 8784

Moon GJ, Sung JH, Kim DH, Kim EH, Cho YH, Son JP, Cha JM, Bang OY (2019): Application of Mesenchymal Stem Cell-Derived Extracellular Vesicles for Stroke: Biodistribution and MicroRNA Study. Transl Stroke Res 10, 509-521

Moriyama Y, Takagi N, Hashimura K, Itokawa C, Tanonaka K (2013): Intravenous injection of neural progenitor cells facilitates angiogenesis after cerebral ischemia. Brain Behav 3, 43-53

Moskowitz MA, Lo EH, Iadecola C (2010): The science of stroke: mechanisms in search of treatments. Neuron 67, 181-198

Murozono M, Matsumoto S, Okada S, Nagaoka D, Isshiki A, Watanabe Y (2009): Reduction of brain infarction induced by a transient brain ischemia in mdr1a knockout mice. Neurochem Res 34, 1555-1561

Musuka TD, Wilton SB, Traboulsi M, Hill MD (2015): Diagnosis and management of acute ischemic stroke: speed is critical. CMAJ 187, 887-893

Naik P, Cucullo L (2012): In vitro blood-brain barrier models: Current and perspective technologies. J Pharm Sci 101, 1337-1354

O'Collins VE, Macleod MR, Donnan GA, Horky LL, van der Worp BH, Howells DW (2006): 1,026 experimental treatments in acute stroke. Ann Neurol 59, 467-477

O'Neill LA, Sheedy FJ, McCoy CE (2011): MicroRNAs: the fine-tuners of Toll-like receptor signalling. Nat Rev Immunol 11, 163-175

Osorio C, Cavalla F, Paula-Lima A, Diaz-Araya G, Vernal R, Ahumada P, Gamonal J, Hernandez M (2015): H2 O2 activates matrix metalloproteinases through the nuclear factor kappa B pathway and Ca(2+) signals in human periodontal fibroblasts. J Periodontal Res 50, 798-806

Park KP, Rosell A, Foerch C, Xing C, Kim WJ, Lee S, Opdenakker G, Furie KL, Lo EH (2009): Plasma and brain matrix metalloproteinase-9 after acute focal cerebral ischemia in rats. Stroke 40, 2836-2842

Patak P, Hermann DM (2011): ATP-Binding Cassette Transporters at the Blood-Brain Barrier in Ischaemic Stroke. Curr Pharm Des 17, 2787-2792

Planas AM (2018): Role of Immune Cells Migrating to the Ischemic Brain. Stroke 49, 2261-2267

Posel C, Moller K, Boltze J, Wagner DC, Weise G (2016): Isolation and Flow Cytometric Analysis of Immune Cells from the Ischemic Mouse Brain. J Vis Exp 108, 53658

Qin SB, Peng DY, Lu JM, Ke ZP (2018): MiR-182-5p inhibited oxidative stress and apoptosis triggered by oxidized low-density lipoprotein via targeting toll-like receptor 4. J Cell Physiol 233, 6630-6637

Qosa H, Miller DS, Pasinelli P, Trotti D (2015): Regulation of ABC efflux transporters at blood-brain barrier in health and neurological disorders. Brain Res 1628, 298-316

Qosa H, Lichter J, Sarlo M, Markandaiah SS, McAvoy K, Richard JP, Jablonski MR, Maragakis NJ, Pasinelli P, Trotti D (2016): Astrocytes drive upregulation of the multidrug resistance transporter ABCB1 (P-Glycoprotein) in endothelial cells of the blood-brain barrier in mutant superoxide dismutase 1-linked amyotrophic lateral sclerosis. Glia 64, 1298-1313

Radu M, Chernoff J (2013): An in vivo assay to test blood vessel permeability. J Vis Exp 73, e50062

Rempe RG, Hartz AMS, Bauer B (2016): Matrix metalloproteinases in the brain and blood-brain barrier: Versatile breakers and makers. J Cereb Blood Flow Metab 36, 1481-1507

Renu A, Amaro S, Laredo C, Roman LS, Llull L, Lopez A, Urra X, Blasco J, Oleaga L, Chamorro A (2015): Relevance of blood-brain barrier disruption after endovascular treatment of ischemic stroke: dual-energy computed tomographic study. Stroke 46, 673-679

Ridder DA, Schwaninger M (2009): NF-kappaB signaling in cerebral ischemia. Neuroscience 158, 995-1006

Ronaldson PT, Davis TP (2012): Blood-brain barrier integrity and glial support: mechanisms that can be targeted for novel therapeutic approaches in stroke. Curr Pharm Des 18, 3624-3644

Sa-Pereira I, Brites D, Brito MA (2012): Neurovascular unit: a focus on pericytes. Mol Neurobiol 45, 327-347

Sakaguchi S, Yamaguchi T, Nomura T, Ono M (2008): Regulatory T cells and immune tolerance. Cell 133, 775-787

Sanchez-Covarrubias L, Slosky LM, Thompson BJ, Davis TP, Ronaldson PT (2014): Transporters at CNS barrier sites: obstacles or opportunities for drug delivery? Curr Pharm Des 20, 1422-1449

Sandoval KE, Witt KA (2008): Blood-brain barrier tight junction permeability and ischemic stroke. Neurobiol Dis 32, 200-219

Santos Samary C, Pelosi P, Leme Silva P, Rieken Macedo Rocco P (2016): Immunomodulation after ischemic stroke: potential mechanisms and implications for therapy. Crit Care 20, 391

Schmidt-Pogoda A, Bonberg N, Koecke MHM, Strecker JK, Wellmann J, Bruckmann NM, Beuker C, Schabitz WR, Meuth SG, Wiendl H, et al. (2020): Why Most Acute Stroke Studies Are Positive in Animals but Not in Patients: A Systematic Comparison of Preclinical, Early Phase, and Phase 3 Clinical Trials of Neuroprotective Agents. Ann Neurol 87, 40-51

Seitz RJ (2016): The pros and cons of intravenous thrombolysis in stroke. Lancet Neurol 15, 997-998

Sharp FR, Zhan X, Liu DZ (2013): Heat shock proteins in the brain: role of Hsp70, Hsp 27, and HO-1 (Hsp32) and their therapeutic potential. Transl Stroke Res 4, 685-692

Shen B, Liu J, Zhang F, Wang Y, Qin Y, Zhou Z, Qiu J, Fan Y (2016): CCR2 Positive Exosome Released by Mesenchymal Stem Cells Suppresses Macrophage Functions and Alleviates Ischemia/Reperfusion-Induced Renal Injury. Stem Cells Int 2016, 1240301

Sokolova V, Ludwig AK, Hornung S, Rotan O, Horn PA, Epple M, Giebel B (2011): Characterisation of exosomes derived from human cells by nanoparticle tracking analysis and scanning electron microscopy. Colloids Surf B Biointerfaces 87, 146-150

Spudich A, Kilic E, Xing H, Kilic U, Rentsch KM, Wunderli-Allenspach H, Bassetti CL, Hermann DM (2006): Inhibition of multidrug resistance transporter-1 facilitates neuroprotective therapies after focal cerebral ischemia. Nat Neurosci 9, 487-488

Su VY, Lin CS, Hung SC, Yang KY (2019): Mesenchymal Stem Cell-Conditioned Medium Induces Neutrophil Apoptosis Associated with Inhibition of the NF-kappaB Pathway in Endotoxin-Induced Acute Lung Injury. Int J Mol Sci 20, 2208

Suofu Y, Clark JF, Broderick JP, Kurosawa Y, Wagner KR, Lu A (2012): Matrix metalloproteinase-2 or -9 deletions protect against hemorrhagic transformation during early stage of cerebral ischemia and reperfusion. Neuroscience 212, 180-189

Takata F, Dohgu S, Yamauchi A, Matsumoto J, Machida T, Fujishita K, Shibata K, Shinozaki Y, Sato K, Kataoka Y, et al. (2013): In Vitro Blood-Brain Barrier Models Using Brain Capillary Endothelial Cells Isolated from Neonatal and Adult Rats Retain Age-Related Barrier Properties. Plos One 8, e55166

Thery C, Witwer KW, Aikawa E, Alcaraz MJ, Anderson JD, Andriantsitohaina R, Antoniou A, Arab T, Archer F, Atkin-Smith GK, et al. (2018): Minimal information for studies of extracellular vesicles 2018 (MISEV2018): a position statement of the International Society for Extracellular Vesicles and update of the MISEV2014 guidelines. J Extracell Vesicles 7, 1535750

Venkat P, Shen Y, Chopp M, Chen J (2018): Cell-based and pharmacological neurorestorative therapies for ischemic stroke. Neuropharmacology 134, 310-322

Wang JD, Khafagy el S, Khanafer K, Takayama S, ElSayed ME (2016): Organization of Endothelial Cells, Pericytes, and Astrocytes into a 3D Microfluidic in Vitro Model of the Blood-Brain Barrier. Mol Pharm 13, 895-906

Wang Y, Kilic E, Kilic U, Weber B, Bassetti CL, Marti HH, Hermann DM (2005): VEGF overexpression induces post-ischaemic neuroprotection, but facilitates haemodynamic steal phenomena. Brain 128, 52-63

Wang Z, Leng Y, Tsai LK, Leeds P, Chuang DM (2011): Valproic acid attenuates blood-brain barrier disruption in a rat model of transient focal cerebral ischemia: the roles of HDAC and MMP-9 inhibition. J Cereb Blood Flow Metab 31, 52-57

Watson PM, Paterson JC, Thom G, Ginman U, Lundquist S, Webster CI (2013): Modelling the endothelial blood-CNS barriers: a method for the production of robust in vitro models of the rat blood-brain barrier and blood-spinal cord barrier. BMC Neurosci 14, 59

Webb RL, Kaiser EE, Scoville SL, Thompson TA, Fatima S, Pandya C, Sriram K, Swetenburg RL, Vaibhav K, Arbab AS, et al. (2018): Human Neural Stem Cell Extracellular Vesicles Improve Tissue and Functional Recovery in the Murine Thromboembolic Stroke Model. Transl Stroke Res 9, 530-539

Weber CR (2012): Dynamic properties of the tight junction barrier. Ann N Y Acad Sci 1257, 77-84

World Health Organization (2020): The top 10 causes of death

Xu SY, Pan SY (2013): The failure of animal models of neuroprotection in acute ischemic stroke to translate to clinical efficacy. Med Sci Monit Basic Res 19, 37-45

Yang C, Candelario-Jalil E (2017): Role of Matrix Metalloproteinases in Brain Edema. Brain Edema 11, 199-215

Yang C, Hawkins KE, Dore S, Candelario-Jalil E (2019): Neuroinflammatory mechanisms of blood-brain barrier damage in ischemic stroke. Am J Physiol Cell Physiol 316, C135-C153

Yang S, Jin H, Zhao Z (2018): Paracellular tightness and the functional expression of efflux transporters P-gp and BCRP in bEnd3 cells. Neurol Res 40, 644-649

Yang Y, Rosenberg GA (2015): Matrix metalloproteinases as therapeutic targets for stroke. Brain Res 1623, 30-38

Yu C, Argyropoulos G, Zhang Y, Kastin AJ, Hsuchou H, Pan W (2008): Neuroinflammation activates Mdr1b efflux transport through NFkappaB: promoter analysis in BBB endothelia. Cell Physiol Biochem 22, 745-756

Zhang J, Zhang M, Sun B, Li Y, Xu P, Liu C, Liu L, Liu X (2014): Hyperammonemia enhances the function and expression of P-glycoprotein and Mrp2 at the blood-brain barrier through NF-kappaB. J Neurochem 131, 791-802

Zhang JW, Gottschall PE (1997): Zymographic measurement of gelatinase activity in brain tissue after detergent extraction and affinity-support purification. J Neurosci Methods 76, 15-20

Zhang L, Graf I, Kuang Y, Zheng X, Haupt M, Majid A, Kilic E, Hermann DM, Psychogios MN, Weber MS, et al. (2021): Neural Progenitor Cell-Derived Extracellular Vesicles Enhance Blood-Brain Barrier Integrity by NF-κB (Nuclear Factor-κB)-Dependent Regulation of ABCB1 (ATP-Binding Cassette Transporter B1) in Stroke Mice. Arterioscler Thromb Vasc Biol 41, 1127-1145

Zhang X, Borg EGF, Liaci AM, Vos HR, Stoorvogel W (2020): A novel three step protocol to isolate extracellular vesicles from plasma or cell culture medium with both high yield and purity. J Extracell Vesicles 9, 1791450

Zheng H, Zhang B, Chhatbar PY, Dong Y, Alawieh A, Lowe F, Hu X, Feng W (2018): Mesenchymal Stem Cell Therapy in Stroke: A Systematic Review of Literature in Pre-Clinical and Clinical Research. Cell Transplant 27, 1723-1730

Zheng X, Zhang L, Kuang Y, Venkataramani V, Jin F, Hein K, Zafeiriou MP, Lenz C, Moebius W, Kilic E, et al. (2020): Extracellular Vesicles Derived from Neural Progenitor Cells--a Preclinical Evaluation for Stroke Treatment in Mice. Transl Stroke Res 12, 185-203

Zhou SF (2008): Structure, function and regulation of P-glycoprotein and its clinical relevance in drug disposition. Xenobiotica 38, 802-832

Zhu BS, Xing CG, Lin F, Fan XQ, Zhao K, Qin ZH (2011): Blocking NF-kappaB nuclear translocation leads to p53-related autophagy activation and cell apoptosis. World J Gastroenterol 17, 478-487

Acknowledgments

This thesis has been written at the Department of Neurology of the University of Göttingen Medical Center (UMG), Germany (director: Prof. Dr. Mathias Bähr). I would like to thank everyone who provided support and encouragement to me through the process of performing the experiments and writing this thesis. However, I would like to especially thank Prof. Dr. Thorsten R. Döppner, M.Sc., for his splendid supervision during all these years. Without him, this thesis would have never been possible. Finally, I would also like to express my gratitude to Prof. Dr. Mathias Bähr for giving me the opportunity to study and work in the Department of Neurology.